IN VITRO MODELING OF NANOMATERIAL TRANSPORT ACROSS THE BLOOD-BRAIN BARRIER (BBB) MODEL DERIVED FROM iPSCs

A THESIS SUBMITTED TO
THE GRADUATE SCHOOL OF NATURAL AND APPLIED SCIENCES
OF
ANKARA UNIVERSITY

by

Cemile GÖKÇE

DEPARTMENT OF BIOMEDICAL ENGINEERING

ANKARA
2024

ABSTRACT

Master's Thesis

IN VITRO MODELING OF NANOMATERIAL TRANSPORT ACROSS THE BLOOD-BRAIN BARRIER (BBB) MODEL DERIVED FROM iPSCs

Cemile GÖKÇE

Ankara University
Graduate School of Natural and Applied Sciences
Department of Biomedical Engineering

Supervisor: Assoc. Prof. Açelya YILMAZER AKTUNA

Blood–brain barrier (BBB) is the main entry to central nervous system (CNS) and considered as the bottleneck of most CNS-related studies like finding new therapeutic canditates against brain tumors such as glioblastoma multiforme (GBM). Maintaining physical BBB and blood–brain-tumor barrier (BBTB) integrity and their well characterization are highly crucial for these studies. For modulating the treatment efficacy of brain tumors, especially GBM, there is a need to understand the behaviors of both BBB and BBTB in further studies. In this regard, decades have been devoted to the investigation and comprehension of the cellular and molecular mechanisms that underlie the development of the BBB and BBTB using in vitro models. Additionally, researchers aim to design nanodelivery systems and/or use nanomaterials (NMs) to cross the BBB and BBTB and therefore successfully deliver them to the brain, for purposes like drug delivery to the tumor site. With the in vitro BBB and BBTB models, it is possible to investigate the transport of these materials/systems from the blood to the brain. For these reasons, in this thesis, useful in vitro human BBB and BBTB models are provided by using differentiation and culturing methods to evaluate the properties of human brain endothelial cells (ECs) and then to investigate the transport of novel fluorescent NMs across the BBB and BBTB. Demonstration of transportation from blood to the brain will pave the way for these NMs to be more preferred in CNS-related studies and even to be used in the treatment of various neurological diseases in future studies.

September 2024, 115 pages

Key Words: In vitro blood-brain barrier model, human brain endothelial cells, human induced pluripotent stem cells, differentiation, disease modeling, glioblastoma multiforme, blood-brain-tumor barrier, fluorescent nanomaterials, nanomaterial transportation

ÖZET

Yüksek Lisans Tezi

uPK HÜCRELERİNDEN ELDE EDİLEN KAN-BEYİN BARİYER MODELİNDE NANOMALZEME GEÇİŞİNİN İN VİTRO MODELLENMESİ

Cemile GÖKÇE

Ankara Üniversitesi
Fen Bilimleri Enstitüsü
Biyomedikal Mühendisliği Anabilim Dalı

Danışman: Doç. Dr. Açelya YILMAZER AKTUNA

Kan-beyin bariyeri (KBB), merkezi sinir sistemine (MSS) ana giriştir ve glioblastom multiform (GBM) gibi beyin tümörlerine karşı yeni terapötik adayların bulunması gibi MSS ile ilgili çoğu çalışmanın önemli bir parçası olarak kabul edilir. Fiziksel KBB ve kan-beyin-tümör bariyeri (KBTB) bütünlüğünün korunması ve bunların karakterizasyonu bu çalışmalar için oldukça önemlidir. Beyin tümörlerinin, özellikle de GBM'nin tedavi etkinliğinin modüle edilebilmesi için ileriki çalışmalarda hem KBB hem de KBTB'nin davranışlarının anlaşılmasına ihtiyaç vardır. Bu bağlamda, in vitro modeller kullanılarak KBB ve KBTB'nin gelişiminin altında yatan hücresel ve moleküler mekanizmaların araştırılmasına ve anlaşılmasına onlarca yıl ayrılmıştır. Ayrıca araştırmacılar, KBB ve KBTB'yi geçmek için nanodağıtım sistemleri tasarlamayı ve/veya nanomalzemeler kullanmayı ve dolayısıyla bunları tümör bölgesine ilaç dağıtımı gibi amaçlarla başarılı bir şekilde beyne ulaştırmayı hedeflemektedir. Oluşturulan in vitro KBB ve KBTB modellemeleriyle bu malzemelerin/sistemlerin kandan beyne taşınmasını araştırmak mümkündür. Bu sebeplerden dolayı, bu tezde, farklılaştırma ve kültür yöntemleri kullanılarak insan beyni endotel hücrelerinin (EH'ler) özelliklerini değerlendirmek ve daha sonra yeni floresan nanomalzemelerin (NM'lerin) KBB ve KBTB boyunca taşınmasını araştırmak için kullanışlı in vitro insan KBB ve KBTB modelleri sağlanmıştır. Kandan beyne geçişinin gösterilmesi, bu nanomalzemelerin MSS ile ilgili çalışmalarda daha çok tercih edilmesine, hatta ileride yapılacak çalışmalarda çeşitli nörolojik hastalıkların tedavisinde kullanılmasının önünü açacaktır.

Eylül 2024, 115 sayfa

Anahtar kelimeler: İn vitro kan-beyin bariyeri modeli, insan beyni endotel hücreleri, insan kaynaklı pluripotent kök hücreler, farklılaşma, hastalık modelleme, glioblastom multiform, kan-beyin-tümör bariyeri, floresan nanomalzemeler, nanomalzeme taşınması

FOREWORD AND ACKNOWLEDGEMENTS

I would like to express my deepest appreciation to my supervisor Doç. Dr. Açelya YILMAZER AKTUNA for her guidance and support in doing my research. I am truly thankful to her for improving my scientific knowledge and sharing her academic experience.

I would also like to extend my deepest gratitude to Prof. Dr. İbrahim Çağatay KARAASLAN for sharing the laboratory and equipment at Hacettepe University and gratefully acknowledge the effort of his doctorate student Büşra KILIÇ throughout the transendothelial electrical resistance experiment of this thesis.

I would like to thank Prof. Dr. Sanjiv DHINGRA for kindly providing the necessary NMs, Mxene Quantum Dots.

I would like to thank my lab colleagues and friends, Cansu GÜRCAN KARATEPE, Ömür BUL BEŞBİNAR, Gökçe Yağmur SUMMAK, Esen KİRİT, Doğantan ÇELİK, Hande YAVUZ, Buse ALTUN, Recep UYAR, and Damla ALKAYA for their unwavering support and valuable advice during my thesis. I had the greatest pleasure of working with them.

I would like to also thank TUBITAK for providing financial support to transduce human iPSCs (hiPSCs) from the peripheral blood mononuclear cells (PBMCs) under the 1004 Center of Excellence Support Program (Project Number: 20AG003-P8).

Finally, I would like to thank my family members, Alime GÖKÇE, Yasin GÖKÇE, İsmail GÖKÇE, Ece Pelin GÖKÇE, and Selda GÖKÇE for their support in my life journey. They have always stood by my side and encouraged me throughout my education and academic career.

Cemile GÖKÇE
Ankara, September 2024

TABLE OF CONTENTS

LIST OF SYMBOLS

Ω	Ohms
μ	Micro
Δ	Delta
≤	Less than or equal to
β	Beta
^{o}C	Degree celsius
cm/s	Centimeter per second
cm^2	Centimeter square
kDa	Kilodaltons
mL	Milliliter
M	Molar
ng	Nanogram
rpm	Revolutions per minute
TM	Trademark
μg/mL	Microgram per milliliter

Abbreviations

2D	Two dimensional
3D	Three dimensional
ABCB1	ATP Binding Cassette Subfamily B Member 1
ALP	Alkaline phosphatase
ASC	Adult stem cell
AT	Adsorptive transcytosis
BBB	Blood-brain barrier
BBTB	Blood-brain tumor barrier
BCECs	Brain capillary endothelial cells
BL	Basal lamina
BMECs	Brain microvascular endothelial cells
BSA	Bovine serum albumin
CO_2	Carbondioxide
cDNA	Complementary DNA
CDH5	Cadherin5 (VE-Cadherin, vascular endothelial-cadherin)
CDs	Carbon dots
CFS	Cerebrospinal fluid
CLDNs	Claudins
CNS	Central nervous system
CoL1	Collagen type I

CoL4	Collagen type IV
Ct	Cycle threshold
DAPI	4’6-diamidino-2-phenylindole
DPBS	Dulbecco’s phosphate-buffered saline
DMSO	Dimethyl sulfoxide
DMEM	Dulbecco′s modified eagle′s medium
dH_2O	Distilled water
EC	Endothelial cell
ECM	Extracellular matrix
ESC	Embryonic stem cells
F	Forward
FBS	Fetal bovine serum
FGF	Fibroblast growth factor
FITC	Fluorescein isothiocyanate
FD	FITC-dextran
FN	Fibronectin
GAPDH	Glyceraldehyde-3-phosphate dehydrogenase
GBM	Glioblastoma multiforme
GTP	Gamma-glutamyl transpeptidase
H	Hours
hCMEC/D3	Human cerebral microvascular endothelial cell line
hiPSC	Human induced pluripotent stem cell
hESFM	Human endothelial serum free medium
ICC	Immunocytochemistry
IF	Immunofluorescence
LAB	Laboratory
ILM	Inverted light microscope
JAM	Junctional adhesion molecule
KDR	Kinase insert domain receptor (VEGFR2, vascular endothelial growth factor receptor 2)
KOSR	Knockout serum replacement
LDH	Lactate dehydrogenase
MEM	Minimum essential medium
MeOH	Methanol
MQDs	MXene quantum dots
NEAA	Nonessential amino acids
NFW	Nuclease-free water
NM	Nanomaterial
NP	Nanoparticle
NVU	Neurovascular unit
OCLN	Occludin
OCT3/4	Octamer-binding transcription factor

PBMC	Peripheral blood mononuclear cell
PCR	Polymerase chain reaction
PDS	Platelet poor plasma derived serum
PDGFR-β	Platelet-derived growth factor receptor- β
PECAM1	Platelet endothelial cell adhesion molecule (CD31, cluster of differentation31)
P-gp	Polyglycoprotein
R	Reverse
RA	Retinoic acid
rhEGF	Recombinant human epidermal growth factor
RMT	Receptor-mediated transcytosis
RNA	Ribonucleic acid
RT	Room temperature
SA	Surface area
SC	Stem cell
SD	Standard deviation
SLC2A1	Solute carrier family 2 member 1 (GLUT1, glucose transporter)
SOX2	Sex determining region y-box transcription factor 2
TEER	Transendothelial electrical resistance
TFRC	Transferrin receptor
TGF-β	Transforming growth factor-β
TJ	Tight junction protein
U87	Human glioblastoma cell line
UM	Unconditioned medium
VTN	Vitronectin
w/o	Without
ZO-1	Zonula occludens-1

LIST OF FIGURES

LIST OF TABLES

1. INTRODUCTION

In well-developed organisms just like the human body, tissues of the brain are preserved from foreign molecules such as infectious agents and toxins via three main physiological barriers in the central nervous system (CNS): blood–cerebrospinal fluid (CSF) barrier, the arachnoid barrier, and blood-brain barrier (BBB) (Abbott, Patabendige, Dolman, Yusof, & Begley, 2010).

BBB is one of the most exclusive ones for homeostasis of the brain, and thus its modeling is extremely important in biomedical applications like CNS drug studies like permeability, screening, and delivery and treatments of brain disorders like neurological diseases and tumors in brain (Bagchi et al., 2019; Z. Liu et al., 2022; Miura et al., 2013; Reddy, Tatiparti, Sau, & Iyer, 2021; Vignone et al., 2022). Regarding this, BBB models can be created under laboratory (LAB) conditions (Hatherell, Couraud, Romero, Weksler, & Pilkington, 2011; J. Helms et al., 2020; Neuhaus et al., 2006; Prashanth et al., 2021).

This thesis provided a basic description of stem cells (SCs) and an overview of BBB anatomy, function, properties, important terms determining BBB integrity, and different transport mechanisms (pathways) present in the BBB. Also, to better understand the thesis aim, different BBB models in vitro in two (2D) and three dimensions (3D), the factors or diseases causing the disruptions in the BBB integrity as well as its function, BBB disease models, NMs' use in biomedical areas like nanodelivery systems in addition to BBB studies including clinical ones are mentioned.

2. LITERATURE REVIEW

2.1 Stem Cells (SCs)

Stem cells (SCs) are undifferentiated cells with potential to differentiate into different cell types within human tissues and organs. SCs may be used in the therapies of various chronic human diseases like diabetes and cancer, replacement of the skin, repair of spinal cord injury, transplantation of brain cells for Parkinson's disease. They are mainly classified as embryonic, hematopoietic or adult, and pluripotent SCs based on their sources (Kalra & Tomar, 2014).

Embryonic SCs (ESCs) are immortalized and self-renewed cells found in the blastocyst's inner cell mass and derived from four-to five-day-old embryos. Pluripotency is shown by these cells, meaning they differentiate into almost any cell type. Adult SCs (ASCs) are found in the umbilical cord, placenta, and mature body tissues. They possess multipotent differential potential by differentiating into a cell family (Kalra & Tomar, 2014). They are widely used in tissue engineering to regenerate dying cells and/or damaged tissues (Eberli & Atala, 2006). Induced pluripotent SCs (iPSCs) are somatic cells, which gain pluripotency by introducing Yamanaka transcription factors, OCT4, SOX2, KLF4, and c-MYC (Takahashi et al., 2007). They possess the capacity for self-renewal and the potential to differentiate to any cell type derived from the three primary germ layers: ectoderm, endoderm, mesoderm (Figure 2.1). They are generated from adults, unlike embryonic tissue, so they do not have ethical issues (Delsing et al., 2020).

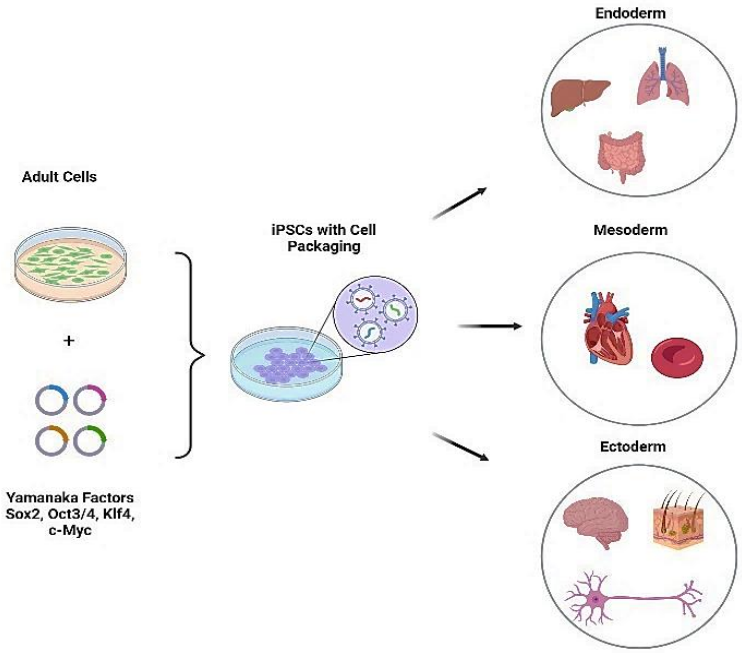

Figure 2.1 iPSCs isolating from adult cells and differentiating into three germ layers (Created by BioRender)

2.2 The blood-brain-barrier (BBB)

2.2.1 Structure and function

BBB, as a selectively semipermeable system, is considered the most regulated and privileged barriers in human body (Alahmari, 2021). Its development starts to occur during fetal life and its proteins' formation by birth. The protection of the CNS in the brain is particularly maintained by the BBB, whose function is to regulate the flow of all kinds of substances from luminal (blood) to abluminal (brain) side or vice versa and thus BBB controls brain's chemical composition for its normal functioning (Nance, Pun, Saigal, & Sellers, 2021).

2.2.2 Neurovascular unit (NVU)

The BBB has the combination of three interfaces: physical barrier with tight junction proteins (TJs) like occludin (OCLN), and claudins (CLDNs) (see Figure 2.3), transport

barrier with transport pathways like diffusion and transcytosis (see Figure 2.4), and metabolic barrier with enzymes like gamma-glutamyl transpeptidase (-GTP) and alkaline phosphatase (ALP) (Abbott, Rönnbäck, & Hansson, 2006; Stamatovic, Keep, & Andjelkovic, 2008). It consists of cells having a comparatively small pore size that inhibit the transcytosis of most solutes and particles (Nance et al., 2021). The critical BBB components are pericytes, astrocytes, and endothelial cells (ECs) creating a neurovascular unit (NVU), as shown in Figure 2.2. In the NVU, the blood capillary walls are formed by ECs, and ECs are connected by TJs, which restrict the flux between these cells (Abbott et al., 2010). Blood vessels are surrounded by end-feet of astrocytes, which have role in maintaining BBB, controlling blood flow, and critical to restore BBB integrity after brain damage (Kubotera et al., 2019). Pericytes, situated very close to the end-feet of astrocytes' end feet, play crucial role in stabilizing vascularization as well as supporting BBB. They contribute to the BBB regulation and functionality through producing transforming growth factor-β (TGF-β) (Alahmari, 2021; Azad et al., 2015). They also produce extracellular matrix (ECM) proteins and regulated activity of ECs (Mo, Pellerino, Soffietti, & Rudà, 2021). In the brain side of BBB, cells, namely microglias, regulate passage of immune cells across the BBB and provide immunity by wrappping foreign particles (Alahmari, 2021; Daneman, 2012).

In the basement membrane (basal lamina, BL), the ECs interact with ECM proteins like collagen (CoL), fibronectin (FN), glycoproteins like tenascin, and proteoglycans like agrin by using integrin receptors and thus manage the BBB to function properly. ECM proteins are prominent because they may promote adhesion, spreading of ECs and monolayer BBB formation (Katt, Linville, Mayo, Xu, & Searson, 2018). In neurological diseases such as stroke, Alzheimer's disease (AD), membrane is disrupted by matrix metalloproteinases disrupt therefore the BBB dysfunctions (Alahmari, 2021; Daneman, 2012; Daneman & Prat, 2015). Furthermore, ECM has great impact on the therapeutic outcome owing to interactions between drug delivery systems or nanoparticles (NPs) and ECM at BBB before reaching brain and then modifies system/particle uptake and releasement to tissues (Henrich-Noack et al., 2019). ECM is also modulated in tumor presence with the partial loss of some ECM components from the blood vessels (Azad et al., 2015; Rascher et al., 2002).

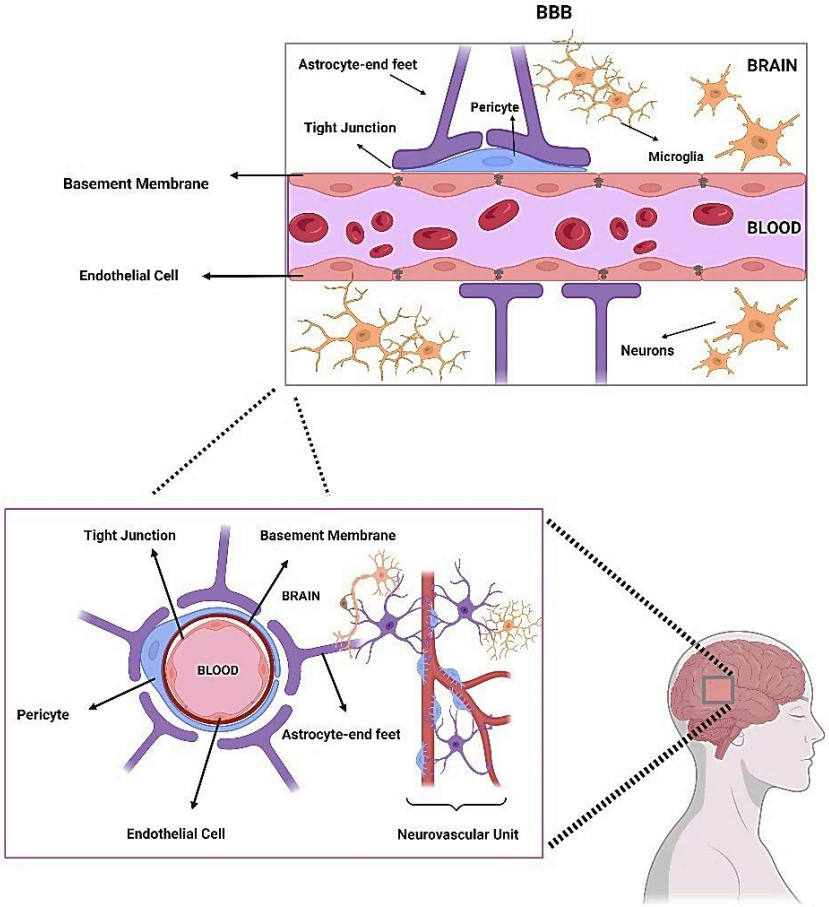

Figure 2.2 Anatomical BBB structure, including BBB vascular view and cross-section (Created by BioRender)

2.2.3 Properties/Characteristics of the BBB

Due to the different areas in the brain and the BBB throughout the vasculature, including capillaries, arteries, veins, and venules, heterogeneity of the BBB is observed (Daneman, 2012). Each vasculating segment has different functional properties. Transport properties-related genes are predominant in venules, whereas immunological properties are enriched in capillaries (Macdonald, Murugesan, & Pachter, 2010).

As described before, TJs form layers of ECs and critical for determining the strength and degree of permeability of the BBB. This is because TJs consist of numerous components, which comprise a sequence of transmembrane proteins including OCLNs, junctional adhesion molecules (JAMs), and more predominanlty claudin family (see Figure 2.3)

(Daneman, 2012; Furuse, Sasaki, & Tsukita, 1999). Out of the family, CLDN-5 seems to be the most prevalent one in endothelial TJs (Morita, Sasaki, Furuse, & Tsukita, 1999). Importantly, the heterogeneous composition of CLDNs within TJs are variable in different cellular barriers and human neurological diseases (Furuse et al., 2002; Nitta et al., 2003). On the other hand, the state of CNS affects the function of the BBB as well as its integrity (Abbott et al., 2010). For example, tumor presence changes the molecular and cellular regulations of the BBB and increases its heterogeneity (Griffith et al., 2020; Papadopoulos et al., 2004). Other than TJ components, adherens junctional proteins such as vascular endothelial-cadherin (VE-Cadherin) and the platelet–endothelial cell adhesion molecule (PECAM1) are identified in brain ECs (Daneman, 2012; Daneman et al., 2010). In addition to the TJs' formation, polarity of the membrane itself affects BBB permeability. Permeability is also associated with molecules' properties to be crossed the barrier such as topological surface area, molecular flexibility, shape, and weight, metabolic stability, and polarity (Cafiso, 2017; Fong, 2015; Stowasser, 2008). Also, the releasement of agents like vasoactive peptides and cytokines and production of reactive oxygen species can regulate it (Abbott et al., 2010; Abbott et al., 2006; Pun, Lu, & Moochhala, 2009).

Another BBB property is transendothelial electrical resistance (TEER), TJs' indicator between brain ECs and its analysis is a way of quantifying the functionality of the TJs. It can be regulated with the phosphorylation of OCLNs in vitro and significantly increased by adding ROCK inhibitor (RevitaCell) to the culture medium, which increase cells to survive and adhere (Katt et al., 2018; Raleigh et al., 2011). However, increased levels of VEGF as seen in patients with Multiple Sclerosis or adding VEGF to ECs result in increment of the permeability and decrease of TEER, by lowering the expression of OCLNs and CLDN-5 (Argaw, Gurfein, Zhang, Zameer, & John, 2009; J. J. Su et al., 2006).

As a consequence, distinct brain areas exhibit specialized functions of the BBB. Also, high TEER, CLDNs and OCLN-positive TJs, and polarized nature of the membrane maintained by P-gp efflux may be counted as characteristics of the BBB. To assess them,

the stiffness of ECM proteins coatings and factors in the culture medium that affect TEER, and permeability values may be screened (Katt et al., 2018).

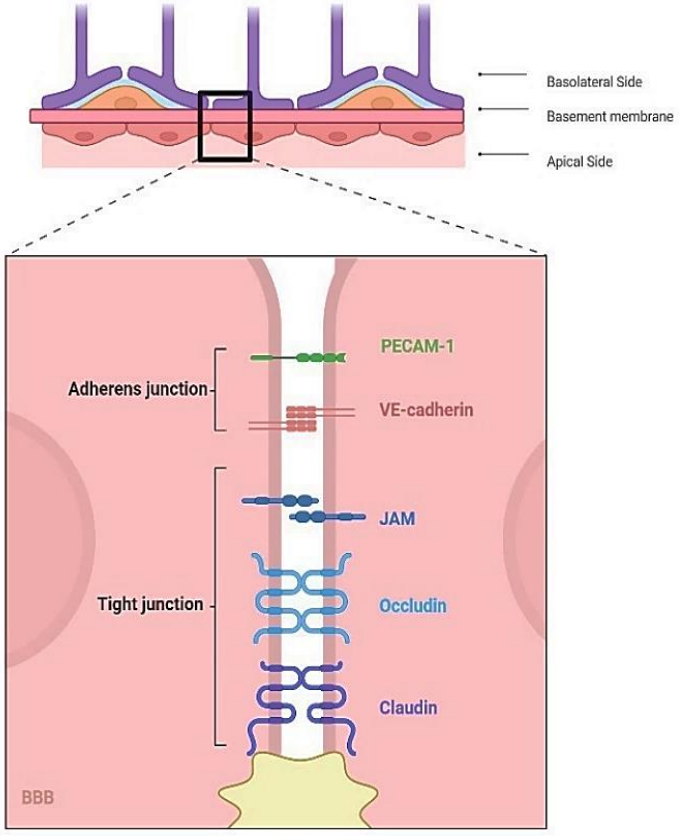

Figure 2.3 Molecular composition of ECs and TJs of the BBB including TJ components junctional adhesion molecules (JAMs), occludin, claudins, and adherent junction components VE-Cadherin, PECAM1 (Created by BioRender)

2.2.4 Transport pathways across the BBB

As mentioned before, the delivery of molecules in and out of the brain is regulated through pumps and by targetting proteins like receptors. In this regard, the BBB has various pathways for the high controllable molecule transport between blood and brain. These pathways mainly are; paracellular aqueous/diffusion pathway, transcellular lipophilic/diffusion pathway, carrier-mediated influx (transporter protein pathway), efflux mechanism, receptor-mediated transcytosis (RMT), and adsorptive transcytosis (AT) (Lalatsa & Butt, 2018) (see Figure 2.4). In paracellular aqueous/diffusion pathway, polar

solute (water-soluble) molecules such as ions may passively transported by utilizing small intercellular pores located in the TJs, which are formed by transmembrane proteins like CLDNs (Y. H. Kim, Kim, D'Argenio, & Crandall, 2021; Wolburg, Wolburg-Buchholz, Liebner, & Engelhardt, 2001). However, the complex inteaction of claudin with occludin and other proteins may block the transportation of these solutes (Lalatsa, Schätchlein, & Uchegbu, 2012). In transcellular lipophilic/diffusion pathway, lipid-soluble and/or amphiphilic solute molecules may diffuse passively through lipid bilayered cell membrane to cross the BBB (Lalatsa & Butt, 2018; Lalatsa et al., 2012). In carrier-mediated influx, numerous essential polar molecules, which may not easily diffuse through the membrane like amino acids, amines, nucleosides, and glucose are transported into the CNS via specialized carries. For instance, aminoacids, nucleosides, low molecular weight drugs, and drug-loaded NPs use large neutral amino acid transporters, and glucose uses the glucose transporter (GLUT1) as their carries (Lalatsa & Butt, 2018). In efflux mechanism, xenobiotics, endogeneous metabolites, or passively penetrating undesirable molecules (e.g. azidothymidine, cyclosporine A, vinca alkaloids) are transported out of the brain ECs via active efflux pumps or carries such as adenosine triphosphate (ATP)-binding cassette transporters (e.g. ATP binding cassette subfamily B member 1, ABCB1) (Löscher & Potschka, 2005; Mahringer & Fricker, 2016). ABCB1 is polyglycoprotein (P-gp), which more likely use high molecular weight lipophilic drugs (e.g. paclitaxel, loperamide, vinblastine, and cyclosporine) as its substrate and therefore prevents their accumulation in the brain (Lalatsa & Butt, 2018). Furthermore, in the brain ECs, endocytosis, intracellular vesicular trafficking, exocytosis are present for transportation, respectively (Pulgar, 2019). The first step involves AT and RMT. AT depends on the charge of the membrane as well as the molecules to be transported across the BBB. The molecules can be positively charged polymers, lipids, polymers, and NPs. They may engage with the membrane and be internalized via AT by forming small surface pits in the membrane, namely caveolae (W. Lu, 2012; Mayor & Pagano, 2007). On the contrary, transportation of various macromolecules such as proteins (e.g. cytokines, insulin, transferrin), peptides (e.g. leptin), viruses (e.g. herpes simplex virus), and particulate formulations (e.g. functionalized NPs, drug and antibody conjugates) occurs through several receptors at the BBB such as transferrin receptor (TFRC), insulin receptor, unlike there is no expression of others such as albumin receptors in the BBB

(Lalatsa & Butt, 2018; Pardridge, Eisenberg, & Cefalu, 1985; Pulgar, 2019). This transportation pathway is called as RMT and based on the specific receptor-ligand interactions on the brain ECs that result in receptor modification and triggering clathrin-coated pits formation. Following intracellular trafficking, the ligand (e.g., transferrin) separates from the receptor, enabling the receptor to be recycled and returned to EC surface in the brain (Brooks, 2009; Nance et al., 2021). In conclusion, the BBB both blocks foreign molecules to pass into brain, and restricts solute molecules to diffuse unregularly out of brain by constraining the pathways.

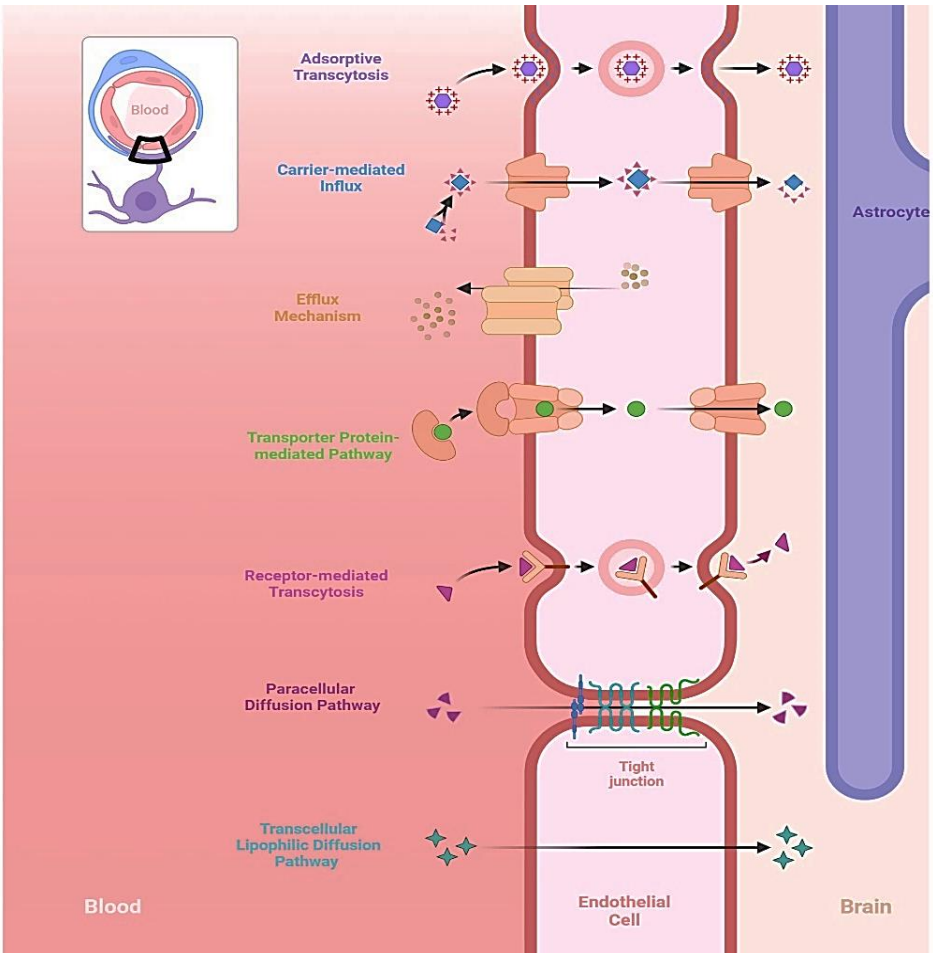

Figure 2.4 Transport routes across the BBB (Created by BioRender)

2.3 In vitro models of the BBB

BBB models have been established in vitro to better mimic in vivo BBB and facilitate studies related to the CNS, including novel drug development and drug delivery to treat a wide range of neurological diseases (He, Yao, Tsirka, & Cao, 2014). Concerning these purposes, in vitro BBB models are categorized as static/transwell (monoculture, co-culture, tri-culture), dynamic, 3D ECM-based, and 3D-microfluidic models (Gomes, Mendes, Martins, & Sarmento, 2016) (see Figure 2.5 and 2.7).

Monoculture BBB models are constructed from monolayers of brain ECs, which are grown in transwell-clear inserts. The well in which the insert is positioned mimics brain side, while insert itself simulates blood side. The exchange of growth factors secreted by the cells as well as small molecules is allowed by membrane of the inserts whereas the cell migration across the two sides is restricted (He et al., 2014; Naik & Cucullo, 2012). These models are the most commonly used, simple, and have only one type of cell, which is brain ECs growth into surface of the inserts, with no physiological stimuli like interaction with different cell types (e.g. astrocytes, pericytes) of the BBB. Thus, they are used in signaling pathways and transporter studies (Gomes et al., 2016; He et al., 2014). Nonetheless, randomly patterned cell adhesion may be observed in ECs formed in the inserts, giving rise to unreliable permeability measurements (Gomes et al., 2016). Moreover, EC dedifferentition may be promoted, fasten the loss of characteristics of the BBB (Naik & Cucullo, 2012). Hence, more complex models BBB models, such as co-culture BBB models, have been created (Abbott, 2013). Co-culture BBB models have been constructed with ECs, growing in interaction with glial cells /astrocytes or pericytes to resemble the BBB phenotype more like in the human body. In these models, brain ECs are seeded inside the inserts, and the incorporation of ECs with astrocytes or pericytes are maintained by growning them either at the well bottom, where the insert located without (w/o) contact, or on the underside of the inserts with direct contact (He et al., 2014). Co-culture with astrocytes may demonstrate high TEER and low permeability to molecules (Dehouck, Méresse, Delorme, Fruchart, & Cecchelli, 1990; Rubin et al., 1991). Similarly, co-culture with pericytes may result in an increase in TEER and influence ECs by means of factor secretion or gap junction interaction, enhancing maturation of endothelium and

barrier functioning (Hayashi et al., 2004; Santaguida et al., 2006). Additionally, co-culture of hCMEC/D3 with human fetal ganglionic eminence-derived neural stem cell line can be an alternative approach to generate an in vitro BBB model owing to the fact that these cell lines yield abundantly homogeneous cell populations (Gomes et al., 2016). Thus, co-culturing enhance formation of TJs, but this improvement is not pronounced as more complex BBB models, like tri-culture models (Hatherell et al., 2011). Tri-culture models are designed to incorporate advanced BBB properties, thereby simulating the neurovascular unit (NVU) structure found in vivo. These models can be formed by brain ECs-pericytes-astrocytes/glial cells by seeding brain ECs inside the inserts, pericytes on the underside of the inserts with direct contact, and astrocytes at the bottom of the well (He et al., 2014). The addition of astrocyes and pericytes to the model have strengthen barrier integrity, contributed to higher TEER and reduced permeability (Nakagawa et al., 2009; Nakagawa et al., 2007). It can be said that tri-culture models appear to be the closest static in vitro model of the in vivo BBB and used for large-scale screenings and pathophysiological studies (He et al., 2014). Nevertheless, static/transwell models are incapable to replicate blood flow-produced-physiological tangential force, essential to preserve BBB structure and function (Naik & Cucullo, 2012; Prabhakarpandian et al., 2013). Furthermore, in the absence of antimitotic signals from flow and laminin, the cell cycle rate tends to accelerate, resulting in the uncontrolled multilayer proliferation of ECs. Therefore, dynamic models have been developed for mimicking blood flow (Gomes et al., 2016; Santaguida et al., 2006). They generate intraluminal flow via pulsatile variable speed pump, which is regulated through viscosity of the medium and capillary-like artificial structural supports, namely hollow fibers to generate shear stress (Naik & Cucullo, 2012). Physiological shear stress induced by blood flow influences the transporters and TJ expressions, in addition to the barrier function (Tarbell, 2010). For example, inclusion of blood flow have been demonstrated to substantially boost the zonula occludens (ZO-1) expression while decreasing the monolayered brain EC permeability (He et al., 2014; Siddharthan, Kim, Liu, & Kim, 2007). In these models, brain ECs are cultivated on the microporous hollow fibers' interior surface in a sealed chamber, and are subjected to continuous fluid flow, whereas other cells (e.g. astrocytes) are seeded in the outer surface of these fibers (Gomes et al., 2016; He et al., 2014). By using dynamic models numerous physiological reactions and functional characteristics

seen at the BBB such as low permability to polar molecules and potassium, expression of BBB-specific proteins related to transportation, high TEER can be replicated (Cucullo et al., 2008). However, they are not preferred for drug permability studies due to time consuming in addition to the need of high cell loading, and technical skills (Naik & Cucullo, 2012). Other than hollow fibers, cells of the BBB can be cultured using 3D supports such as self-polymerizing ECM protein scaffolds (e.g. matrigel) with the advancement of tissue culture technology. This in vitro BBB, namely 3D ECM-based models, mimics ECM environment with close interaction and communication of cells, and biochemical gradient formation required in cell signaling. Nonetheless, they are not as convenient and cheap as static models (Naik & Cucullo, 2012). Moreover, 3D-microfluidic models better represent dynamic models to form BBB in vitro developed to address the limitations of dynamic models (Booth & Kim, 2012; Yeon et al., 2012). They use multilayered microfluidic device including two channels crossing perpendicularly and a thin porous membrane where channels intersect. The membrane permits ECs and astrocytes cultured together and the channels allow both shear stress and dynamic flow (He et al., 2014). They have been used in permeability studies, and monitoring of migration of cells and alterations in function of the BBB (Booth & Kim, 2012; Griep et al., 2013; Prabhakarpandian et al., 2013). In conclusion, choosing the BBB models out of various models in vitro is dependent on research area. Also, the best BBB model in vitro meeting putative BBB properties in vivo has not been established so far and its creation is still challenging (Cardoso, Brites, & Brito, 2010; Gomes et al., 2016).

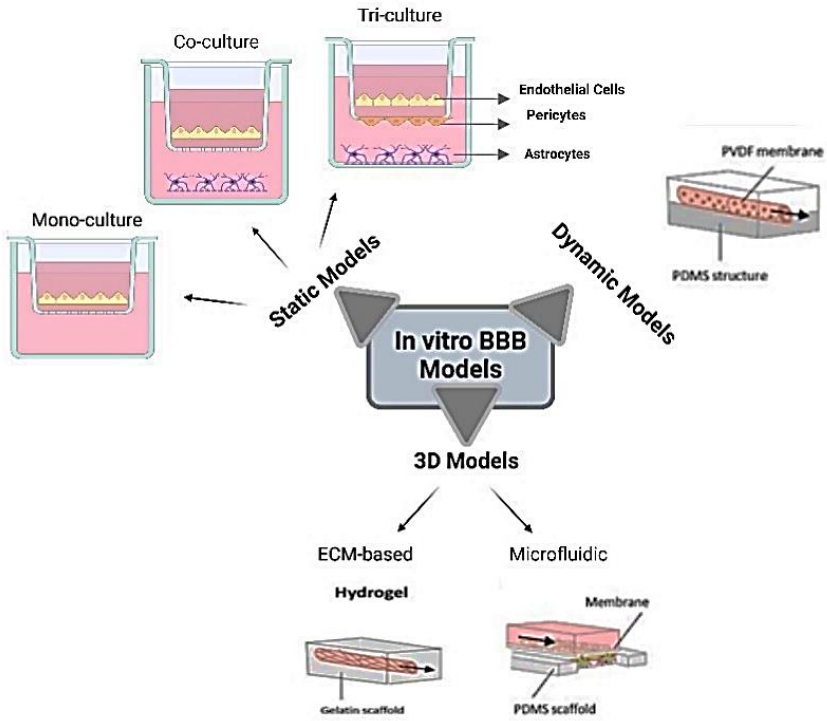

Figure 2.5 Different configurations of BBB Models (Created by BioRender)

Model Type	Advantages	Disadvantage
Epithelial cells overexpressing Transporters model	• Cheap • Easy to standardize	• Differences between epithelial and endothelial cells • Non-physiologically high levels of transporter
Transwell monoculture model - Cerebral endothelial cells on microporous membranes	• Uses brain endothelial cells • Inexpensive	• Effect of other cellular components of the neuro-vascular unit (NVU-astrocytes, pericytes) is neglected • No shear stress
Co-cultures models - Co-culture of cerebral microvascular endothelial cells with astrocytes • Co-culture models using pericytes • Triple cell co-culture models (astrocytes, endothelial and pericytes) • Co-culture of brain endothelial cells with neuronal precursors	• Takes into account the influence of other elements of the neurovascular unit (NVU)	• Relatively expensive and time-consuming • No shear stress
Dynamic in vitro (DIV) model	• Mimics in-vivo situation possibility of co-culture	• Expensive • No possibility to optically monitor the cells • Special skills required to culture cells in these conditions
Microfluidic model	• Mimics in-vivo situation possibility of co-culture	• Not well-established models presently expensive
iPSC (Pluripotent stem cells) based model	• Generate models similar to the human complexity observed in-vivo • Very high TEER values	• Differential procedure depends upon random and permanent insertion of transcription factors, • Complicated procedure with meagre yield • Rigid removal of epigenetic markers related to environmental exposure or age

Table 2 Comparison of different in vitro BBB models for drug transport

Model Type	Other brain cell required	Sheer Stress produced	Time to stable TEER (d)	Appropriate for migration assay	Cost	Technical requisite
Monolayer	No	No	3–4 d	Yes	Low	Low
Co-culture	Yes	No	3–4 d	Yes	Low to moderate	Moderate
Cone-plate apparatus	No	Yes	3–4 d	No	Low	Low to moderate
Dynamic in vitro BBB	Yes	Yes	9 −12 d	No	High	High
Microfluidic based model	Yes	Yes	3–4 d	Yes	High	Moderate
iPSC based model	No	Yes	>1 Week	Yes	High	High

Figure 2.6 Advantages and disadvantages using BBB models in vitro (Prashanth et al., 2021)

2.4 Sources of BBB Models

Over the years, different BBB models in vitro have been established for several BBB-related studies, such as drug targeting, and may be categorized as non-human (animal) and human models. None of the models have the same barrier properties based on structure, function, and behavior in vitro, which give rise to their benefits and drawbacks and make it a challenge to obtain the best model for a particular research.

2.4.1 Non-human models

BBB models in vitro may be derived from animals like rodents (e.g. mouse and rats), porcine, and bovine because of the difficulty in obtaining the brain ECs from humans and their primary culture (Hans C Helms et al., 2016). The first attempts at modeling have started with the brain capillaries' isolation from rats (Joo, 1973). These capillaries have been treated with an enzyme mixture to isolate the primary brain capillary ECs (BCECs) (Bowman et al., 1981). Primary brain ECs isolated from animals retain quite tight BBB in vitro, which makes them useful for studying paracellular transport (Patabendige & Abbott, 2014). However, an issue in rat models that the researchers deal with is increasing the purity of the primary isolation of the rat brain ECs. This is achieved by treating the cells with P-gp substrate, puromycin (Perriere et al., 2005). Rat models can be formed by culturing with astrocytes and/or pericytes together to examine their characterization and study the cell interactions (Fan et al., 2019; Gaillard et al., 2001; Nakagawa et al., 2007). On the other hand, mouse brain ECs as an immortalized cell line (e.g. bEND.5) can be preferred because they may yield large cell numbers, and having stable BBB characteristics independent of the increase in passage number (Hans C Helms et al., 2016). They can be created from a mouse, which is genetically modified via the expression of polyoma middle T antigen (Wagner & Risau, 1994). Mouse models have been co-cultured with astrocytes and displayed a well-characterized BBB with tight barriers and high TEER (Coisne et al., 2005). Rodent brain ECs are widely used in the field as immortalized cell lines (Burek, Salvador, & Förster, 2012), can be targeted with antibodies, and therefore rodent models are very suitable for large cohort studies (T. M. Lu et al., 2021). Their in vitro co-culture with neural cells better mimics the NVU and

demonstrates enhanced TEER (Abbott, Dolman, Drndarski, & Fredriksson, 2012; Coisne et al., 2005). Furthermore, due to the need for larger species to generate enough brain ECs, porcine brain ECs have been firstly isolated from brain capillaries (Mischeck, Meyer, & Galla, 1989). Porcine models have demonstrated very high TEER both in monocultures and co-cultures with the help of hydrocortisone in the culture medium and astrocytes in co-culturing. Therefore, these models exhibit limited permeability to molecules at small sizes (Hoheisel et al., 1998; Patabendige, Skinner, & Abbott, 2013; Patabendige, Skinner, Morgan, & Abbott, 2013; Yan Zhang et al., 2006). Bovine models have been sourced from BCECs since the early beginning (Bowman, Ennis, Rarey, Lorris Betz, & Goldstein, 1983). Similar to porcine models, bovine models may show high TEER values both in mono- and co-cultures, which are greater than 800 Ω x cm^2, but also show lower TEER of 150-300 Ω x cm^2 in the same in vitro model. Many researchers have also found the TEER even lower than 150 w/o the BBB transporter activity (Hakkarainen, Rilla, Suhonen, Ruponen, & Forsberg, 2014; Hans Christian Helms et al., 2014). The wide range of differences in TEER can be a disadvantage for bovine models. Fortunately, their co-cultured models have shown drug-induced changes in TJs, affecting drug permeability and thus being used in drug transport studies (Gaillard & de Boer, 2000). Both porcine and bovine BBB models can be easily established owing to their ability to be isolated in large quantities, which enhance their use in several BBB studies related to transcytosis and permeability (T. M. Lu et al., 2021).

In conclusion, in vitro animal models have sustained insight into the BBB, although there is a lack of precise reproducibility caused by varied BBB phenotypes and TEER values, as well as major differences in the BBB cellular phenotype relative to the human BBB (Hans C Helms et al., 2016; T. M. Lu et al., 2021).

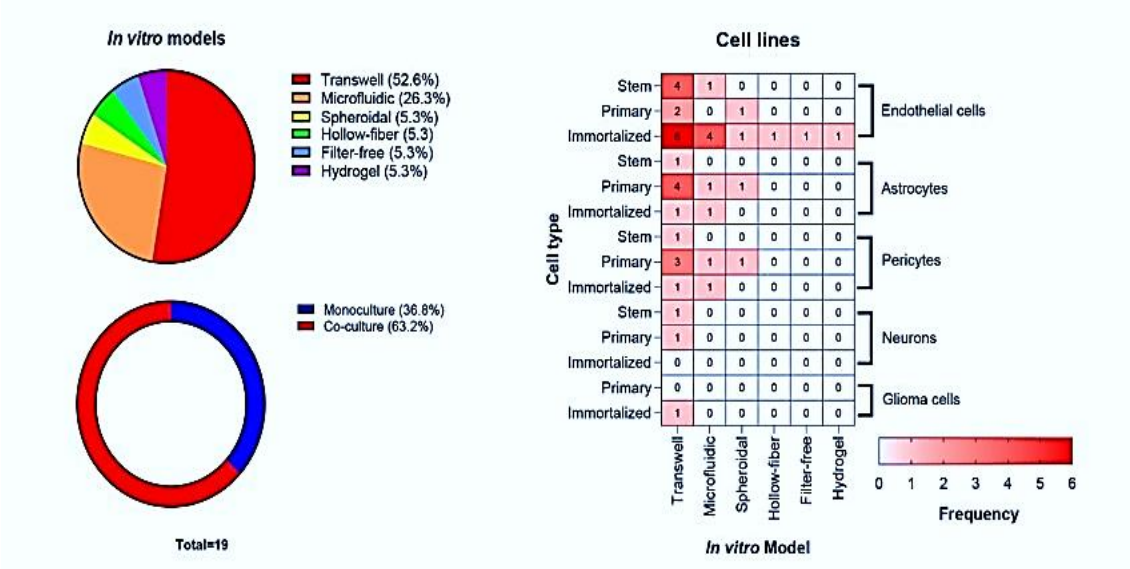

Figure 2.7 Charts of employment of models and culture types in studies and heat-map of usage of different cell types forming BBB models with frequencies (Prashanth et al., 2021)

2.4.2 Human models

The restrictive barrier capacity of non-human models as well as the difference of expression of transporters specific to brain ECs between different species have emerged a need for enhanced BBB models in vitro (Syvänen et al., 2009; Urich, Lazic, Molnos, Wells, & Freskgård, 2012). Therefore, human BBB models are preferred over animal BBB models because of the precise reproducibility with certain human BBB models (T. M. Lu et al., 2021). However, there are concerns over the use of commercial primary BMECs as BBB models due to their lack of detailed experimental data such as cell isolation and sourcing. In addition, the exclusive endothelial identity and barrier properties of these BMECs may not be well maintained in vitro over extended periods (Hans C Helms et al., 2016; T. M. Lu et al., 2021). These limitations have been overcomed by establishing immortalized human brain EC lines (Rahman & Meyding-Lamadé, 2016; BB Weksler et al., 2005).

2.4.2.1 The human immortalized endothelial cell line: hCMEC/D3

In the literature, there are many immortalized human brain EC lines used for permeability studies, such as BB19, HCEC, and HBMEC/3 cells, demonstrating various BBB phenotypes with advantages and limitations (Babette Weksler, Romero, & Couraud, 2013). Out of them, the human cerebral microvascular EC line (hCMEC/D3) is a well characterized, reproducible, and easy-to-use human in vitro BBB model, having stable growth and enhanced proliferation even in high passage numbers (BB Weksler et al., 2005). It expresses proteins important for TJ integrity, seen in BBB in vivo, like zonula occludens-1 (ZO-1), PECAM1, VE-cadherin, OCLN, CLDNs (Hans C Helms et al., 2016; Ohtsuki et al., 2013). Expression of these proteins, particularly CLDNs and OCLN, is best detected when the cells approach confluency. hCMEC/D3 also expresses proteins of transport pathways such as ABC transporters (e.g.ABCB1), essential for studying drug delivery through the BBB (Babette Weksler et al., 2013). For example, in a study, transporter expression levels and their functional activities in hCMEC/D3 have been measured. The transport rates of a number of molecules with various molecular weights and physicochemical characteristics have been examined to assess the barrier tightness and distinguish low and high transport rates (Poller et al., 2008). The clearance mechanism of amyloid beta from the CNS has also been studied in this cell line to avoid neurotoxicity and vasculotoxicity consequences, including the emergence of neurological diseases such as Alzheimer's disease (Tai, Loughlin, Male, & Romero, 2009). In conclusion, hCMEC/D3 is a unique BBB model to examine the human brain endothelium.

hCMEC/D3 arranges itself into extended cell monolayers on collagen type I (CoL1) with surface inhibition (Hans C Helms et al., 2016; BB Weksler et al., 2005). hCMEC/D3 monolayers show 5-fold higher concentrations of TJs on transwell-clear inserts than well-plates. Furthermore, the TEER of these monolayers ranges from 30 to 50 Ω x cm^2 (Babette Weksler et al., 2013). Similar to non-human models, this value may be increased with co-culturing hCMEC/D3 with astrocytes (Hatherell et al., 2011) as well as the addition of hydrocortisone because corticosteroids modulate the expression of proteins of TJs (Förster et al., 2008). Nevertheless, ECs can be dysfunctional, and paracellular transport of dextrans is increased through the induction of cytokines and/or chemokines

(Lopez-Ramirez et al., 2012). Recently, new preparations of pure brain ECs with higher expression of TJs and transporters from the isolation of stem cells to construct a highly efficient in vitro human BBB model than EC lines have been developed.

2.4.2.2 Human iPSCs (hiPSCs)-derived brain microvascular endothelial cells (BMECs) for BBB model

Recent progress in SC technologies allows BMECs to generate from diverse SC sources with expandable and renewable capabilities, such as circulating endothelial progenitors (Ponio et al., 2014), hematopoietic stem cells (Cecchelli et al., 2014), and human iPSCs (hiPSCs) (Lippmann et al., 2012).

As mentioned before, obtaining primary brain ECs from healthy individuals and/or patients is highly difficult, and immortalized BMECs may have lower expression of TJ specific genes such as OCLN than in vivo as well as non-sustainable functional barrier phenotypes (T. M. Lu et al., 2021). So, brain-related studies have been an issue until the use of hiPSCs has been included. hiPSCs-derived BMECs are widely used by researchers to study the development and maintenance of the BBB as well as the effects of neurological diseases like Huntington's disease (Lim et al., 2017), CNS-related antimicrobial infections (Alimonti et al., 2018; B. J. Kim et al., 2017) by disease modeling (Canfield et al., 2017; Delsing et al., 2020; Lippmann, Al-Ahmad, Azarin, Palecek, & Shusta, 2014; Workman & Svendsen, 2020). They demonstrate more restricted barrier properties correlating with the in vivo BBB than many primary ECs or immortalized EC lines from both animal and human origins. They may provide information about transport pathways for drug delivery and earlier drug discovery (Ribecco-Lutkiewicz et al., 2018; Roux et al., 2019) and their 2D and 3D models provide the opportunity for studies related to examining both static and dynamic changes in the BBB. This is why models created from these cells have facilitated the broader application of standardized BBB in vitro (Eigenmann et al., 2013). However, using high potential of iPSCs requires reliable and robust culture and differentiation protocols (Delsing et al., 2020). Different protocols of hiPSCs culture and their differentiation into BMECs have been released during the years since 2012 (Delsing et al., 2018; Hollmann et al., 2017; Lippmann et al., 2014; Lippmann

et al., 2012; Neal et al., 2019; Park et al., 2019; Pong, Lizano, & Karmacharya, 2020; Praça et al., 2019; T. Qian et al., 2017; Stebbins et al., 2016; Wilson, Canfield, Hjortness, Palecek, & Shusta, 2015). In the protocols, these cells are basically derived from hiPSCs followed by the purification of endothelial progenitor cells selectively and further be BMECs under the differentiation culture conditions (T. M. Lu et al., 2021). Additionally, long-term cryopreservation of BMECs is crucial for enabling the production and storage of these cells at large scales w/o deforming the expression of BBB markers, and the high TEER similar to non-frozen BBB. It also decreases the time to generate purified BMECs (Wilson, Faubion, Hjortness, Palecek, & Shusta, 2016). All in all, hiPSCs-derived BMECs have a significant impact on enhancing knowledge about both human BBB development and disease.

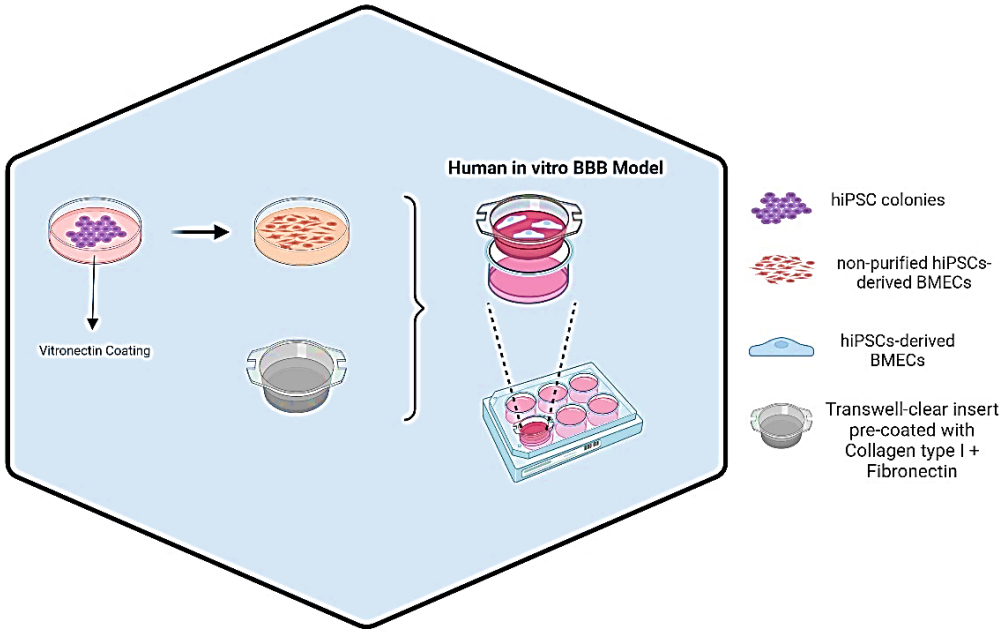

Figure 2.8 hiPSCs-derived BBB model construction in vitro (Created by BioRender)

2.4.2.2.1 Characterization of hiPSC-derived BMECs phenotype

After obtaining hiPSC-derived BMECs, several characterization assays can be conducted for these BMECs to be validated as a BBB model. For example, expression of BMECs-related marker genes and proteins like TJs (e.g. OCLN) preventing paracellular diffusion, and efflux transporters (e.g. P-gp) preventing transcellular flux can be observed via real-

time quantitative reverse transcription polymerase chain reaction (RT-qPCR), flow cytometry, and visually localized via immunocytochemistry assay (Czupalla, Liebner, & Devraj, 2014; Delsing et al., 2020). Other than these, the integrity of BMECs is achieved by a electrophysiological measurement that gives the overall BMEC monolayer resistance such as TEER, a hallmark of brain ECs. On the other hand, impedance spectroscopy monitors BMEC monolayer to better give informations about the BBB integrity (Benson, Cramer, & Galla, 2013). Additionally, administration and delivery of therapeutics through the BBB, like drugs and NMs, is hindered by natural functional activity of the BBB, so they either fail to enter the brain or have limited bioavailability (Czupalla et al., 2014; Pardridge, 2005). Therefore, permeability assays can be performed to characterize the transport of these therapeutics as well as the transport of usually tested molecules (e.g. FITC-dextran, sodium fluorescein, lucifer yellow) across the BBB by finding the BMEC monolayer permeability coefficients (Canfield et al., 2017; Katt et al., 2018; Natarajan, Northrop, & Yamamoto, 2017; Sun et al., 2022). In all these characterization assays, a transwell setup including transwell-clear inserts with a porous membrane is the preferred growing surface for more functional assays. Because the behavior of BMECs varies in accordance with their growing surface, whenever possible, all experiments should be conducted on the identical growing surface (Czupalla et al., 2014). Thus, determining the methods are important to obtain reliable BBB characterization.

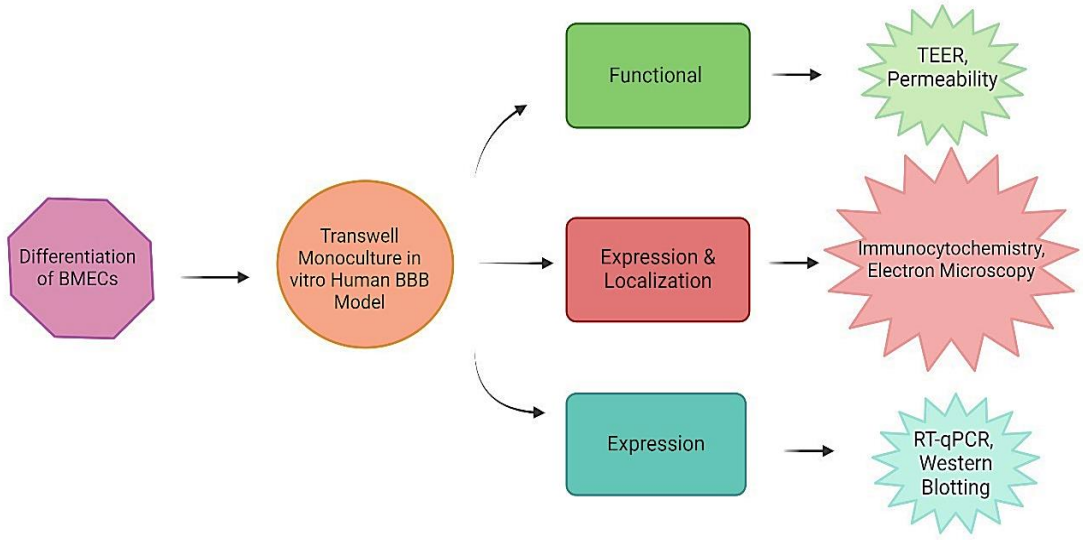

Figure 2.9 Different assays performed for BMEC characterization (Created by BioRender)

2.5 BBB in presence of brain tumors: Blood-brain-tumor barrier (BBTB)

BBB integrity may be altered and disrupted in various neurological diseases, such as the most common primary brain tumor, glioblastoma multiforme (GBM). The BBB is renamed as blood-brain-tumor barrier (BBTB) (Van Tellingen et al., 2015). The disruption depends on the stage and type of the disease and therefore impacts drug delivery and therapeutic efficacy (Mo et al., 2021). Characteristics of the BBTB are shown as increased caveolae and fenestrations in GBM vessels. NVU is altered by pericyte' detachment, reactive astrocytes' number increase, the schrinkage of end-feet of astrocytes, ECM thickening and change by the loss of ECM molecules such as agrin and tenascin in the BL (Rascher et al., 2002). Fenestrated vessels form highly permeable BBTB and cause molecules to diffuse into brain (Mo et al., 2021). Also, in BBTB, the reduced expression of TJs and platelet-derived growth factor receptor beta (PDGFR-β) are observed as a consequence of increased vascular endothelial growth factor (VEGF) secretion and metalloproteinases like MMP2-MMP9 from the tumors (Arvanitis, Ferraro, & Jain, 2020). Some genes that are normally expressed in ECs of the CNS, such as a type of transporter called solute carrier family 2 member 1 (SLC2A1), are downregulated by activating WNT/β-catenin pathway, signal transduction pathway regulating tissue regeneration, and homeostasis (Jung & Park, 2020; Phoenix et al., 2016).

Because BBTB has a leaky vasculature, some may think that theureputic efficacy and drug delivery are no longer limited in the treatment of GBM. However, the disruption of BBB integrity is heterogeneous, meaning that the undamaged parts of BBTB prevent the bypassing of molecules to the diseased brain side and thus protect some parts of malignant brain tumors from therapeutic drugs and/or NPs (Griffith et al., 2020; Mo et al., 2021). Therefore, methods must be provided, like the blockage of drug metabolizing enzymes, and transport systems must be exploited (receptor-mediated transcytosis) and/or blocked (efflux mechanism) to overcome the BBTB (Deligne et al., 2020; Van Tellingen et al., 2015).

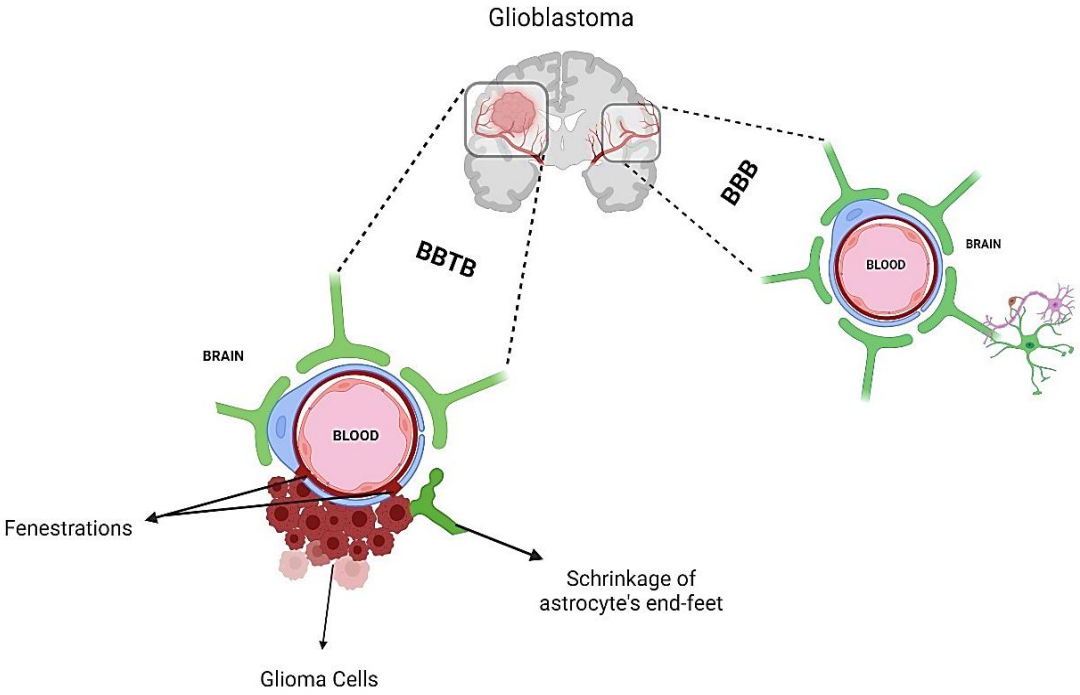

Figure 2.10 BBB in tumor presence and absence (Created by BioRender)

2.6 Neurological disease studies using BBB models

As mentioned earlier, the barrier structure and function are altered in presence of nearly all neurological diseases compared to healthy controls (Obermeier, Daneman, & Ransohoff, 2013; Sweeney, Sagare, & Zlokovic, 2018). Therefore, it is extremely important to model the BBTB as well as diseases in vitro for better understanding of the barrier breakdown, dysfunction, pathological proteins in various type of fields including drug permeability and delivery, neurological diseases and cancer treatment, infectious diseases, NVU cell-to-cell interactions (Workman & Svendsen, 2020). In this regard, iPSCs-based BBB models with disease mechanisms are provided (Wu, Sonninen, Peltonen, Koistinaho, & Lehtonen, 2021). They have been recently preferred and be used as disease models for preclinical and clinical researchs (Chang et al., 2020; de Rus Jacquet, Denis, Cicchetti, & Alpaugh, 2021; Pasteuning-Vuhman, de Jongh, Timmers, & Pasterkamp, 2021). For example, Katt et al. have used with different iPSC lines to conduct a comprehensive study correlating the defects of brain ECs causing BBB to mutate and dysfunction in various neurological diseases (Katt et al., 2019). In AD, risks have been declared by researchers (Rieker et al., 2019). Moreover, the phenotype and potential

mechanisms of iPSCs-derived brain ECs, harboring the mutation of presenilin-1, have been described to infer how to clear toxic amyloid beta peptides and deliver drugs (Oikari et al., 2020; Raut, Patel, & Al-Ahmad, 2020). Besides, 3D ECM-based disease model on matrigel with culturing of hiPSCs-derived brain ECs, astrocytes, and pericytes have been constructed to reveal cerebral amyloid angiopathy pathology in AD and to highlight the targets of therapy like apolipoprotein-4 gene (Blanchard et al., 2020).

Other than iPSCs-based BBB models, immortalized cell lines-based BBB models have been used. As an example, TY08 cell line co-cultured with human pericytes have developed a BBB model to study the effects of diabetic encephalopathy, resulting in dimentia, in the BBB for its prevention and treatment (Shimizu et al., 2013). Bamji-Mirza et al. have constructed a BBB model using hCMEC/D3 to demonstrate the protection of BBB dysregulation, caused by amyloid beta inducement in AD (Bamji-Mirza et al., 2014). Another study has used the same cell line, that releases metalloproteinases such as TIMP-1 and TIMP-2 and it has been exposed to simvastatin, favorably effecting to treat acute stroke (Reuter et al., 2015). Furthermore, a BBTB model by co-culturing hCMEC/D3 and human glioblastoma cell line (U87) has been constructed to characterize the barrier properties in brain tumors to investigate novel drugs or systems to conduct effective tumor treatment (Mendes et al., 2015). Advanced BBB models have been also developed. A 3D BBTB model has been engineered to study drug response and delivery in the treatment of GBM in vitro (Seo, Nah, Lee, Choi, & Kim, 2022). More recently, a BBTB model, using both primary brain ECs and U87, have been developed to study spatial organization of brain tumors and the resistance of drug, temozolomide (Lam et al., 2023). Therefore, it can be concluded that disease models can help to prevent the development of neurological diseases and offer insights on how to cure them.

2.7 Use of nanomaterials (NMs) in the biomedical field

Nanomedicine are playing a major role in therapeutic and diagnostic studies of various diseases in the biomedical field. Due to the difficulty in targeting brain areas, both periclinal and clinical studies have been devoted to neurological disease therapy including AD and especially GBM by using nanoparticles (NPs) and 2D NMs.

In this section, various types of NMs and nanodelivery systems crossing the normal and diseased BBB will be mentioned.

2.7.1 Nanomaterials and delivery systems overcoming the BBB and BBTB

Due to BBB existence and the lack of neurotherapeutics like nanodelivery systems and/or NMs crossing BBB and BBTB, neurological or CNS-related diseases therapy remains an important issue. The restricted delivery of these compounds to the brain by the barriers is significant factor contributing to challenges in disease treatment. Solution to this issue will necessitate collaborations among government, industry and academics (Neuwelt et al., 2008; Reddy et al., 2021).

In addition to the conventional neurotherapeutics' inability in crossing barriers, they may fail pre-clinically and clinically because of their severe side effects, their poor distribution, and unfavorable prognosis of the disease (Z. Liu et al., 2022). Size effects and distribution of these compounds can be affected by their characteristics (e.g. chemical composition, charge, shape, size, hydrophobicity). These factors also influence their clearance and reactions to the immune system (Nance et al., 2021). Fortunately, as shown in Table 2.1, nanotechnology has promising opportunities regarding to the delivery of drugs such as doxorubicin, paclitaxel, and temozolomide across the BBB via various nanodelivery systems, which are polymers (e.g. polymeric NPs and micelles), lipids (e.g. liposomes, and solid lipid NPs), dendrimers, amphiphilic cyclodextrins, inorganic NMs (e.g. gold, silver, and iron oxide NPs), carbon nanotubes, carbon dots (CDs), and quantum dots (Calabrese et al., 2021; Chakraborty et al., 2022; Mc Carthy, Malhotra, O'Mahony, Cryan, & O'Driscoll, 2015). Nanodelivery systems can include ligands (e.g. peptides, and antibodies) on their surface for an enhanced targeting, mediated by receptors and thus are useful to maintain sustained releasement of the drugs to the infected area and/or tumor site (Madane & Mahajan, 2016; Reddy et al., 2021). Other than receptor-mediated delivery, systems conjugated or encapsulated with the drugs can be accumulated in brain tumor tissues via enhanced permeability and retention (EPR) effect.

Table 2.1 Nanomaterials/ Nanodelivery systems used in the therapy of brain tumors

Clinical / Preclinical Study	Type of Tumor	Nanomaterial / Nanodelivery System	References
Clinical	GBM	Liposome + Temozolomide (TMZ) + SGT-53	NCT02340156
		Liposome + Rhenium 186	NCT01906385
	Refractory Non-brainstem Malignant Glioma	Liposome + Doxorubicin (DOX)	NCT02861222
	Refractory Solid Tumors	Liposome + HCL+ DOX	NCT00019630
	GBM, Relapsed and refractory primary CNS lymphoma	Liposome + PEG + DOX	NCT01848652
	Brain Metastases	Liposome + Irinotecan (CPT-11)	NCT03328884
		Gadolinium-based NP (AGuIX)	NCT03818386
	Diffuse Intrinsic Pontine Glioma	Convection-enhanced delivery of Liposome + Irinotecan	NCT0202264, NCT03086616
	GBM	AGuIX + TMZ	NCT04881032
		Gold NPs + NU-0129	NCT03020017
		Albumin-based NPs + Rapamycin	NCT03463265
	Brainstem Glioma	Platinum Acetylacetonate + Titania (NPt-Ca)	NCT03250520
Preclinical	GBM	Liposome + DOX + CB5005	(Yanyu Zhang et al., 2018)
		Liposome + Paclitaxel (PTX) + Rg3	(Zhu et al., 2021)
		Liposome + Super paramagnetic iron oxide NPs (SPIONs) + DOX + P1NS + TNC	(Zhu et al., 2021)
		Liposome + Rapamycin + MTI-31 + VAP	(X. Wang et al., 2019)

Table 2.1 Nanomaterials/Nanodelivery systems used in the therapy of brain tumors (continued)

Clinical / Preclinical Study	Type of Tumor	Nanomaterial / Nanodelivery System	References
Preclinical	GBM	Liposome + DOX + CB5005	(Yanyu Zhang et al., 2018)
		siPLK Micelle + TMZ + Angiopep-2 (Ang2)	(Shi et al., 2020)
		Micelle + Platinum + cyclic RGD (cRDG)	(Miura et al., 2013)
		Dendrimer (PAMAM) + DOX + Ang2	(Han et al., 2018)
		PAMAM + Arsenic trioxide + cRGD	(Y. Lu et al., 2018)
		PAMAM + TRAIL + Transferrin (Tf)	(Gao, Li, Jiang, Hong, & Hao, 2015)
		PAMAM + Tamoxifen + DOX + PEG + Tf	(Y. Li et al., 2012)
		Cyclodextrin + butylidenephthalide	(Lin et al., 2020)
		Magnetic Double Emulsion Nanocapsules + Lactoferrin	(Fang et al., 2014)
		Spherical Nucleic Acid NPs (Gold NPs)	(Jensen et al., 2013)
		SPION + HAPtS	(Sallem et al., 2019)
		Silver (Ag) NPs + Verapamil + AS1411	(Zhao et al., 2021)
		Iron oxide NPs + Cisplatin + Folate Acid	(Yulin Zhang et al., 2020)
		Polybutylcyanoacrylate (PBCA) NPs + Cisplatin	(Ebrahimi Shahmabadi et al., 2014)
		PLGA NPs + Methotrexate / PTX + Poloxamer 188	(Madani et al., 2024)
		BSA NPs + DOX + PEG + Lactoferrin	(Z. Su et al., 2014)
		Ph-dye NPs + ApoE	(J. Wang et al., 2022)
		Polylevodopamine NPs + DOX + Indocyanine green	(Dube, Kumar, Bishnoi, & Panda, 2021)
		Ag-In-S ternary quantum dots + Cysteine + KLA	(Mansur et al., 2022)

Table 2.1 Nanomaterials/Nanodelivery systems used in the therapy of brain tumors (continued)

Clinical / Preclinical Study	Type of Tumor	Nanomaterial / Nanodelivery System	References
Preclinical	GBM	Carbon Nitride Dots	(Liyanage et al., 2020)
		Graphene Quantum Dots	(Patel & Shah, 2023; Perini et al., 2020)
		Carbon Dots (CDs)	(Deng et al., 2023; M. Qian et al., 2018; L. Qiao, Sun, Zheng, Zheng, & Xie, 2018; Zhou et al., 2019)
		CDs + DOX + Tf	(S. Li et al., 2016)
		Iron-doped Orange Emissive CDs	(S. Liu et al., 2022)
		Boron CDs + Exosome	(J. Li et al., 2021)
	Small Orthotopic Glioma	Sugar CDs	(Y. Wang et al., 2021)
	GBM and Diffuse Intrinsic Pontine Glioma (DIPG)	CDs + Pep1 + Epirubicin + TMZ	(Cilingir et al., 2022)

As in compounds of nanodelivery systems, various formulations have been revolutionized to treat challenging brain tumors. For instance, Boltman et al., have used cell-penetrating peptide-based NPs, namely chlorotoxin (CTX) NPs, to treat GBM and neuroblastoma by considering the ability of CTX to bind to tumors and kill tumors by hyperthermia via these NPs (Boltman, Meyer, & Ekpo, 2023). CTX can also combined with other molecules like cancer drugs, DOX, and polymers like chitosan to increase the efficiency of cytotoxicity in brain tumors. In studies, CTX has been conjugated to a fluorescent molecular probe, cyanine 5.5 (Cy5.5) to be used as a tumor paint, and to PEGylated-chitosan branched copolymer NPs. As a result, this formulation has demonstrated capability to pass BBB, targeted tumors in brain, caused prolonged

retention in tumors and cytotoxicity (Jeong et al., 2010; Veiseh et al., 2009). Furthermore, CTX conjugated with DOX-loaded liposomes have been studied against U87 in vitro and significantly inhibited tumor growth in vivo (Xiang et al., 2011). Also, gold nanorods entrapped in PLGA NPs with CTX and Cy5.5 have exhibited binding ability to U87 and have led to damage of tumor cells in vitro (Locatelli et al., 2014). Lee and co-workers have perfused fluorescent polystyrene (PS) NPs, and novel rhodamine-labeled polyurethane (PU) NPs to the in vitro 3D BBB microvasculature model. They have observed same permeability of PU NPs and PS NPs. They have also functionalized these NPs with holo-transferin (Tf) and found that the Tf has increased NPs' permeability the BBB and so easier delivery across the BBB (Lee et al., 2020). Qiao et al. have developed a lactoferrin (Lf)-conjugated and PEG-coated nanodelivery probe with iron oxide (Fe_3O_4) NPs for facilitated passage of NPs from the BBB by using RMT via Lf receptors present on the BBB (R. Qiao et al., 2012). Moreover, due to the studies regarding superparamagnetic iron oxide NPs (SPIONs) causing cytotoxicity on monolayers of BMECs (See Table 2.1), in a study by Theumer et al., BBB model suitability in both 3D and 2D with BMECs and spheroids, have been demonstrated by investigating the interactions of SPIONs interactions with these models (Theumer et al., 2015).

As a concluence, the BBB-related preclinical studies with existing and novel NMs and/or nanodelivery systems are still ongoing, and their accelerated development specialized for GBM therapy to the clinic highlights the therapeutic potential of nanomedicine and improves the therapeutic outcomes of patients with brain tumors.

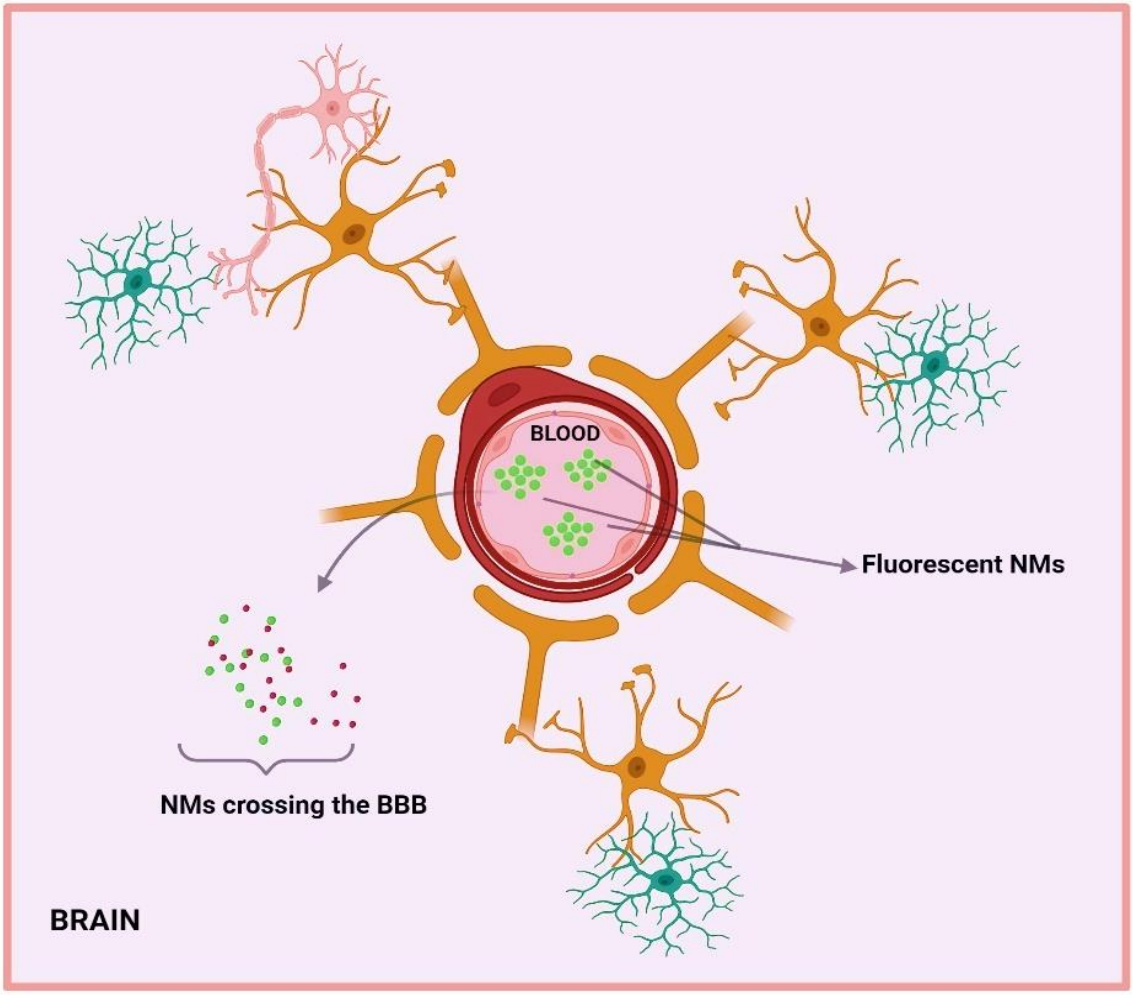

Figure 2.11 Nanomaterials by-passing the BBB with NVU to enter CNS (Created by BioRender)

The thesis's aim was raised from the issue that there is no perfect human in vitro BBB model for personalized modeling. hiPSCs transduced from the blood of one healthy human can offer a way for this type of modeling. Also, the easy passage of neurotherapeutics across the BBB via transport pathways as well as their detection inside brain tumors needed for the treatment of GBM. In this thesis, the BBB was modeled by using brain microvascular ECs (BMECs) derived from hiPSCs and the transport of fluorescent NMs, namely titanium carbide/oxide ($Ti_3C_2T_x$) MXene quantum dots (MQDs), across both BBB and BBTB models and their uptake by brain tumors in BBTB model, used hiPSCs-derived BMECs and U87 were investigated.

3. MATERIAL AND METHODS

3.1 Materials

Table 3.1 Materials used in the thesis

Materials & Reagents	**Cell Lines (hCMEC/D3, U87) Culture**	-EndoGRO™ MV Complete Media Kit (Cat. No. SCME004, Merck, Millipore) -Recombinant Human FGF-basic (FGF2) (Lot. No. 1563542C, Invitrogen Gibco) -Collagen type I, Rat tail (Lot. No. SLBW1777, Sigma) -DPBS (1X, Cat. No. 14190094, Gibco) -Trypsin-EDTA Solution with Phenol Red (1X, 0.25 %, Cat. No. 25200056, Gibco) -Trypsin-EDTA (1X, 0.05 %, Cat. No. A1413201, BI) -DMSO (5X, D2650, Sigma) -FBS, heat inactivated (Cat. No. 10500064, Gibco) -Penstrep Solution (Penicillin-Streptomycin) (Cat. No. 15140122, Gibco) -MEM (1X, Lot. No. 2411746, 31095-029, Gibco)

Table 3.1 Materials used in the thesis (continued)

Materials & Reagents	**hiPSCs Culture**	-rhVTN-N (A31804, Gibco) -E8 (A15169-01, Gibco) -E8 Supplement (Lot. No. 2313787, A15171-01, Gibco) -RevitaCell™ Supplement (A26445-01, Gibco) -EDTA Buffer (0.5 mM, Cat. No. 15575020, Thermo) -PSC Cryomedium (A26444-01)
Materials & Reagents	**BMECs Culture (Induction, Expansion & Purification)**	-DMEMF12 (31330-038, Gibco) -KnockOut Serum Replacement for ESCs/iPSCs (KOSR, Lot. No. 2517495, 10828-010, Gibco) -MEM NEAA (100X, 1954599, Gibco) -Glutamax-1 (100X, 35050-061, Gibco) -2-Mercaptoethanol (50mM, Lot No.2099616, 31350-010, Gibco) -RA (Lot No. SLBB5473V, R2625 100 mg, Powder, Sigma) -DMSO Molecular Biology Grade (Serva, 220551) -RevitaCell™ Supplement (A26445-01, Gibco)

Table 3.1 Materials used in the thesis (continued)

Materials & Reagents	**BMECs Culture (Induction, Expansion & Purification**	-hESFM (11111-044, Gibco) -Human PDS (P2918, Sigma) -Collagen type I, Rat Tail (4.1 mg/mL, Lot. No. 3951247, 08-115, Merck, Millipore) -Collagen type IV from human cell culture (0.3 mg/mL, C6745) -Fibronectin (Bovine Plasma, 1mg/mL, 341631, Millipore) -StemPro Accutase Cell Dissociation reagent (A11105-01, Gibco)
Materials & Reagents	**Assays (ICC, Permeability, cDNA, RNA Isolation, RT-qPCR, TEER, Flow Cytometry, LDH, Mycoplasma)**	-MeOH-BioReagent (Lot. No. SHBF0179V, 494437, Sigma) -BSA (Cat. No. ALB001.100, BioShop) -TritonX_100 (TRX506-100, Bioshop) -Mounting Medium with DAPI solution (ab104139, Abcam) -FITC-Dextran (FD4-250 MG, Lot. No. BCBZ1714, Sigma) -Technic Ethanol (%96, EYA-01, Emir) -iScript™ cDNA Synthesis Kit (Cat. No. 170-8891, BIO-RAD)

Table 3.1 Materials used in the thesis (continued)

Materials & Reagents	**Assays (ICC, Permeability, cDNA, RNA Isolation, RT-qPCR, TEER, Flow Cytometry, LDH, Mycoplasma)**	-Ultra pure water / NFW (Lot. No. 1719421, 01-8661A, BI) -Macherey-nagel NucleoSpinRNA Mini Kit (Cat. No.740955.50) -β-Mercaptoethanol (62689-25ML-F, Sigma) -Sso Advanced™ Universal SYBR® Green Supermix (Cat. No. 172-5271. BIO-RAD) -Microseal 'B' Seals (Cat. No. MSB1001, BIO-RAD) -TC-Inserts (24 Well, PET 0,4 µm, TP, Lot. No. 21410116, 83.3932.041, Sarstedt) -Black Polystrene 96 well-plate (Lot No. 2631022, Corning) -Titanium Carbide/Oxide ($Ti_3C_2T_x$) MXene Quantum Dots (University of Manitoba, Winnipeg, Canada) -CyQUANT™ LDH Cytotoxicity Assay (Cat. No. C20301, Thermo) -EZ-PCR Mycoplasma Detection Kit (Cat. No.BI20-700-20, BI) -EZ Load 1 kb Molecular Ruler (80 µg/mL, 1708355, BIO-RAD) -SafeView™ Classic (Cat No. G108, abm)

Table 3.1 Materials used in the thesis (continued)

Devices & Equipments	-Fluorescence Microscope (Zeiss) -Fluorescent Plate Reader (Mithras^2 LB 943, Berthold Technologies) -NanoDrop (BioSpec) -BIORAD Thermal Cycler (CFX96) -Volt-Ohmmeter (MERS00002, Millicell® ERS-2, Millipore) -STX2 Electrodes (World Precision Instruments) -Ultrasonic Bath Sonicator (Elmasonic S80H, Elma-Hans GmbH) -Flow Cytometer (BD Accuri C6 Plus, BD Biosciences)

3.2 Methods

In this thesis, NMs, namely $Ti_3C_2T_x$ MQDs was kindly provided by Prof. Sanjiv Dhingra, faculty member in the Physiology and Pathophysiology Department at the Rady Faculty of Health Sciences at Manitoba University, Winnipeg, Canada. $Ti_3C_2T_x$ MQDs have been synthesized via hydrothermal method (in distilled water), are zero dimensional, and have sizes of 4.58 nm in diameter each (Rafieerad, Yan, Amiri, & Dhingra, 2020). Their surface area is abundant with highly active functional groups. They may exhibit intrinsic anti-inflammatory effects for regenerative medicine to treat cardiac allograft vasculopathy and stem cell therapy as well as infectious diseases caused by viruses (Rafieerad et al., 2019; Yan et al., 2023; Yilmazer et al., 2023). Moreover, they are considered as fluorescent NMs due to their excellent autofluorescence abilities at various excitation/emission wavelengths, especially in 586 nm/647 nm, which could be easily trackable by emitting

red light (Rafieerad et al., 2020). Regarding these red-emitting fluorescence and immunomodulatory properties, they have been tracked inside the breast tumor and how they may change the tumor microenvironment has been studied using spatial omics techniques (Ceylan et al., 2024).

The cell lines were obtained commercially and hiPSCs were obtained from human peripheral blood mononuclear cells (PBMCs) programmed via Sendai-virus (SeV) vector encoding Yamanaka Factors (Sox2, Oct3/4, c-Myc, Klf4) and characterized under TUBITAK ARDEB 1004 Center of Excellence Support Program. Also, 4 kDa FITC-dextran were kindly provided by Prof. İbrahim Çağatay Karaaslan, faculty member in Molecular Biology and Deputy Director in Sciences Institute at Hacettepe University.

As for experiments of the thesis, most of them were carried out in Cell and Tissue Culture Research LAB, and Nanomedicine LAB at Ankara University, Biomedical Engineering Department. Fluorescence Detection of $Ti_3C_2T_x$ MQDs, 4 kDa FITC-dextran, and antibody stainings were carried out in Ankara University, Stem Cell Institute. In addition, TEER experiment and its measurement by Volt-Ohmmeter were performed in Cell Culture LAB at Hacettepe University, Molecular Biology Department.

3.2.1 Culture of the cell lines

Cell growth in a LAB is known as cell culture. In this thesis, 2 types of cell lines were used; which are U87 obtained from ATCC, and hCMEC/D3 obtained from Sigma-Aldrich. Additionally, a human iPSCs (hiPSC) obtained by transducing PBMCs, and BMECs differentiated from the hiPSCs were used. hCMEC/D3 was used as human monoculture BBB model in vitro and this model was used as control group for the human BBB modelled by using BMECs differentiated from hiPSCs (hiPSCs-derived BMECs). These cells were then separately co-cultured together to model human BBTB in vitro. The detailed informations of all of these cells are shown in Table 3.2.

For all culturing processes, a Laminar class II cabinet (a laminar flow hood) was used with sterilization provided by ultraviolet light.

3.2.1.1 Thawing of the cell lines

To thaw cell lines, the cryovial was taken from liquid nitrogen and immediately incubated in a water bath at 37ºC until a piece of ice remains. As soon as cell line was thawed, vial's outer surface was disinfected with 70% ethanol and it is taken inside the cabinet. Cell line was transferred to sterile conical falcon tube (15 mL), made up the volume to 5 mL by slowly adding its medium and then centrifuged 5 minutes 300 x g. Supernatant was aspirated, and cell line was suspended with its freshly prepared medium (appropriate amount usually 7-8 mL). Cells were gently disturbed by slowly pipetting up and down a few times for homogenizing cell suspension. The cell suspension was then transferred to a culture plate (generally T25 flask) and was left for incubation at 37ºC and 5% CO_2.

3.2.1.2 Passaging and seeding of hCMEC/D3

For preparation of passaging cells, CoL1 was diluted with DPBS at 1:10 dilution rate as described in Table 3.3. Appropriate culture plate was coated with this CoL1+DPBS solution and incubated at least 1 hour at 37 ºC.

EndoGRO™ basal medium was completed with EndoGRO™-MV supplements and 1 ng/mL FGF2 in dark. To use 1 ng/mL FGF2, 10 µg of lyophilized FGF2 was dissolved in 1 mL DPBS including 0.1% bovine serum albumin (BSA) solution, which was thoroughly mixed by vortex and presterilized by filtration. To prepare a 50 mL EndoGRO™ medium, 100 µL of EndoGRO™ LS supplement, 50 µL rhEGF, 50 µL hydrocortisone hemisuccinate, 50 µL ascorbic acid, 50 µL heparing sulfate included in the EndoGRO™-MV media kit, and 5 µL of FGF2 from already prepared 10 µg/mL stock concentration were added to 47.5 mL of the EndoGRO™ basal medium.

DPBS was aspirated from the coated culture plate and freshly completed EndoGRO™ medium was added to the plate. hCMEC/D3 was thawed in this completed EndoGRO™ medium according to a protocol described just above. After thawing, hCMEC/D3 was plated into already coated culture plate. Day after thawing, the media was changed with freshed one. When cells have reached over 30% confluency, they were passaged with Trypsin-EDTA (0.25%).

For passaging cells, culture plate was freshly coated with CoL1. After coating, old media was aspirated. Cells were washed with DPBS (3 mL to T25 flask). The DPBS was aspirated, and Trypsin-EDTA was added (1 ml to T25 flask) and incubated 2-4 minutes at 37ºC. Cells were detached by tapping culture plate with hand palm and were observed under an inverted light microscope (ILM). Trypsin-EDTA was deactivated with 3 times amount of the medium. To continue their expansion, only needed amount of cell-medium-Trypsin-EDTA suspension was taken and volume was completed with fresh medium (total volume should be 4-8 mL for T25 flask). The cells were put in an incubator with appropriate cell culture environment (5% CO_2, 37°C). If not used, they were freezed with its freezing medium prepared according to Table 3.2 for later experiments.

For seeding cells, after deactivation of Trypsin-EDTA with medium, cell suspension was transferred to a sterile conical falcon tube and centrifuged 5 minutes 300 x g. Supernatant was aspirated, cell pellet was gently disturbed by flicking falcon, and resuspended with medium. Cell suspension was mixed by pipetting up and down a few times. Cell suspension (10 µL) was taken to be counted on a hemocytometer. Only the 4 circular areas shown in red, consisting of 1x1 cm^2 squares, shown in Figure3.1 were counted. The average of all 4 circular areas was taken and then was multiplied by 10^4 to calculate cell number in cell suspension (1 mL). From 1 mL cell suspension, the total cell number in the suspension and desired cell suspension volume needed for seeding were calculated.

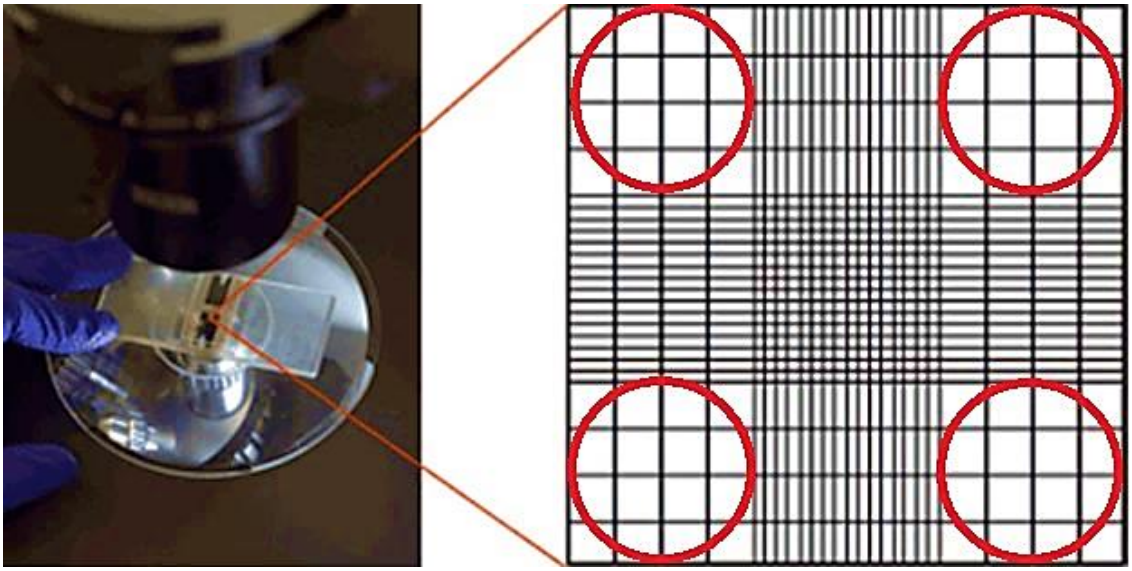

Figure 3.1 Counting cells on hemocytometer and visualized under ILM

3.2.1.3 Subculturing of hCMEC/D3

For in vitro modeling of monoculture BBB, Table 3.4 was used for appropriate working volumes and seeding densities.

Transwell-clear inserts were carefully placed into wells of the plates and the microporous polystrene (PET) membrane (0.4 µm) of these inserts were coated with CoL1 (see Section 3.2.1.2). Cell suspension was seeded onto these pre-coated inserts drop by drop using a 200-gauge micropipette to distribute cells evenly over the surface. Only its fresh medium (500 µL) was added to basolateral (lower) side of the insert.

3.2.1.4 Freezing of hCMEC/D3

Before beginning to the freezing, cryovials were labelled with informations of the cells such as name, passage number, and the date which the cells were freezed.

For freezing cells, old media was aspirated. Cells were then washed with DPBS (add 3-4 mL for T25 flask). DPBS was aspirated, and Trypsin-EDTA was added directly onto the cells (1 mL to T25 flask). The cells with Trypsin-EDTA were incubated 3-5 minutes at

37ºC. After incubation, Trypsin-EDTA was deactivated with 3 times amount of the medium. Cell suspension was then transferred to a sterile conical falcon tube and centrifuged 5 minutes 300 x g. Supernatant was aspirated and resuspended with its freezing medium described in Table 3.2 (1 mL cell-freezing medium for each cryovial). The cryovials were placed in freezing container with isopropanol (Mr. frosty) overnight at 80ºC. The next day, they were transferred to tank with liquid nitrogen at -176 ºC for storage.

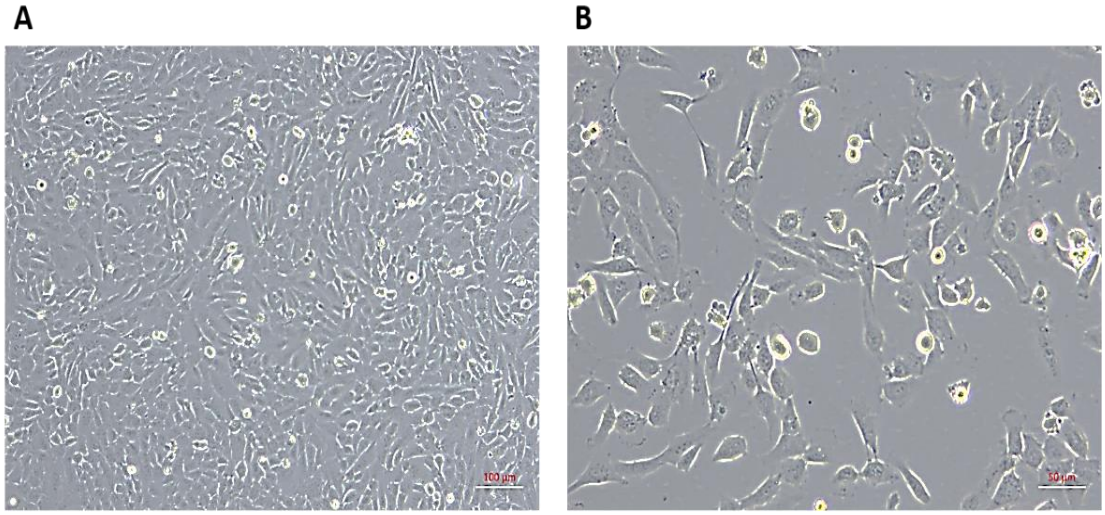

Figure 3.2 ILM images of hCMEC/D3 cell line at passage +4 (A. Magnification: 10X, scale bar: 100 µM, B. Magnification: 20X, scale bar: 50 µM)

3.2.1.5 Culturing of U87 (Thawing, passaging, seeding, and freezing)

Before beginning to culture U87, MEM medium was completed with 10% FBS and 1% penicillin-streptomycin. U87 was thawed in this completed MEM medium according to a previously described thawing protocol. After thawing, U87 was plated into an appropriate plate. When the cells reached 70-80% confluency, they were passaged with Trypsin-EDTA (0.05%). For passaging, seeding, and freezing same protocols were used in hCMEC/D3, referring to Tables 3.2, 3.3, and 3.4.

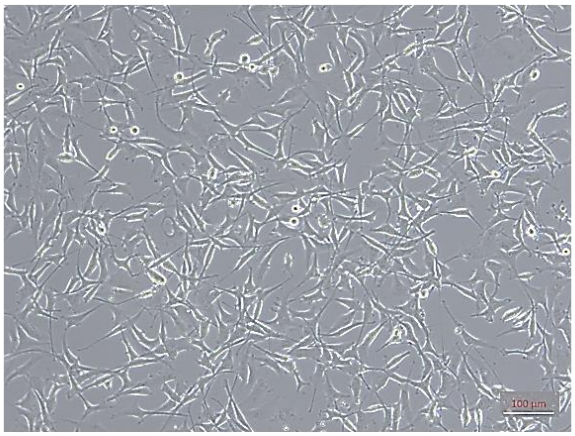

Figure 3.3 ILM image of U87 at passage +7 (Magnification: 10X, scale bar: 100 µM)

Table 3.2 Cells used with their culturing informations

Passage Number	Cell Name	Cell Type	Media	Passaging Agent	Coating
26	hiPSCs obtained from PBMCs' transduction	Human Induced Pluripotent Stem Cell	Culture: E8 Basal Medium + E8 supplement (Completed E8) Freezing: PSC Cryomedium or 90% Completed E8 + 10% DMSO	0.5 mM EDTA	VTN diluted in DPBS
0	hiPSCs-derived BMECs	Human Brain Microvascular Endothelial Cell	Culture: hESFM + 1% PDS (Culture Medium) Freezing: 60% EC Medium + 30% FBS + 10% DMSO	Accutase	CoL1 + FN + dH_2O
+6	hCMEC/D3	Human Cerebral Microvascular Endothelial Cell Line	Culture: EndoGRO™-MV Media Kit + 1 ng/ml FGF2 (Completed EndoGRO™ Medium) Freezing: 90% Completed EndoGRO™ Medium + 10% DMSO	0.25% Trypsin-EDTA	CoL1 diluted in DPBS
+8	U87	Human Glioblastoma Cell Line	Culture: MEM+ 10% FBS+ 1%Penicillin-Streptomycin Freezing: 90% FBS + 10% DMSO	0.05% Trypsin-EDTA	-

3.2.2 Culturing hiPSCs

In all steps or experiments in which hiPSCs were used, attention was paid to the sterilization of all materials used, as the risk of contamination would be greater due to the absence of the use of Penicillin-Streptomycin in the medium.

For preparation of culturing hiPSCs, VTN was prepared in DPBS as described in Table 3.3. Appropriate culture plates (e.g. T25 flasks or petri dishes) were coated with this VTN for an hour at RT. If not used, leftover coated culture plates were stored at +4 for later use for a maximum of 1 week. Essential 8 (E8) medium was completed by adding 1 mL E8 Supplement to 49 mL E8 Basal Medium.

For culturing hiPSCs, hiPSCs was thawed in this freshly completed E8 medium by adding RevitaCell™ Supplement (50 µL supplement to 5 mL medium) to reduce large amount of cell death and get optimal post-thaw cell recovery. DPBS was aspirated from coated plate and hiPSCs colony was plated by pipetting up and down one-two times w/o damaging the colonies. The spent medium was changed with freshly completed E8 medium w/o RevitaCell™ (4 mL for T25 flask) every 24 H to prevent uncontrollable differentiation of hiPSCs to any type of cell.

3.2.2.1 Passaging and Freezing of hiPCSs

When hiPSC colonies were covered 80% of the surface area (SA) of the culture plate, they were non-enzymatically passaged by 0.5 mM EDTA prepared in DPBS (add 50 µL pure EDTA to 50 mL DPBS). Also, non-enzymatic passaging was continued until the mature hiPSCs (passage number > 20) was observed, according to the characterization data of hiPSCs shown in Appendix 8.

For non-enzymatic passaging of hiPSCs, old media was aspirated and the colonies were washed with DPBS (add 3 mL to T25 flask). The DPBS was aspirated, EDTA in DPBS was added (3 ml to T25 flask) and incubated 4 minutes at 37ºC. The half detachment of

colonies from plate surface were observed under an ILM. EDTA in DPBS was aspirated. 500-1000 µL of completed E8 medium was quickly released onto the colonies by using micropipette to completely detach the best colonies. A small amount (10-20 µL for T25 flask) was taken from the colony-media suspension with a micropipette, transferred to a new coated culture plate and the volume is completed with fresh medium (4 mL for T25 flask). The cells were put in an incubator with appropriate cell culture environment (5% CO_2, 37°C).

For freezing of hiPSCs, if not used, they were freezed by gently spraying the medium over the colonies a few times for better collection and then the same protocol mentioned in Section 3.2.1.4 and informations in Table 3.2 were used.

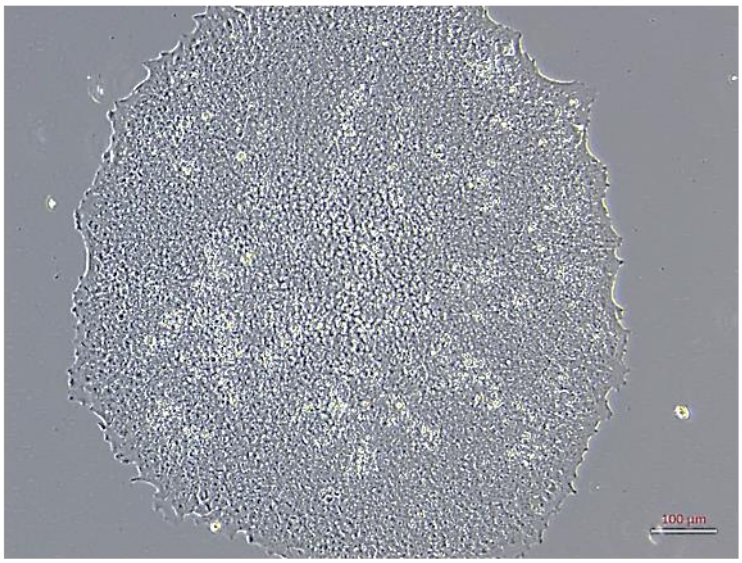

Figure 3.4 ILM image of hiPSCs colony 4 at passage 25 (Magnification: 10X, scale bar: 100 µM)

Table 3.3 Volumes for ECM coating solutions

Coating Type	Usage of the Coating	Plate/Transwell/Flask Type	Working Volume	Coating Time
VTN	Independent from the volume, dependent only surface area of the culture plate, and must be used within enough DPBS (1X) covering the surface	T25 Flask	25 µL in 4 mL DPBS	Wait 1H at RT before usage
		T75 Flask	75 µL in 7 mL DPBS	
		6-well Plate	9.6 µL in 2 mL DPBS	
		24-well Transwell-clear Insert	1.9 µL in 1 mL DPBS	
CoL1 + FN + dH_2O	Mixture ECMs as: CoL1: 4 µL FN (1 mg/mL): 1 µL dH_2O: 5 µL in total of 10 µL of the mixture	6-well Plate	1.5 mL of already prepared mixture	Wait 24H at 37 °C before usage
		24-well Plate	500 µL of already prepared mixture	
		24-well Transwell-clear Insert	100 µL of already prepared mixture	
CoL1	Dilution ratio is 1:20 For exp. Take 1 mL of CoL1 and mix with 19 mL of DPBS (1X)	T25 Flask	200 µL in 4 mL DPBS	Wait at least 1H at 37 °C before usage
		T75 Flask	350 µL in 7 mL DPBS	
		24-well Plate	500 µL of already diluted CoL1	
		24-well Transwell-clear Insert	50 µL of already diluted CoL1	

3.2.3 Differentiation of hiPSCs into BMECs

The differentiation was started with seeding of singularized hiPSCs (Day -3), and was continued with induction (Day 0-5), expansion (Day 6-7), and purification of BMECs (Day 8-11), as demonstrated in Figure 3.5. Also, differentiation was performed using procedures in the literature with some differences like coating types (Stebbins et al., 2016).

3.2.3.1 Seeding of Singularized hiPSCs and Their Expansion for Differentiation

Before starting the experiment, hiPSCs should be reach 80% confluency (lasted ~7 days).

Day -3: 5 x 6-well plates were coated with VTN (see Section 3.2.2 for steps and Table 3.3 for appropriate volumes). Old medium was aspirated, then colonies were washed with DPBS. DBPS was aspirated and hiPSC colonies were then enzymatically dissociated with cold accutase for 3 minutes to observe singularization. Completed E8 medium (see Section 3.2.2) was gently sprayed over the surface a few times to collect all the single cells off the culture plate. Cells were then collected to a conical falcon tube and centrifuged 5 minutes at 1000 rpm. After centrifugation, the supernatant was aspirated. The cell pellet was resuspended in Completed E8 medium with RevitaCell™ (see Section 3.2.2) by pipetting a few times, and counted on a hemocytometer (see Section 3.2.1.2). 100.000 cells/1.5 mL media were seeded on each well of 6-well plate. One well was marked as a counting well to count the cell density and determine the starting day of induction, Day 0. The plates were placed in an incubator with appropriate cell culture environment (5% CO_2, 37°C) and shaked forth and back, paused, shaked right-to-left, paused. This shaking was repeated three times for even cell distribution.

Day -2 and Day -1: Medium was changed with fresh E8 Medium w/o RevitaCell™ (2 mL of medium for each well) after 24 H. Medium change was repeated every 24 H for three days until an appropriate cell density (250.000-400.000 cells/per well) was counted.

3.2.3.2 Induction of BMECs

Day 0: Unconditioned medium (UM) was prepared by adding 10 mL KOSR, 0.5 mL NEAA, 250 µL glutamax, and 0.35 µL 2-mercaptoethanol to 39.25 mL DMEM-F12. The cells in the marked counting well were dissociated with cold accutase (see Section 3.2.3.1), counted as 320.000 cells/per well, which is an ideal starting density for induction. After counting, old medium of the other wells was changed with UM for 6 days until day 5 (2 mL for each well).

3.2.3.3 Expansion of BMECs

Day 6: To prepare 10 µM RA (3 mg/mL), 10 mM (40 mg/mL) stock concentration of RA was made by dissolving 100 mg of RA powder in 2.5 mL DMSO and then diluted as 1:1000. Endothelial cell (EC) medium was prepared by adding 0.5 mL PDS, 100 µL FGF2, 50 µL RA to 50 mL hESFM. For expansion of BMECs, UM was changed with EC medium (2 mL for each well). Medium was not changed at day 7.

Day 8: If not used, BMECs were freezed.

3.2.3.4 Freezing of BMECs

Due to the absence of some reagents like PDS, and FN, BMECs are freezed at day 8 as non-purified cells based on previously published protocol (Wilson et al., 2016). Protocols are same for non-purified and purified (the cells at day 11, which were seeded onto coated plates) BMECs.

For freezing hiPSCs-derived BMECs, old medium was taken and cells were washed with DPBS. DPBS was taken, and cells were incubated with cold accutase at 37ºC (waited 30 minutes for BMECs on day 8, 15 minutes for BMECs on day 11) until single cells were observed. After incubation, EC Medium was added onto cells w/o aspirating accutase, suspension was gently sprayed a few times for each well and then centrifuged 5 minutes 300 x g. Supernatant was aspirated and cell pellet was resuspended with its freezing medium (see Table 3.2) and stored (see Section 3.2.1.4)

3.2.3.5 Thawing of BMECs and their subculturing for purification

All experiments of the thesis were carried out by thawing the non-purified BMECs at day 8 (Wilson et al., 2016). The protocols are same for non-purified and purified BMECs.

Thawing medium was prepared by adding 50 µL FGF2, 0.5 mL PDS, and 500 µL RevitaCell™ to 50 mL hESFM. The culture medium was prepared by adding 1% PDS to hESFM. To mimic basement membrane components, culture flasks or transwell-clear inserts were coated with ECM coating solution (CoL1 + FN + dH_2O) according to Table 3.3. 24 H later, cells were thawed by using thawing medium (see Section 3.2.1.1). After thawing, cells were immediately seeded like in Section 3.2.1.2 with appropriate volumes and seeding densities in Table 3.4. For in vitro modeling of monoculture hiPSCs-derived BBB, cell suspension was seeded onto pre-coated inserts like in Section 3.2.1.3. Beginning from post-thawing, every 24 H until day 11, thawing medium was changed to culture medium for removing non-adherent cells and thus maximize TEER.

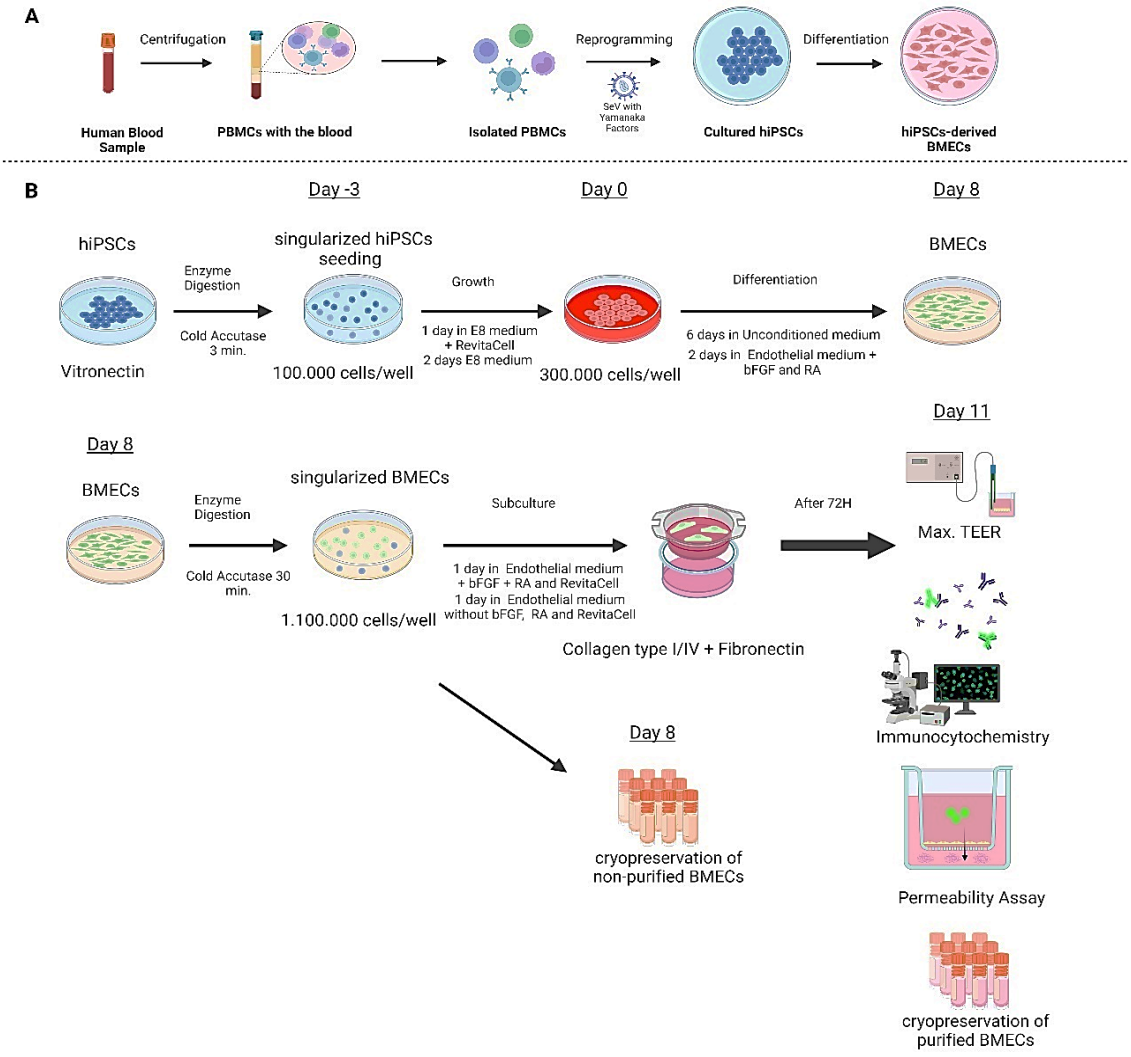

Figure 3.5 A. Steps of BMECs' differentation starting from PBMCs' isolation, B. BMECs' derivation from hiPSCs on 6-well plates (Created by BioRender)

3.2.4 Formation of in vitro BBTB models

After TEER has reached its maximum value, brain ECs (hCMEC/D3 and hiPSCs-derived BMECs) were separately co-cultured with U87 by using transwell systems. Table 3.4 was used for seeding densities of cells and working volumes of both models.

3.2.4.1 Models with hCMEC/D3 and U87

Before seeding the cells, transwell-clear insert was placed into a well-plate and then it was coated with CoL1 (see Sections 3.2.1.2 and 3.2.1.3). U87 cells were subcultured on an empty well of the well-plate which had the insert. Cells were incubated 1-2 H for adherence. hCMEC/D3 cells were seeded on the apical (upper) side of the insert. Two days later (after 48 H), the insert including cultured hCMEC/D3 cells supplemented with completed EndoGRO^{TM} medium was transformed to the well where U87 cells were cultured and supplemented with completed MEM Medium. Before the experiments including co-culturing, it was waited for 2 H to ensure that both cells were communicating.

3.2.4.2 Models with BMECs and U87

Transwell-clear insert was coated with CoL1 and FN (see Section 3.2.3.5). After 24H, non-purified BMECs were subcultured on upper side of insert. Next day, media of non-purified BMECs was changed with its fresh culture medium (hESFM + 1% PDS) and U87 cells were seeded on an empty well of well-plate which had insert including BMECs. Two days later (after 48 H), insert including purified BMECs supplemented with hESFM + 1% PDS was transformed to well where U87 cells were cultured and supplemented with completed MEM Medium. Before experiments including co-culturing, it was waited for 2 H to ensure that both cells were communicating.

Table 3.4 Seeding densities and working volumes in subculturing of the cells used

		Plate/Transwell Type	Seeding Density	Working Volume/well
Cell Name	hiPSCs	6-well Plate	100.000 cells/well	1.5 to 2 mL
		24-well Transwell	3.500 cells/well	Upper Chamber: 100 to 300 µL
				Lower Chamber: 500 µL
	hCMEC/D3	24-well Plate	104.500 cells/well	500 µL to 1 mL
		24-well Transwell	16.500 cells/well	Upper Chamber: 100 to 300 µL
				Lower Chamber: 500 µL
	hiPSCs-derived BMECs	24-well Plate	250.000 cells/well	500 µL to 1 mL
		24-well Transwell	330.000 cells/filter	Upper Chamber: 100 to 300 µL
				Lower Chamber: 500 µL
	U87	24-well Plate	60.000 cells/well	500 µL to 1 mL

3.2.5 Immunocytochemistry (ICC)

For immunocytochemistry (ICC) experiment, cells (hCMEC/D3, BMECs) were seeded on 24-well plates. Fixation was performed on day the cells (BMECs and hCMEC/D3) reached maximum TEER value. It was done to observe specific markers related to brain ECs.

In the experiment, aspiration and DPBS washing were done. Then, cold methanol (MeOH) was added to cover wells and incubated 15 minutes, -20ºC. MeOH was removed and allowed to dry in the hood. DPBS washing and its aspiration were applied to cells. To block non-specific bindings and to improve permeabilization of dyes and intensity of staining, a solution (50 µL tritonX_100 and 0.5 g BSA in 50 mL DPBS) was prepared and vortexed thoroughly until it has completely homogenized. The wells were then covered by adding 200 µL this solution to each and incubated for 1 H at room temperature (RT). After incubation, the solution was taken and the cells were washed 3 times with DPBS. Primary antibodies (CD31 and OCLN) were diluted in prepared solution separately according to Appendix 1. After washing, 100 µL prepared antibodies were added to determined wells and incubated at +4°C overnight. Primary antibodies were aspirated and cells were washed 3 times with DPBS. The secondary antibody (AF488) was diluted in prepared solution separately according to Appendix 1 in dark. After washing, 100 µL prepared antibodies were added to determined wells and left for incubation 1-2 H at RT. After incubation, solution was aspirated and cells were washed 3 times with DPBS. To stain cell nuclei, 4’6-diamidino-2-phenylindole (DAPI) was diluted (ratio 1: 100) and added to all wells in dark. Then, the stained wells were examined under a fluorescence microscope.

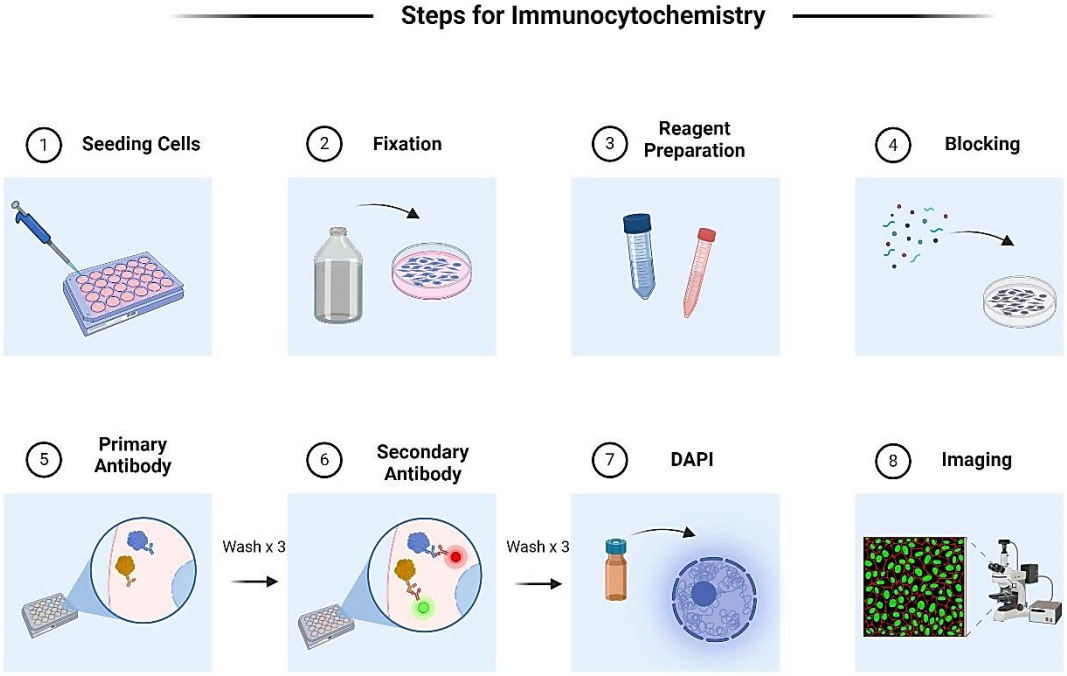

Figure 3.6 Steps of ICC experiment (Created by BioRender)

3.2.6 Real-time quantitative reverse transcription polymerase chain reaction (RT-qPCR)

RT-qPCR detects and quantifies RNA. It was done to get expression profiles of genes related to brain ECs with three biological replicates.

Firstly, the RNAs of hiPSCs, BMECs, and hCMEC/D3 cells were separately isolated by using column method as in the protocol of the Macherey-nagel nucleospin RNA mini kit. To prepare the lysis solution, 250 µl β-mercaptoethanol was added to the 25 mL lysis solution included in the kit. For all cell types, they were thoroughly lysed with 350 µL this solution by pipetting a few times and transferred into an eppendorf microcentrifuge tube. After lysis, the steps from the Mini Kit were applied. At the last step, 50 µL nuclease-free water (NFW) was added to the isolated RNA in the tube, and this step was repeated. Then, the RNA samples were stored at -20°C.

Secondly, complementary DNA (cDNA) was synthesized from 1000 nanograms (ng) each RNA sample (ng/µL) by following the protocol in the iScriptTM cDNA synthesis kit. To observe whether pure RNA was obtained and to calculate the amount of RNA to be taken from the RNA sample to prepare 1000 ng RNA, 2 µL NFW was dropped as blank, and then 2 µL RNA sample was dropped on the NanoDrop device (BioSpec). The cDNA synthesis solution was prepared by taking 1 µL the iScript reverse transcriptase enzyme and 4 µL iScript reaction mix per sample, both of which were contained in the kit. 5 µL this solution were then added to the total 15 µL calculated 1000 ng RNAs and NFW, for 20 µL total volume. After that, this mixture (1000 ng RNA, NFW, and cDNA synthesis solution) in a PCR tube was incubated with the BIORAD thermal cycler device (CFX96) 5 minutes 25°C, 20 minutes 46°C, and 1 minute 95°C. The synthesized cDNAs were diluted with RNase-free water at 1:2 and stored at -20°C.

Lastly, for RT-qPCR, primer sequences were designed using "NCBI Primer Blast" and outsourced to "Oligomer" company, as shown in Appendix 2, were used by following the protocol of Sso Advanced™ Universal SYBR® Green Supermix. Commercially obtained lyophilized forward (F) and reverse (R) primers were solved with NFW according to designer's instructions and thus 100 µM main stocks were prepared. After that, running stocks were prepared by adding 475 µL of NFW to the 25 µL of main stock. RT-qPCR reaction mixture was prepared by taking 10 µL SsoAdvanced Universal SYBR® Green Supermix, 1 µL F primer, 1 µL R primer, and 6 µL NFW per sample. For each sample, 18 µL of the mixture was transferred into 96-well PCR plates and each sample was repeated 3 times. Except for the no template, 2 µL cDNA was added to them. Total volume was 20 µL for each well. After that, this plate was covered with an adhesive PCR plate seal and placed in BIORAD thermal cycler device (CFX96) and the reaction was taken place 10 minutes 95°C, 15 seconds 95°C (40 cycles), and1 minute 60°C (40 cycles). After the reaction has completed, cycle threshold (Ct) value for all genes were obtained ($Ct \leq 40$). This value was used to calculate the amount of gene expression for the obtained samples compared to the control group. To calculate this, the difference between the samples and the house-keeping/reference gene (GAPDH) was found (ΔCt). Then, the difference between samples' ΔCt value and control group's ΔCt value was found (ΔΔCt) and finally the analysis were performed by averaging the $2^{-\Delta\Delta Ct}$ values. The data

normalized to the expression levels of GAPDH was carried out using the following formula: $2^{-\Delta Ct} \times 100$.

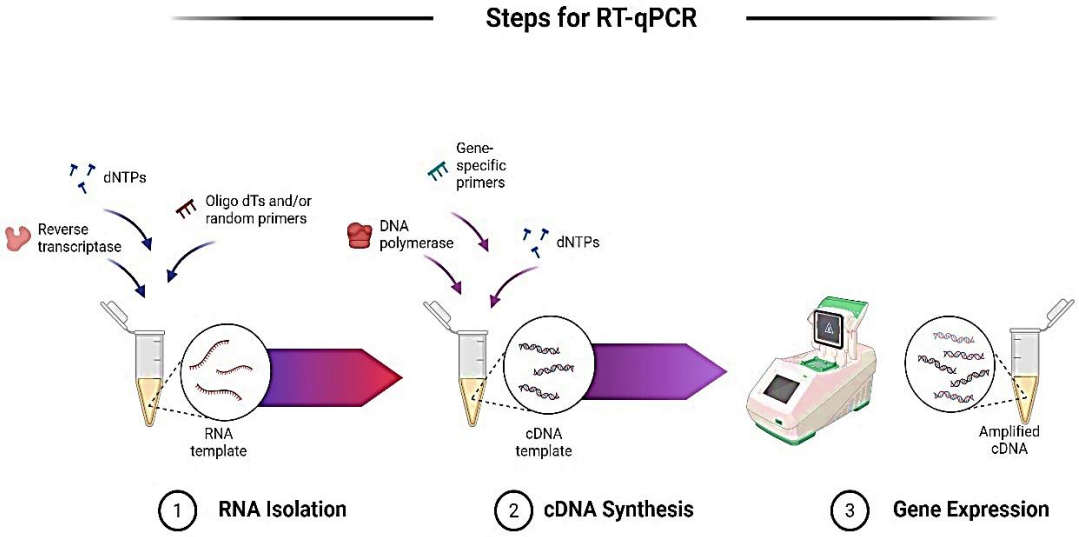

Figure 3.7 Steps of RT-qPCR, summarized (Created by BioRender)

3.2.7 Evaluation of the BBB impermeability/permeability

3.2.7.1 Transendothelial electrical resistance (TEER) measurement

Transendothelial electrical resistance (TEER) measurement was carried out for determining barrier integrity. For this experiment, the cells (hiPSCs, hCMEC/D3, and BMECs) were subcultured into 24-well transwell-clear inserts with three biological replicates at densities described in Table 3.4. To obtain the actual TEER value of the cells, ECM coatings (CoL1 and CoL1+FN) were used as blanks; therefore, the inserts were coated only. hiPSCs, as the negative control group, were thawed onto VTN coating and cultured until big colonies were observed. Then, they were singularized with Accutase and subcultured into the inserts, which were pre-coated with CoL1 and FN. hCMEC/D3, as the positive control group, was subcultured into the inserts pre-coated with CoL1 (see Section 3.2.1.3). BMECs at day 8 were thawed and immediately subcultured into the inserts pre-coated with CoL1 and FN (see section 3.2.3.5). Each group was subcultured in a separate 24-well plate. After subculturing, TEER was measured in a sterile hood via

STX2 electrodes and A volt-ohmmeter (MERS00002, Millicell® ERS-2, Millipore) every 24 H for 4 days, with 3 technical replicates for each insert.

Before starting the measurement, the electrodes were kept in 70% ethanol for 10 minutes, then immersed in sterile DPBS, and then each insert was quickly measured at RT. When different groups were measured, the ethanol-DPBS process was repeated, and the inserts were immediately measured. Meanwhile, others were kept at 37°C to avoid fluctuations in TEER values resulting from temperature changes. At the end of each measurement day, the medium of all inserts was replaced with fresh ones.

All measurements were recorded as ohms (Ω). To obtain TEER (in Ω x cm^2), the average of the triplicate values of insert with cells (in Ω) was taken and subtracted from the average of the values of their blanks. Then, the becoming value was multiplied by the SA of the 24-well transwell-clear insert (0.3 cm^2). This was repeated for other biological replicates of the groups to obtain TEER values with standard deviations (SD).

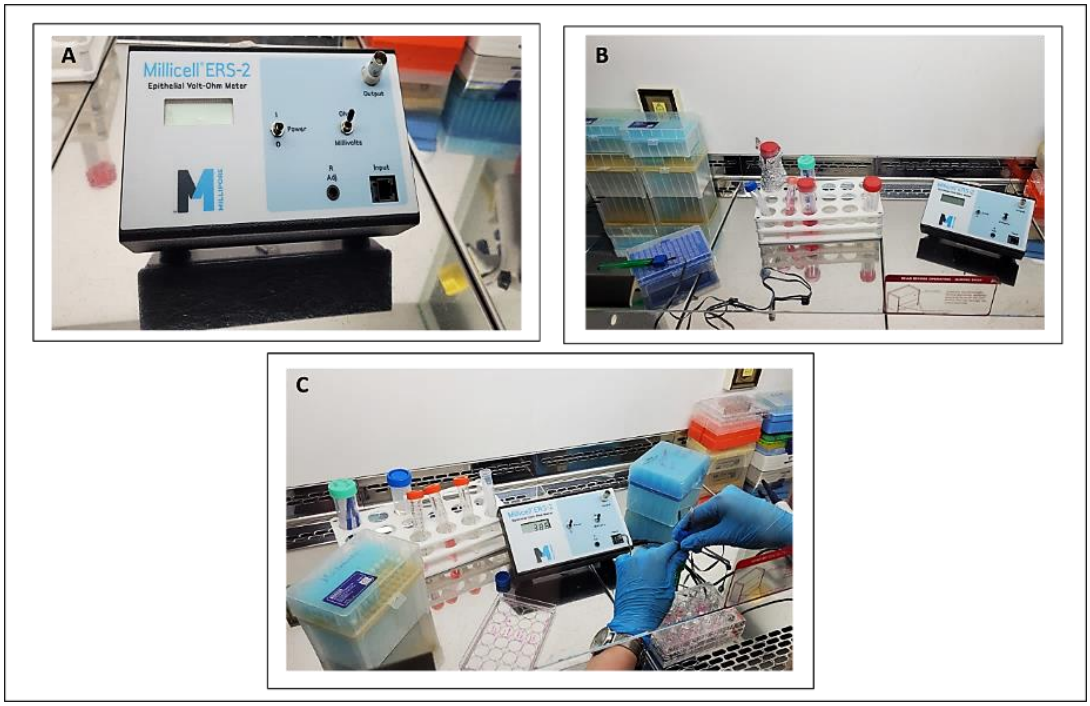

Figure 3.8 A. Voltohmmeter device, B. Voltohmmeter with STX2 electrodes, C. In vitro TEER measurement

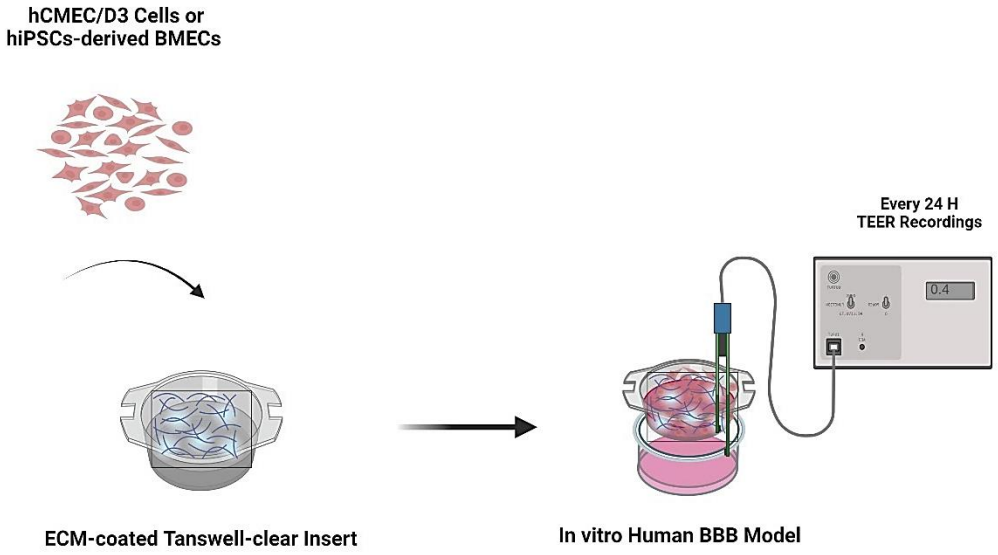

Figure 3.9 BBB model in vitro ilustration used for TEER measurements (Created by BioRender)

3.2.7.2 Permeability assay: Measurement of FITC-dextran

The permeability assay was done by using a commercially available tracer, fluorescein isothiocyanate (FITC) labeled dextrans (FD), to determine barrier permeabilization and if the tracer permeability paralleled with TEER measurements. Additionally, it was conducted to set a standard for the permeability of fluorescent materials through the BBB and BBTB models.

For this experiment, small molecular weight (4 kDa) FD (FD4) was used. The cells (hCMEC/D3 and BMECs) were subcultured into 24-well transwell-clear inserts with and w/o U87 cells, which were seeded on lower side of insert, well of plate, according to Section 3.2.4. As in the TEER measurement experiment, blank inserts were also included. Therefore, the groups were monocultures (hCMEC/D3 only and BMECs only), cocultures (hCMEC/D3 + U87 and BMECs + U87), and blanks (CoL1 and CoL1+FN).

After seeding and/or waiting for cells to communicate, monocultures were transferred to clean wells of the well plate. The old media of all groups from both sides of the inserts were aspirated. The medium of the lower side of all inserts was replaced with fresh

medium. FD4 was prepared in the fresh medium of the relevant cell by adding 24 µL FD4 to 276 µL medium in the dark. 300 µL prepared FD4 per insert was dropped from upper side of inserts of all groups in dark and incubated 2 H, 37°C. After incubation, 100 µL of the medium was taken from both sides of each insert of all groups and distributed to the wells of the black polystyrene 96 well-plate (fluorescence plate) in the dark. To find the actual fluorescent intensity (FI) of FD4, 100 µL of fresh medium from all cells was also distributed to the wells of the fluorescence plate.

FI by FD4 was measured via a fluorescent plate reader (Mithras2 LB 943, Berthold Technologies) at an excitation/emission wavelength of 490 nm/520 nm. After measurement, spontaneous passage of FD4 transported across the barriers (%) and permeability coefficients (P_e, cm/s) were calculated as:

Spontaneous passage (%) = [initial FI (concentration) of lower side of insert / initial concentration of lower side of blank insert] x 100,

P_e (cm/s) = [(volume of lower side of insert in cm^3 x the diffusion concentration of lower side of insert) / (SA of insert in cm^2 x diffusion time in seconds x the initial concentration of upper side of insert)].

3.2.8 Studies with fluorescent nanomaterials in BBB and BBTB models

3.2.8.1 Permeability measurement of MQDs

Permeability measurement of MQDs was carried out to quantify transport of this material across BBB and BBTB models. Groups were the same as in permeability measurement of FD4.

In experiment, same protocol as in the Section 3.2.7.2 were followed. Different from this protocol, in the dark, main stock MQDs at 225 µg/mL concentration were vortexed thoroughly and used amount was sonicated in a sterile amber bottle for 20-25 minutes in an ultrasonic bath sonicator (Elmasonic S80H) at RT by preventing temperature rise

above 30°C. After sonication, MQDs were vortexed again and 50 µg/mL of MQDs were prepared by diluting the main stock MQDs with the fresh medium related to cell type. Dilution ratio was found as; 225 µg/mL / 50 µg/mL = 1:4,5. The brain ECs were separately treated with this vortexed and pipetted 50 µg/mL of MQDs, which was determined by LDH Cytotoxicity Assay, as its analysis described in Appendix 4. The FI of MQDs was measured via the fluorescent plate reader at an excitation/emission wavelength of Texas Red (586 nm/647 nm).

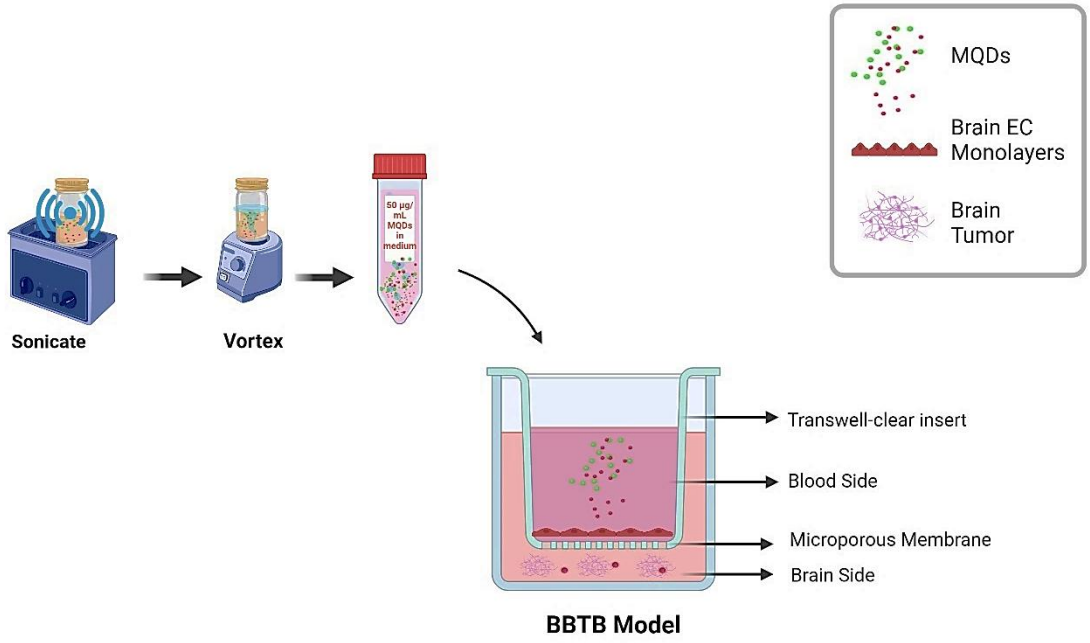

Figure 3.10 Treated cells with MQDs in BBB/BBTB models (Created by BioRender)

3.2.8.2 Detection of MQDs by flow cytometry

Flow cytometry was done to investigate if MQDs were transported across brain ECs and thus were uptaken by U87 by measuring the distribution of cell FI via flow cytometer. The measurement was obtained on 10.000 events (cells) at medium fluidics and averaged between three replicates.

In the experiment, 24-well transwell-clear inserts were used, and the cocultures (hCMEC/D3 + U87 and BMECs + U87) were treated with MQDs, namely treated groups, as well as the no treatment (naïve) groups.

To conduct the experiment, the brain ECs were cocultured with U87, as previously described in Section 3.2.4. After that, the old media were aspirated. The medium of both sides of naïve groups and the medium of the lower side of inserts of treatment groups were replaced with fresh medium. MQDs were made ready for use just as in the permeability measurement of MQDs. The brain ECs of treatment groups were separately treated with 50 µg/mL MQDs in the dark and incubated 24 H, 37°C. After treatment, media were aspirated, and the cells were washed with DPBS. All the cells were then detached from the surface of inserts and/or wells by an appropriate enzyme (trypsin-EDTA for hCMEC/D3 and U87, and cold accutase for BMECs). The enzyme was deactivated with the medium related to cell type. The cells were centrifuged at 1500 rpm for 3 minutes. Cell pellets were resuspended with cold MeOH for 20 minutes for fixation. After fixation, cells were centrifuged again 3 minutes, 1500 rpm, and resuspended in 1 mL DPBS and then immediately measured (samples that could not be measured immediately were stored at +4°C). Before starting measurement and between mesurements of each different group, flow cytometer was rinsed with detergent (FACS) and dH_2O respectively.

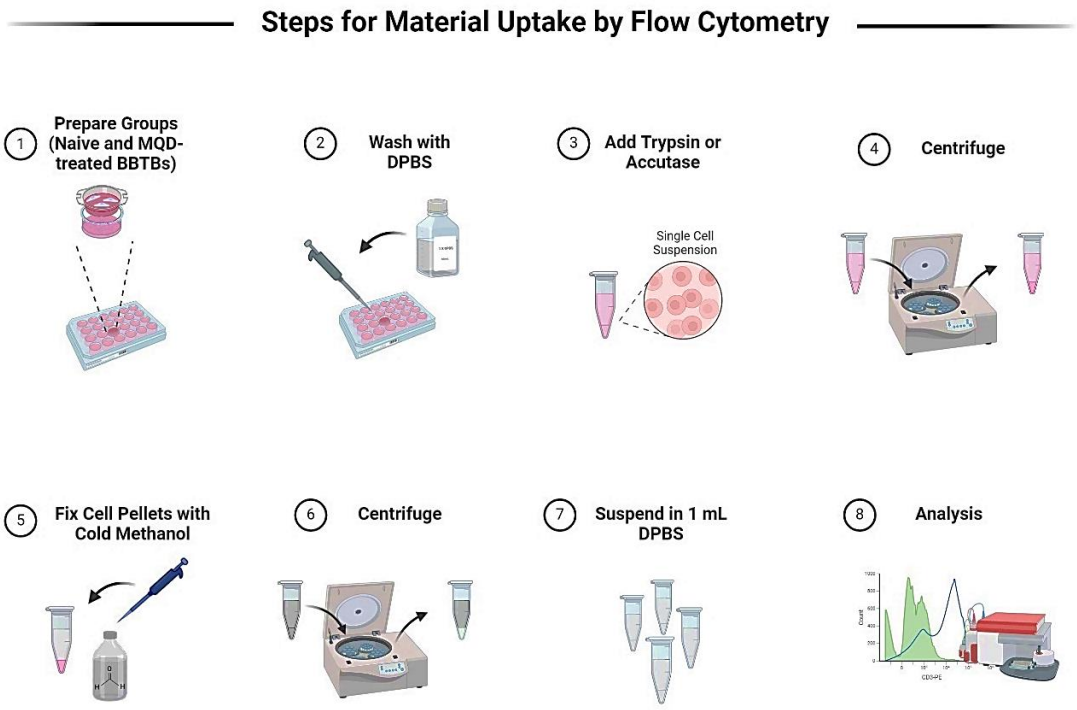

Figure 3.11 Flow cytometry (Created by BioRender)

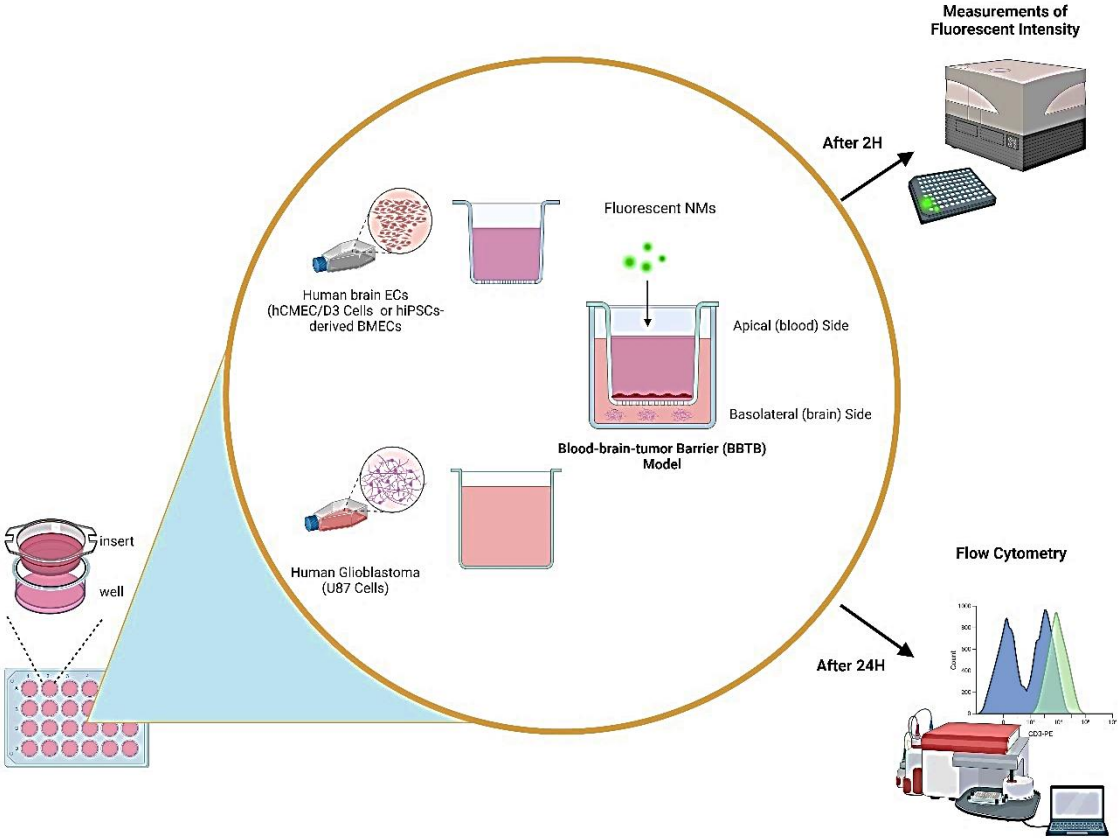

Figure 3.12 llustration of in vitro BBTB model used for permeability measurements and flow cytometry (Created by BioRender)

3.3 Statistical analysis

Experimental data was analyzed statistically via GraphPad Prism software (version 9). For the evaluation of statistical difference, ordinary one-way analysis of variance (ANOVA), and two-way ANOVA followed by Tukey's multiple comparison test were conducted where appropriate. The results in graphs were demonstrated as mean ± standard deviation and significance by statistics was considered as $p < 0.05$.

4. RESULTS

4.1 Derivation of BMECs from hiPSCs

For developing human BBB model in vitro similar to in vivo, hiPSCs were cultured and then differentiated into BMECs as described in sections 3.2.2 and 3.2.3. To depict the differentiation of hiPSCs into BMECs and observe the change in morphology, bright field images of the differentiation process were taken day-by-day via ILM at a magnification of 10X, as shown in Figure 4.1. On day (-2), the starting day of seeding singularized hiPSCs, the morphology is the same as hiPSCs until the day (0). After one day of culture in UM, the colonies of hiPSCs began to merge, grow, and differentiate but retained their cellular morphology. As the cells continued to culture in this media, residual undifferentiated hiPSCs were eliminated. On day 3, morphological changes started to be observed and they appeared as beads between days 4-6 in UM. On day 8, the cells were elongated, distinctly different from hiPSCs, and acquired a cobblestone-like appearance in EC media. The cells were purified on days 10 and 11 and became larger with a cobblestone pattern and connections similar to neural and endothelial cells.

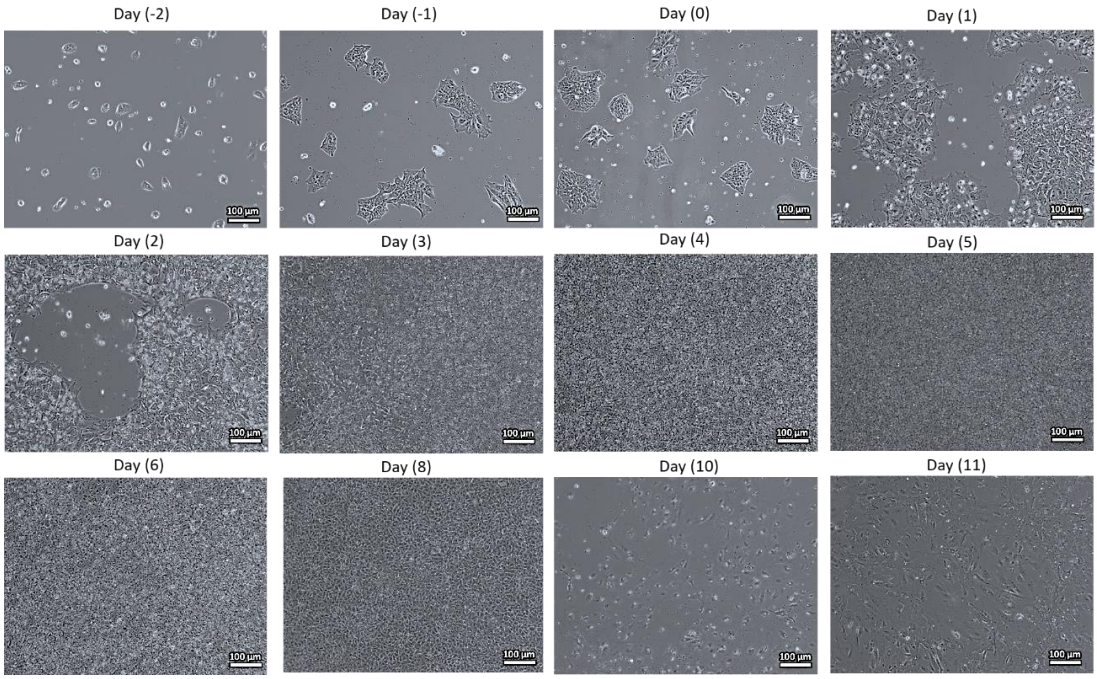

Figure 4.1 ILM images of differentiation of BMECs from hiPSCs (Magnifications: 10X, Scale bars: 100 µM)

4.2 TEER analysis

From the analysis of BBB characterization, TEER is the most crucial one, demonstrating the structural integrity and functional ability of brain ECs. It is also important to determine the starting day of other related experiments, like ICC staining and permeability assays. Therefore, it was done as a part of this thesis, as described in section 3.2.7.1.

As part of this thesis, the TEER values of hiPSCs, hCMEC/D3, and hiPSCs-derived BMECs were measured. This was crucial to observe the difference in resistance of these cells. hiPSCs were counted as the negative control group whereas hCMEC/D3 positive control group. Here, 24 H represented the time after subculturing the cells onto 24-well transwell-clear inserts.

The TEER experiment was repeated two times, and different results were obtained, as shown in Figure 4.2. The differences were the brand of CoL1 and the starting time to measure TEER. The result of the first trial, shown in Figure 4.2A, indicated that the TEER of hCMEC/D3 cell line monolayers lay between 30-40 Ω x cm^2 with a maximum TEER of 36 similar to the literature (Babette Weksler et al., 2013). As for the hiPSCs, TEER values were found to be quite low, around 3 Ω x cm^2 w/o a peak, which came out as expected and were convenient given the characteristics of this cell (Pong et al., 2020). In monolayers of hiPSCs-derived BMECs, these values increased with time and were found close to the values of the positive control group, hCMEC/D3, especially after 96 H, with a maximum value of 23 Ω x cm^2.

As for the second trial of the experiment, shown in Figure 4.2B, the measurement was started 24 H after the subculturing of the cells and repeated every 24 H for 4 days. Here, line graphs much more resembled the graphs in the literature than the first trial although the values were different. According to this, the TEER values of hiPSCs-derived BMECs increased with time, were close to the values of hCMEC/D3 w/o a significant difference, and with a maximum value of 11 Ω x cm^2 at 72 H ($p=0.3$). Also, they were significantly higher than the values of hiPSCs at 72 H ($p =0.05$). Importantly, at 72 H, hiPSCs-derived

BMECs could be counted as purified BMECs to start permeability, ICC, and flow cytometry experiments.

As in the literature, both results demonstrated that the values of TEER could be variable and were dependent on the cell seeding density, culture medium and supplements, coating type and concentration, time, electrode type, transwell pore size, growth area, type, and brand. In addition, the temperature of the experimental environment was highly associated with obtaining the TEER values (Czupalla et al., 2014; Eigenmann et al., 2013; Pong et al., 2020).

A

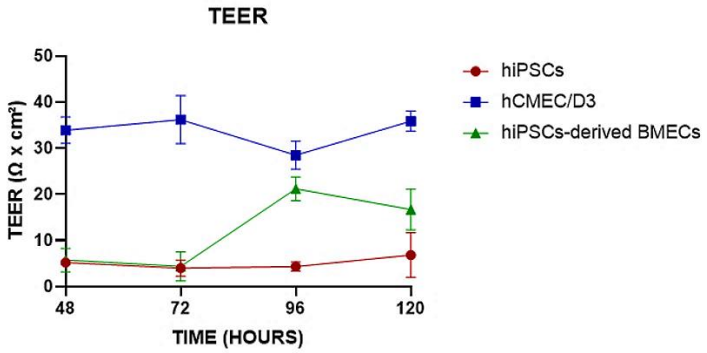

B

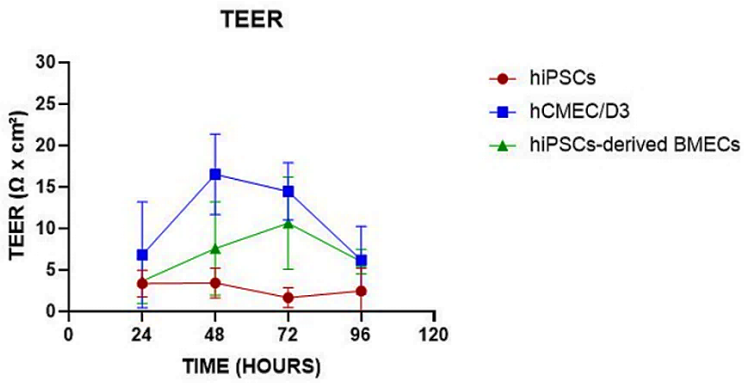

	iPSCs vs hCMEC/D3	iPSCs vs hiPSCs-derived BMECs	hCMEC/D3 vs hiPSCs-derived BMECs
24	0.12033019	0.38841543	0.168717998
48	0.049169011	0.044211512	0.232686243
72	0.04109462	0.052603058	0.368039588
96	0.004624254	0.019272061	0.123033174

Figure 4.2 TEER measurements graphs (A. First trial TEER data, B. Last trial TEER data and ANOVA analysis, $p \leq 0.05$ with standard errors)

4.3 Immunocytochemistry staining

ICC experiment is another characterization assay that visualizes the expression of protein or gene markers specific to cells. Here, the brain ECs (hCMEC/D3 cell line and hiPSCs-derived BMECs) stained on the day maximum TEER observed or on the day purified BMECs observed. They observed whether expressed CD31 and OCLN genes or not, as described in section 3.2.5 and according to Appendix 1. CD31 encodes a human protein, playing a role in EC adhesion and maintaining vascular endothelial barrier function, while OCLN encodes a human TJ.

ICC staining in Figure 4.3 showed that both genes were observed in both cells. However, the expression of OCLN marker were significantly better than hiPSCs-derived BMECs than hCMEC/D3 while CD31 marker was slightly observed. Especially, the formation of TJs in hiPSCs-derived BMECs was seen homogeneously around each of the nuclei.

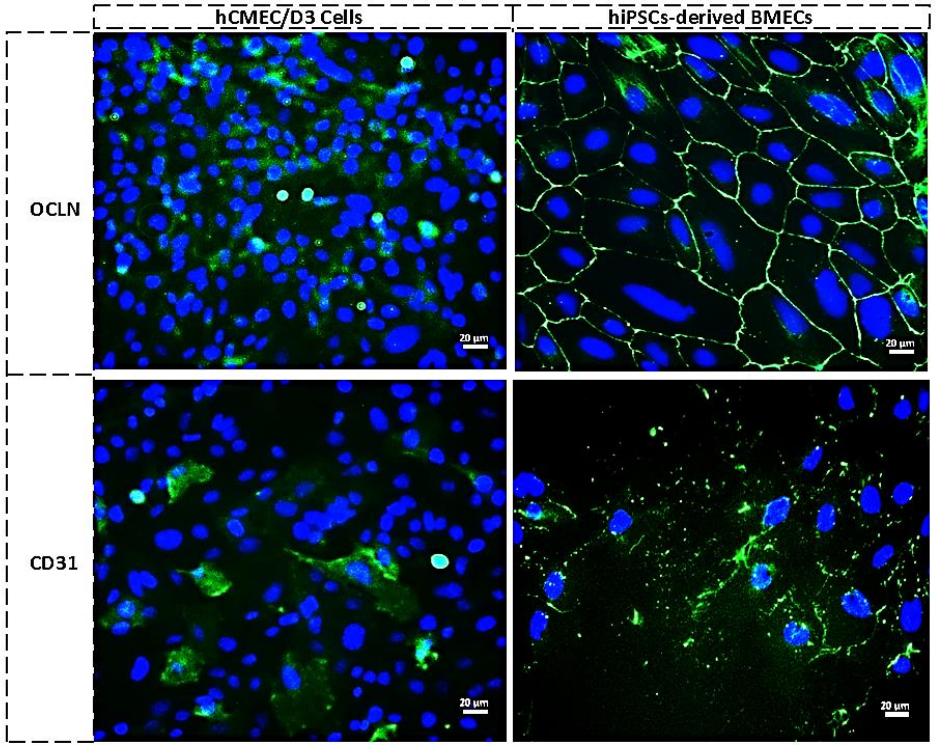

Figure 4.3 Fluorescence microscope images of hCMEC/D3 cells and hiPSCs-derived BMECs at max. TEER, day 10 (48 H) and day 11 (72 H), respectively (Magnifications: 40X, scale bars: 20 µM)

4.4 RT-qPCR

RT-qPCR is a numerical observation of gene expressions specific to cells in real-time and thus it is the best way of showing which genes are expressed out of the variety of genes or proteins of the BBB. In this experiment, based on the literature, several commercially obtained genes, shown in Appendix 2, were tested in hiPSCs, hCMEC/D3, and hiPSCs-derived BMECs as in section 3.2.6 (T. Qian et al., 2017).

GAPDH was used as a house-keeping gene. The normalizations of each gene, reported as a percentage of GAPDH expression (% GAPDH) were shown in Appendix 6.

4.4.1 Gene expression profiles of hCMEC/D3

As shown in Appendix 5, the positive control cell of hiPSCs-derived BMECs of this thesis, hCMEC/D3, was normalized to a cell assured to have no endothelial-specific gene expression, which is hiPSCs. Here, CDH5, CD31, and ABCB1 genes were expressed by hCMEC/D3. The expressions of endothelial marker genes CDH5 and CD31 were prominently greater than hiPSCs. There were no expressions of genes specific to hiPSCs, which are PAX2, SOX2, OCT4, and NANOG genes, the intermediate mesoderm and pluripotency transcription factor genes, respectively. Furthermore, the expressions of glucose transporter gene SLC2A1, vascular endothelial gene CDH5, efflux pump gene ABCB1, TJ protein gene OCLN, and vascular endothelial growth factor or EC progenitors gene KDR in hCMEC/D3 monolayers were significantly increased at 48 H after seeding them on pre-coated transwell-clear inserts. Transporter genes SLC2A1 and ABCB1 were highly expressed in hCMEC/D3 monolayers 72 H after seeding on pre-coated transwell-clear inserts.

4.4.2 Gene expression profiles of hiPSCs-derived BMECs throughout differentiation

As for RT-qPCR results of hiPSCs-derived BMECs, 12 genes including genes specific to brain ECs (CDH5, CD31, ZO-1, OCLN, ABCB1, SLC2A1, TFRC, KDR), hiPSCs (SOX2, OCT4, NANOG), and intermediate mesoderm gene (PAX2) were examined for

their expressions by hiPSCs-derived BMECs day-by-day from the start of the induction (day 0), as shown in Figures starting from Figure 4.4 until 4.10. Here, the legends of figures were inferred from Figure 3.5B as well as the section 3.2.3 and the changes in gene expressions were normalized to positive control, hCMEC/D3 at passage +5. Also, the effect of RA-included EC medium (day 8) on gene expression of hiPSCs-derived BMECs was investigated by changing their culture in UM to EC media 1 day before the protocol described in section 3.2.3.2 (sample D).

In Figure 4.4, there was no expression of the CDH5 gene by hiPSCs-derived BMECs at induction (samples A and B). RA-included EC media has increased the expression of CDH5 (samples C and D), and on day 10, where the cells were purified on ECM mixture, this expression was prominently greater than both hiPSCs-derived BMECs and hiPSCs. Furthermore, hCMEC/D3 had a prominent expression of the CD31 gene. On day 10, where hiPSCs-derived BMECs were subcultured on pre-coated transwells, they expressed CD31 more than hiPSCs but less than hCMEC/D3.

In Figure 4.5, OCLN expression in hCMEC/D3 was less than in hiPSCs. It may be because the iPSCs are transduced from blood cells, PBMCs. Fortunately, hiPSCs-derived BMECs express more OCLN than both hCMEC/D3 and hiPSCs, although there is no gradual increase day-by-day. This better expression was parallel with Figure 4.3, and this gene has been positively affected by both UM and EC medium plus RA. Moreover, the expression of ZO-1 was higher in hiPSC-derived BMECs than both hiPSCs (sample G) and hCMEC/D3 (sample F) and substantially increased in hiPSC-derived BMECs. This increment was gradual and reached a much higher value on day 10 (sample E).

In Figure 4.6, SLC2A1 gene expression was observed by hiPSC-derived BMECs on day 8 (samples C and D). However, at day 10 (sample E), the expression of this gene decreased even though it was much more expressed than hCMEC/D3 and hiPSCs (2-fold). Therefore, SLC2A1 was significantly affected by the presence of RA, and withdrawing RA resulted in a decrease in its expression. However, ABCB1 was highly expressed by hCMEC/D3 than hiPSCs-derived BMECs. Unfortunately, the expression of

this gene by hiPSCs-derived BMECs was little, unlike the literature (Delsing et al., 2018; Lippmann et al., 2014; T. Qian et al., 2017).

In Figure 4.7, hiPSC-derived BMECs expressed the TFRC gene. On day 8, they expressed this gene nearly the same as hCMEC/D3 and on day 10, they expressed more of this gene than on day 6 (2.5-fold) as well as hiPSCs (3-fold) and than hCMEC/D3 (2-fold). Therefore, differentiation and subculturing processes increased its expression.

KDR gene was expressed less by hCMEC/D3 than hiPSCs. On day 0, KDR expression by hiPSC-derived BMECs was the same as hiPSCs. On day 6, its expression was decreased and on day 10, hiPSC-derived BMECs started to express this gene again. The decrease in KDR expression might be due to the fact that the growth area of BMECs decreases day-by-day on 6-well plates and increases when subculturing on 24-well transwells.

In Figure 4.8, there was no PAX2 gene expression by hCMEC/D3 and hiPSCs. In hiPSC-derived BMECs, its expression highly increased on day 6 and was at a fairly high value on day 10. These increments were statistically non-significant and might be because the maximum TEER was observed on day 11, so the purification process of BMECs has not finished yet. hiPSCs expressed SOX2 gene prominently higher than hCMEC/D3. In hiPSC-derived BMECs at day 0, the expression was still preserved as much as hiPSCs. On day 10, the expression was 3-fold less than hiPSCs.

In Figure 4.9, the OCT4 gene was more highly expressed by hiPSCs than hCMEC/D3. In hiPSC-derived BMECs on days 0 and 6, its expression was slightly more than in hiPSCs, but it was non-significant. On day 10, there was lower expression of OCT4, just as in the SOX2 gene. That could be because RA induces differentiation by inhibiting OCT4 (Hanley, Rastegarlari, & Nathwani, 2010; J. Zhang et al., 2015). Finally, there was no NANOG gene expression by hCMEC/D3, and hiPSCs highly expressed this gene. In hiPSC-derived BMECs at days 0 and 6, its expression was less than in hiPSCs. On day 10, its expression was none. Additionally, these results for SOX2, OCT4, and NANOG were consistent with the graph D in Appendix 8.

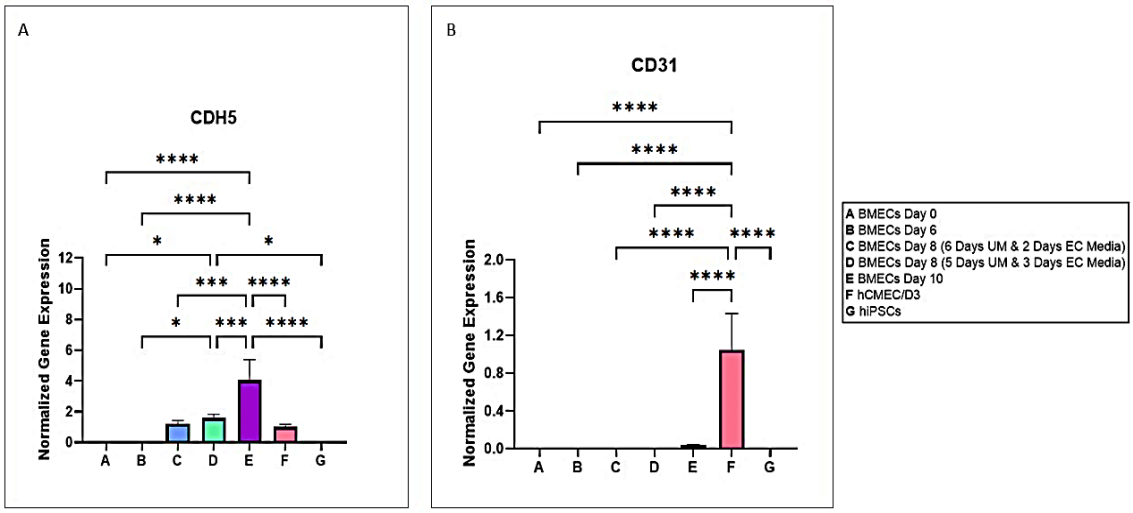

Figure 4.4 RT-qPCR results of normalized endothelial marker gene expressions of hiPSCs-derived BMECs throughout the differentiation, and hiPSCs according to hCMEC/D3 (A. CDH5, B. CD31, *p < 0.05 with standard errors). hCMEC/D3 were cultured on pre-coated T25 flask, hiPSCs were cultured and induced on pre-coated 6-well plates, hiPSCs-derived BMECs were subcultured on pre-coated 24-well transwells on day 9

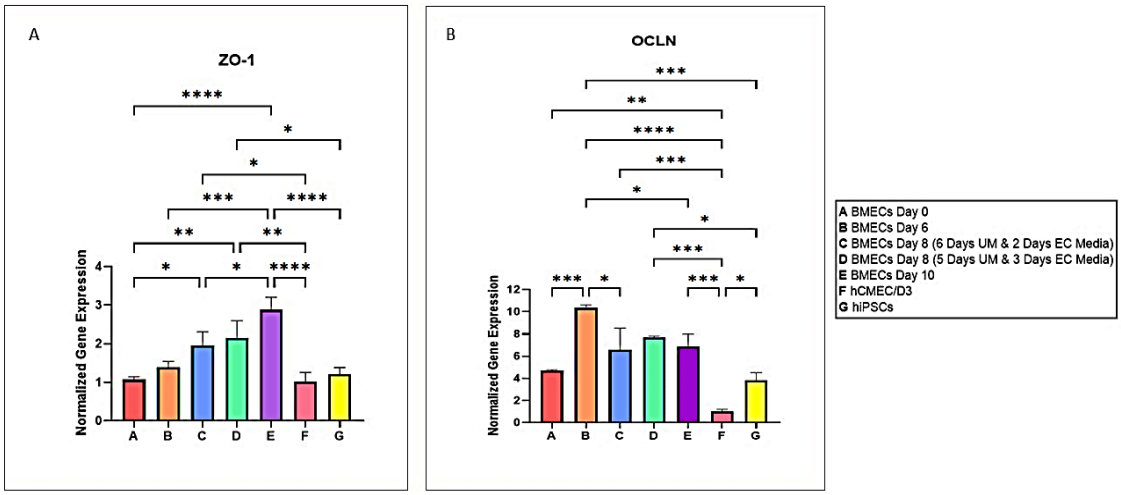

Figure 4.5 RT-qPCR results of normalized TJs gene expressions of hiPSCs-derived BMECs throughout the differentiation, and hiPSCs according to hCMEC/D3 (A. ZO-1, B. OCLN, *p < 0.05 with standard errors). hCMEC/D3 were cultured on pre-coated T25 flask, hiPSCs were cultured and induced on pre-coated 6-well plates, hiPSCs-derived BMECs were subcultured on pre-coated 24-well transwells on Day 9

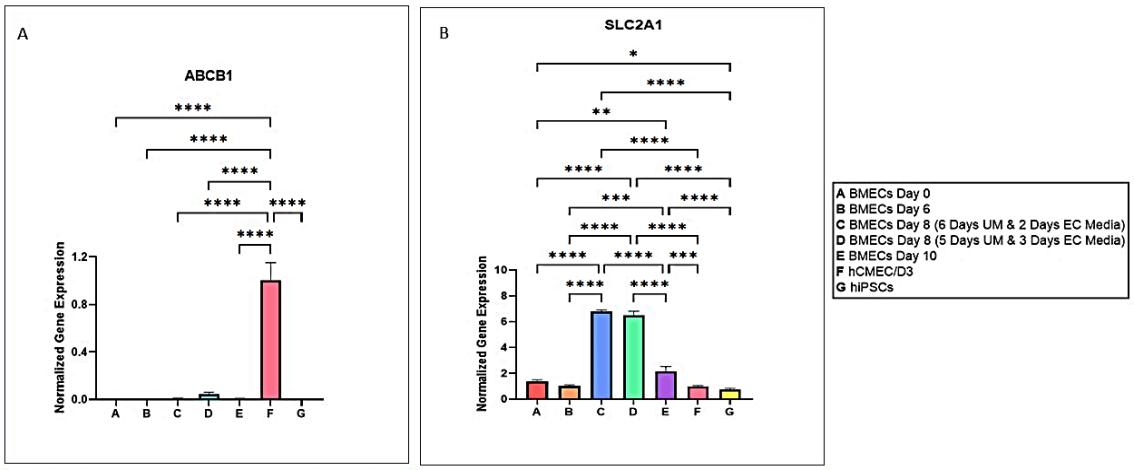

Figure 4.6 RT-qPCR results of normalized transporter gene expressions of hiPSCs-derived BMECs throughout the differentiation, and hiPSCs according to hCMEC/D3 (A. ABCB1, B. SLC2A1, *p < 0.05 with standard errors). hCMEC/D3 were cultured on pre-coated T25 flask, hiPSCs were cultured and induced on pre-coated 6-well plates, hiPSCs-derived BMECs were subcultured on pre-coated 24-well transwells on Day 9

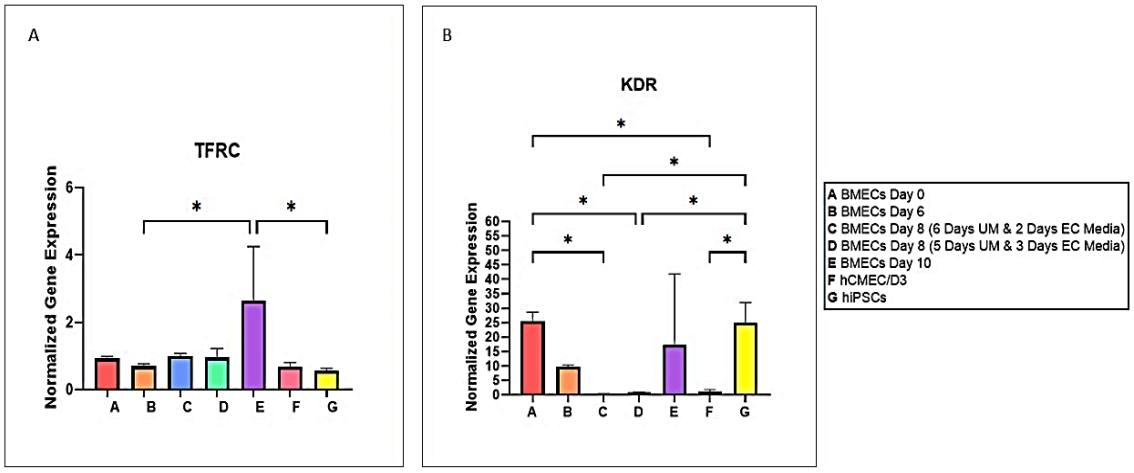

Figure 4.7 RT-qPCR results of normalized gene expressions of hiPSCs-derived BMECs throughout the differentiation, and hiPSCs according to hCMEC/D3 (A. TFRC, B. KDR, *p < 0.05 with standard errors). hCMEC/D3 were cultured on pre-coated T25 flask, hiPSCs were cultured and induced on pre-coated 6-well plates, hiPSCs-derived BMECs were subcultured on pre-coated 24-well transwells on Day 9

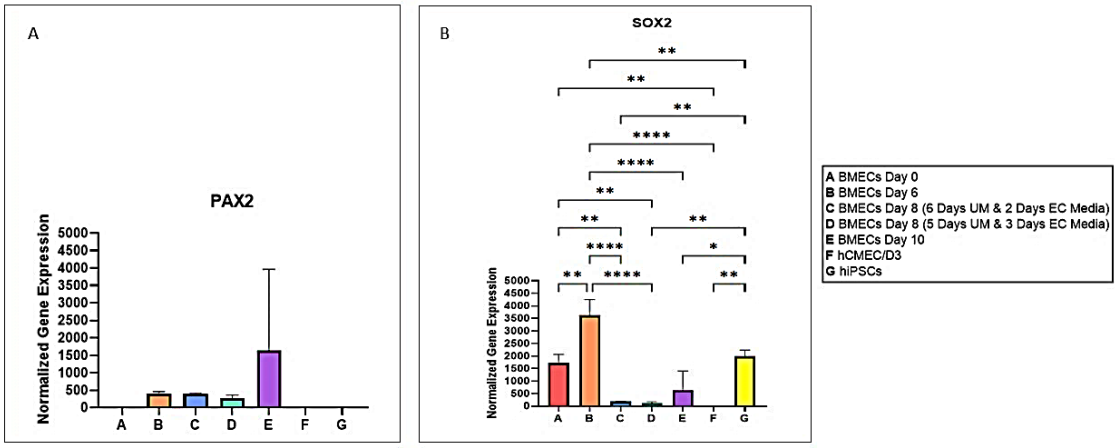

Figure 4.8 RT-qPCR results of normalized gene expressions of hiPSCs-derived BMECs throughout the differentiation, and hiPSCs according to hCMEC/D3 (A. PAX2, B. SOX2, *p < 0.05 with standard errors). hCMEC/D3 were cultured on pre-coated T25 flask, hiPSCs were cultured and induced on pre-coated 6-well plates, hiPSCs-derived BMECs were subcultured on pre-coated 24-well transwells on Day 9

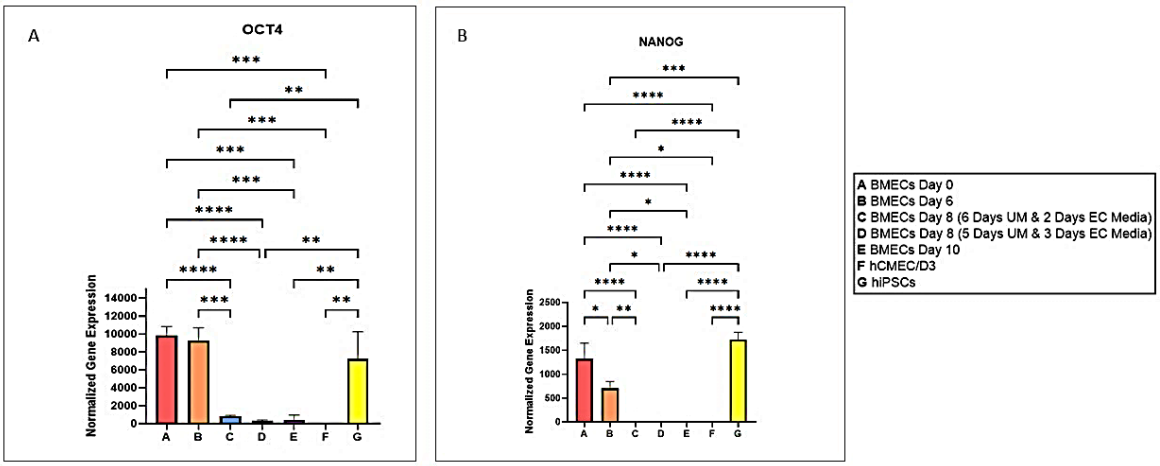

Figure 4.9 RT-qPCR results of normalized gene expressions of hiPSCs-derived BMECs throughout the differentiation, and hiPSCs according to hCMEC/D3 (A. OCT4, B. NANOG, *p < 0.05 with standard errors). hCMEC/D3 were cultured on pre-coated T25 flask, hiPSCs were cultured and induced on pre-coated 6 well plates, hiPSCs-derived BMECs were subcultured on pre-coated 24-well transwells on Day 9

4.4.3 Gene expression profiles of hiPSCs-derived BMECs during subculture/purification process

Figures 4.10, 4.11, and 4.12 demonstrated RT-qPCR results of hiPSCs-derived BMECs after subculturing them onto 24-well transwells, previously coated with CoL1 + FN. These results were normalized to 48 H after subculture of hCMEC/D3 on 24-well transwells previously coated with CoL1. Here, only 5 genes (CDH5, OCLN, ABCB1, SLC2A1, KDR) out of 12 were examined because hiPSCs-derived BMECs better expressed these genes than hCMEC/D3. Samples were chosen to observe brain ECs-specific gene expressions during the purification process of hiPSCs-derived BMECs and whether this information correlated with the TEER data in Figure 4.2B. Sample A represented 48 H after subculturing, just as in TEER, because purifying BMECs started when the cells were subcultured onto pre-coated transwell-clear inserts. Similarly, sample B represented 72 H, and sample C was 96 H.

According to these results, SLC2A1, CDH5, ABCB1, OCLN, and KDR genes' expressions were different between purification days 10, 11, and 12. SLC2A1 and CDH5 were highly expressed on day 10, whereas ABCB1, OCLN, and KDR expression were the most on day 12. In Figure 4.10, the expression of CDH5 by hiPSCs-derived BMECs was statistically higher on day 10 than on days 11 and 12. In all these days, its expression by hiPSCs-derived BMECs was generally better than its expression by hCMEC/D3. Especially, in hiPSCs-derived BMECs at maximum TEER (sample B), OCLN expression was statistically higher than hCMEC/D3 at maximum TEER (sample D). Also, its expression by hiPSCs-derived BMECs increased day-by-day and reached its highest value on day 12. In Figure 4.11, the expression of ABCB1 was similar to the expression of OCLN but with less expression number. Moreover, hiPSCs-derived BMECs expressed SLC2A1 with a decrease day-by-day and at maximum TEER; they expressed this gene as much as hCMEC/D3 at maximum TEER. In Figure 4.12A, hiPSCs-derived BMECs expressed the KDR gene almost the same they expressed the OCLN gene.

From Figure 4.12B, in purified BMECs (day 11 or 72 H according to TEER data in Figure 4.2B), the best-expressed gene was found to be OCLN, which is nearly 5-fold higher than

the OCLN expression of hCMEC/D3. This result was parallel with the results of ICC staining shown in Figure 4.3. The nearest expression to OCLN was observed to be the KDR gene.

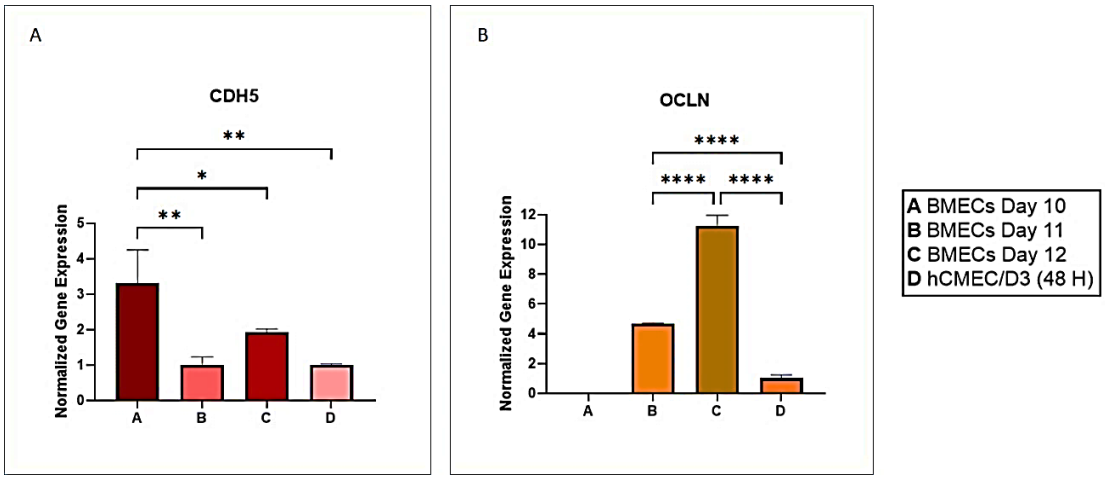

Figure 4.10 RT-qPCR results. (normalized gene expression of hiPSCs-derived BMECs on CoL1 + FN coated-transwells according to hCMEC/D3 on CoL1-coated transwells at maximum TEER, A. CDH5, B. OCLN, *p < 0.05 with standard errors)

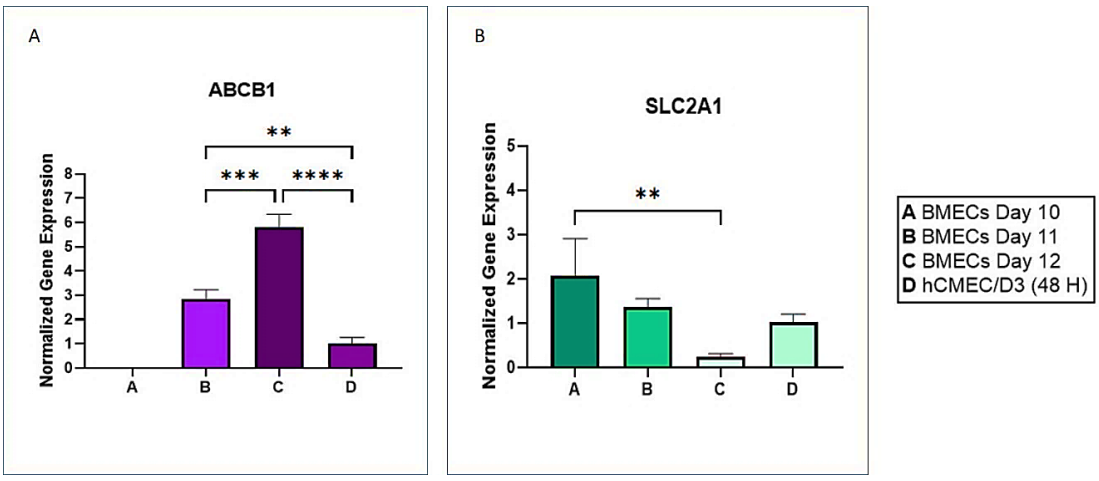

Figure 4.11 RT-qPCR results. (Normalized gene expression of hiPSCs-derived BMECs on CoL1 + FN coated-transwells according to hCMEC/D3 on CoL1-coated transwells at maximum TEER, A. ABCB1, B. SLC2A1, *p < 0.05 with standard errors)

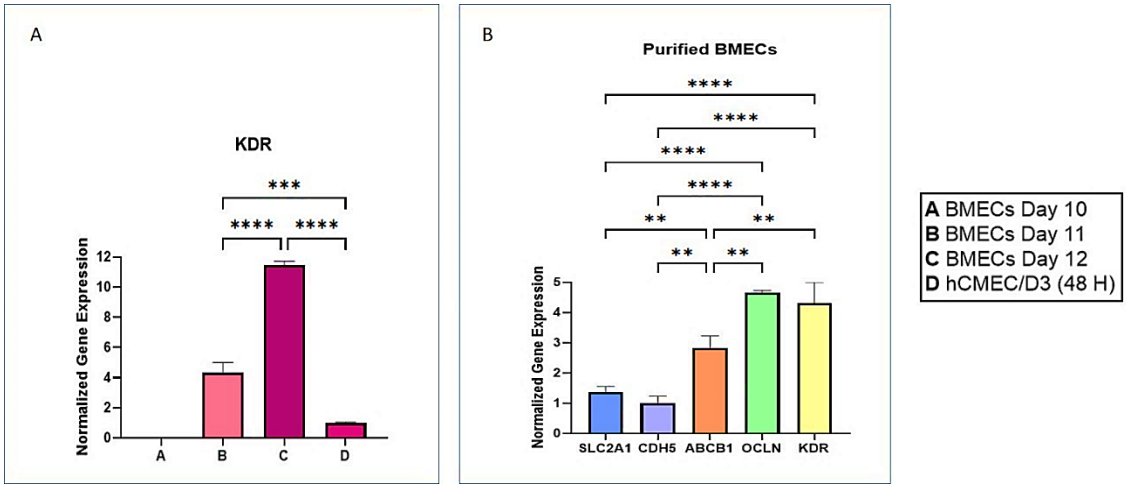

Figure 4.12 RT-qPCR results. (Normalized gene expression of hiPSCs-derived BMECs on CoL1 + FN coated-transwells according to hCMEC/D3 on CoL1-coated transwells at maximum TEER, A. KDR, B. All gene expressions of hiPSCs-derived BMECs at maximum TEER, day 11, *$p < 0.05$ with standard errors)

4.5 Permeability studies

Permeability, as an important phenomenon, evaluates BBB integrity and more importantly, molecules crossing the BBB. Before studying the permeability of novel molecules like MQDs in this thesis, the permeability of already studied molecules in the BBB, such as FD, might be determined as a part of the characterization of the BBB and BBTB before the actual study with MQDs. Therefore, the permeability of both 4 kDA FD and 50 µg/mL MQDs were investigated as described in sections 3.2.7.2 and 3.2.8. The concentration of MQDs was chosen regarding results of LDH assay in Appendix 4. Just as in ICC staining, it was conducted on the day at which the peak was observed, and the TEER value reached its maximum value (Figure 4.2B).

In Figures 4.13B and 4.14B, the groups that transwells previously coated with CoL1 or CoL1 and FN mixture (blanks) were normalized as 100%.

According to the permeability measurements of FD, as shown in Figure 4.13B, the most important result was that adding brain ECs (hCMEC/D3 or hiPSCs-derived BMECs) to the blanks decreased FD passage to the brain side. This result might be possible according

to previous studies (Mendes et al., 2015; Ragnaill et al., 2011). FD4 passage in the monoculture BBB model with hiPSCs-derived BMECs was found to be higher than in the same model with hCMEC/D3. This might be because of the abundancy of TJs, like ZO-1 and OCLN playing role in paracellular transport, in hiPSCs-derived BMECs than in hCMEC/D3. Furthermore, in both co-culture models, BBTBs, the crosstalk between glioblastoma (U87) and brain endothelial cells (hCMEC/D3 or hiPSCs-derived BMECs) impacts BBB integrity and thus decreased FD4 passage. This decrease could be caused by lower expressions of TJs in BBTBs than in BBBs.

As for permeability coefficients in Figure 4.12A, P_e relied between 22-24 x 10^{-5} and there was no statistical significance between all related groups.

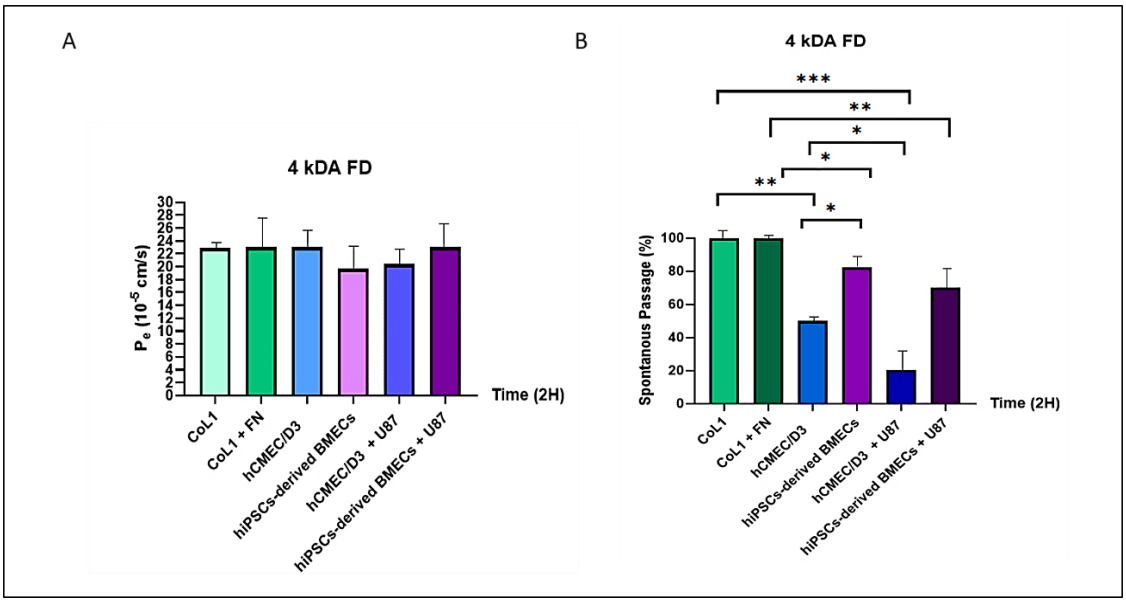

Figure 4.13 Permeability measurement of FITC-dextran (FD) after 2 H of incubation (A. Apparent permeability coefficients, B. Spontaneous passages at excitation/emission: 490/520, *p < 0.05 with standard errors)

As for the permeability of the MQDs, the situation turned out to be slightly different from that of the FD4. The results shown in Figure 4.14B demonstrated that the spontaneous passage of MQDs from hCMEC/D3 monolayers to the brain side was a bit less than the passage of these MQDs from CoL1-coated transwells w/o cells, which was again might reasonable regarding the passage of FD4. Also, adding U87 to the brain side and thus

modeling BBTB caused a statistically significant decrease in the passage of MQDs and therefore, their transition could become problematic. This finding might be due to the fact that the BBTB may have an inhibitor protein that blocks the pathway for MQDs, or the pathway was broken.

Therefore, the blood-to-brain transit behavior of MQDs was similar to that of FD in BBB and BBTB models with hCMEC/D3 and hCMEC/D3 + U87, respectively.

In the BBB model with hiPSCs-derived BMECs, the MQDs' passage was slightly higher than the passage from (CoL1+ FN)-coated transwell alone w/o statistical significance. This could be because proteins specified for the transcytosis of MQDs were expressed in hiPSCs-derived BMECs, as opposed to hCMEC/D3. Also, the time (2 H) was insufficient to observe MQDs' transport across the BBB and get reliable permeability data. Unlike the BBTB model with hCMEC/D3 and U87, co-culturing hiPSCs-derived BMECs with U87 led to a significant increase in MQDs passage. Here, adding U87 could cause a leaky BBTB presenting fenestrations for MQDs to be quickly passed to the brain side in 2 H.

Additionally, in Figure 4.14A, MQDs' permeability coefficients while crossing both BBTBs were statistically higher than when crossing the BBBs. The permeability coefficient of the hiPSCs-derived BMECs + U87 group was the highest one (324×10^{-6}). The permeability coefficient in the blank group, CoL1 was higher than both the BBB model with hCMEC/D3 and the BBTB model with hCMEC/D3 + U87. For the second blank group, CoL1 + FN, the permeability coefficient was lower than the BBTB model with hiPSCs-derived BMECs + U87. These findings might occur owing to the same reasons for spontaneous passages.

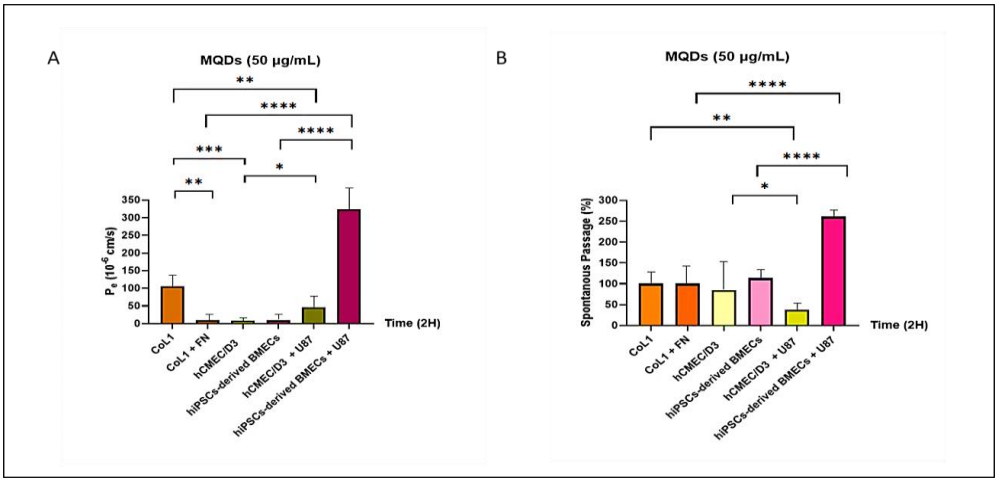

Figure 4.14 Permeability measurement of MQDs after 2 H of incubation (A. Apparent permeability coefficients, B. Spontaneous passages at excitation/emission: 586/647 nm, Texas Red, *p < 0.05 with standard errors)

4.6 Flow cytometry analysis

For the second experiment with the models and MQDs, due to the fluorescence property of MQDs, flow cytometry was conducted as described in section 3.2.8.2 instead of visualization via a fluorescence microscope. This demonstrated quantitative and more accurate data than the fluorescence microscopy technique. This analysis determined the passage from the BBTB models and then the nanomaterials' uptake by the cells in the brain side.

Firstly, as shown in Figures 4.15A and 4.17A, the regions where the cluster of cells was positioned were determined by drawing them as red gates, and then axes were determined over the untreated group, namely naïve. On these axes, the percentage of cells in the positive (right) region of the axis automatically appeared and indicated NM presence in tumor cells (Figures 4.15B and 4.17B).

According to Figure 4.15B, the positive cells' percentage in the group treated with 50 µg/mL MQDs was 10 times higher than naïve, meaning that most of the MQDs passed through the barrier and were taken up by U87 cells after 24 H. Its analysis, shown in Figure 4.16, showed the slight slip of the treated group as well as the significant uptake of MQDs.

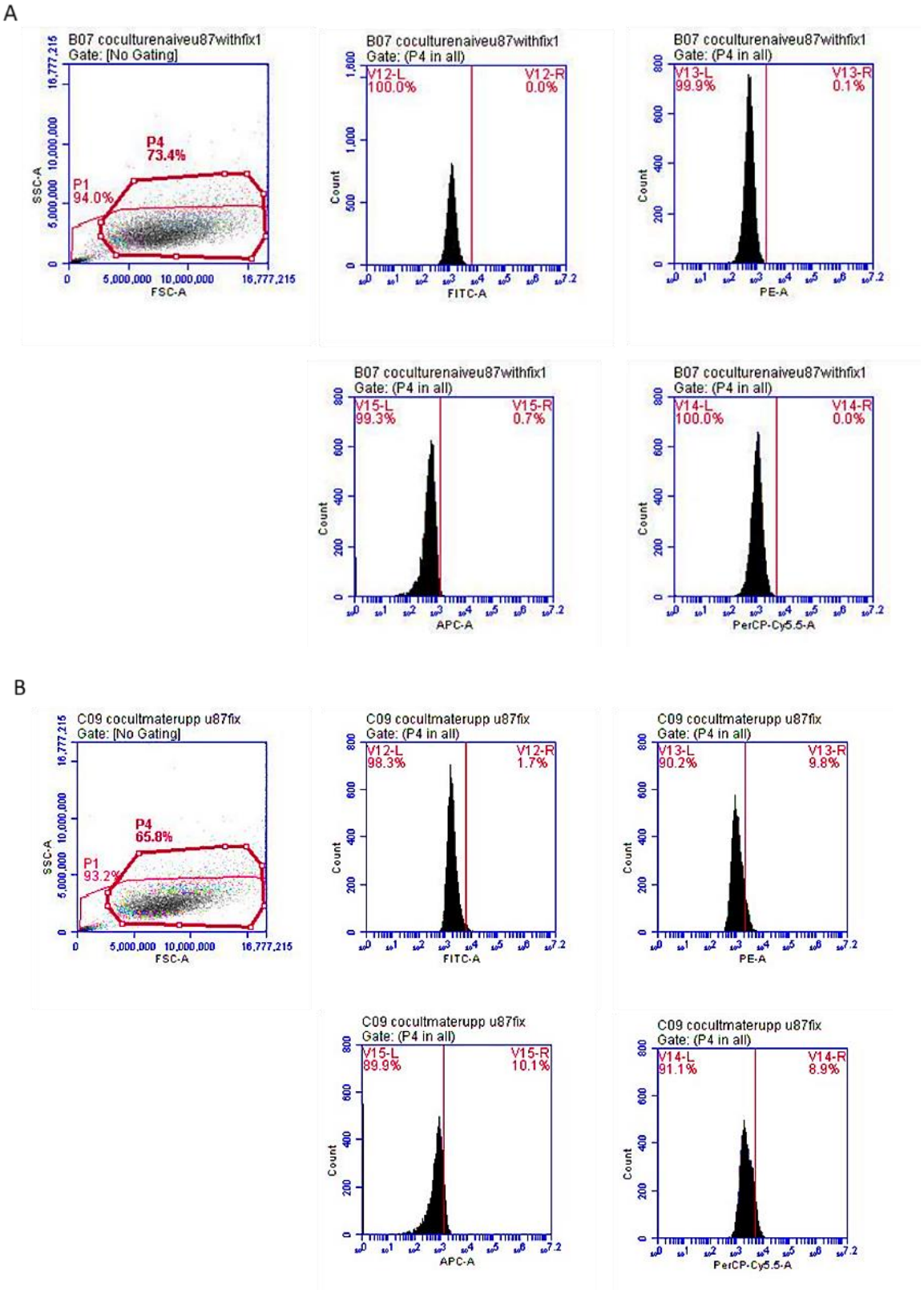

Figure 4.15 Flow cytometry data of co-cultured BBB model (BBTB with hCMEC/D3 + U87) (A. Fixed untreated / Naïve U87 cells, B. Fixed U87 cells treated with MQDs from the upper chamber)

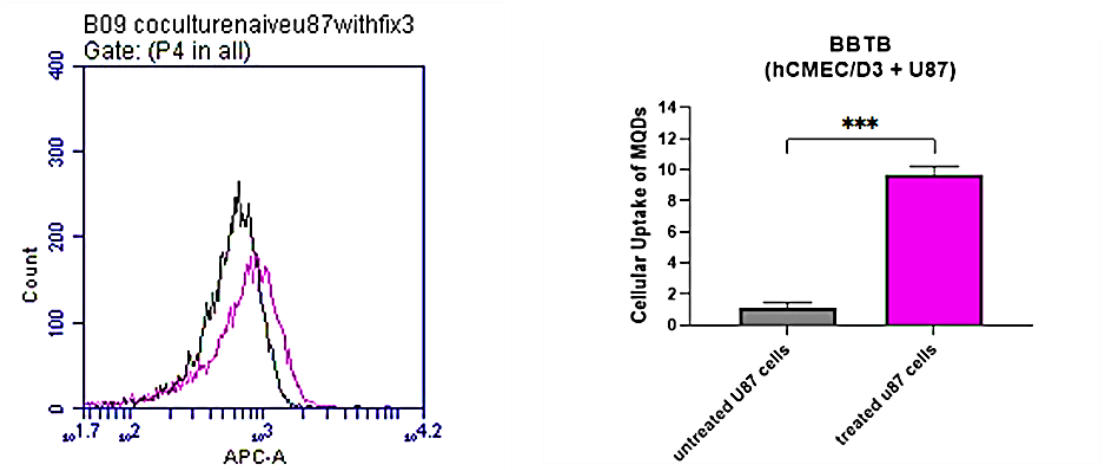

Figure 4.16 Fluorescent data by flow cytometry analysis showing MQDs' uptake by U87 cells in hCMEC/D3 BBTB model (*p < 0.05 with standard errors)

In Figure 4.18, the positive number of cells in the treated group was slightly higher than the naïve group (3-fold), so MQDs passed through the barrier and therefore were taken up by U87. However, the percentage of MQDs' uptake in the BBTB model formed by hiPSCs-derived BMECs was lower than in the hCMEC/D3-formed BBTB model. The reason was that all MQDs could not pass through the blood and reach the brain; some of them may be recognized by efflux transporters, like P-gp encoded by highly expressed ABCB1 gene, in these hiPSCs-derived BMECs, and were efficiently shuttled back into the blood.

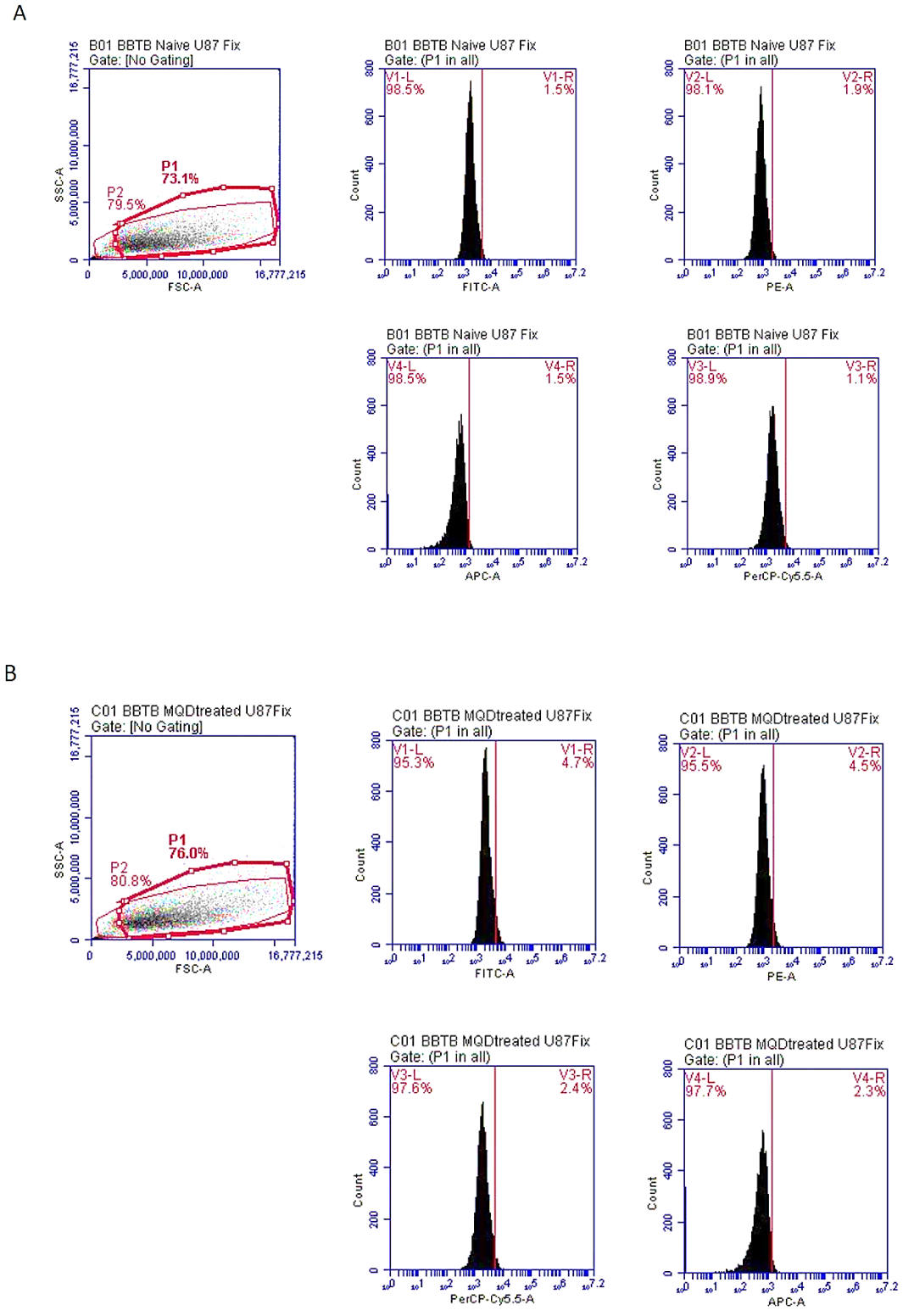

Figure 4.17 Flow cytometry data of co-cultured BBB model (BBTB with hiPSCs-derived BMECs+ U87) (A. Fixed untreated / Naïve U87 cells, B. Fixed U87 cells treated with MQDs from the upper chamber)

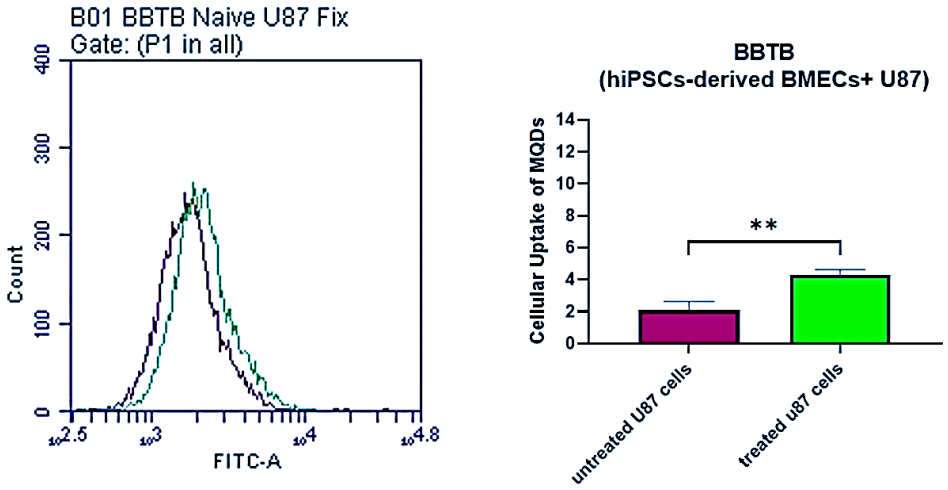

Figure 4.18 Fluorescent data by flow cytometry analysis showing MQDs' uptake by U87 cells in hiPSCs-derived BBTB model (*p < 0.05 with standard errors)

5. DISCUSSION

hCMEC/D3 is a previously used cell line in studying the biology of brain endothelium, the CNS and its drug candidates, and the treatment of neurological diseases (Babette Weksler et al., 2013; BB Weksler et al., 2005). It could demonstrate most of the unique characteristics of the BBB by expressing several genes related to the structural and functional formation of brain endothelium w/o the need to culture it with another BBB-related cell (Appendix 5). Therefore, it was an excellent choice to use as a positive control group in this thesis study.

Nevertheless, researchers found achieving a fully developed brain EC phenotype requires the influence of other NVU components, such as astrocytes and pericytes, which modulate gene expression. Alternatively, enhancing the hCMEC/D3 cell culture medium with soluble factors could support further cell maturation toward BBB-like phenotype. However, those factors increase the cost and time needed to model the BBB in vitro. Therefore, a more intricate model in vitro might be necessary to replicate the BBB accurately (Babette Weksler et al., 2013). Using hiPSCs, better BMECs could be formed to develop patient-specific BBB models.

Besides, animal models ultimately fail in clinics despite the promising outcomes observed with numerous drug candidates in these models (Perrin, 2014). his failure highlights the urgency for more refined BBB models in vitro that offer greater translational relevance to humans in vivo. In this regard, these sophisticated BBBs might be models derived from hiPSCs.

Like primary cells, co-culturing human BMECs with other hiPSC-derived cells in NVU can enhance TEER values and barrier function. However, adding cells may be unnecessary for BMECs to reach TEER levels physiologically. They mainly improve barrier properties when initial conditions are suboptimal or under stress (Jamieson, Linville, Ding, Gerecht, & Searson, 2019; Workman & Svendsen, 2020). Thus, hiPSCs-drived BMEC monolayers alone might be enough to encounter the properties of the BBB, just as in this thesis study.

The TEER values of hCMEC/D3 cell line and hiPSCs-derived BMECs of this thesis study were close and statistically higher than the TEER values of hiPSCs. Therefore, the BBB integrity was managed in hiPSCs-derived BMECs.

Maximum TEER was a crucial phenomenon in BBB characterization. When TEER was at its maximum value, one can conclude that the barrier integrity was relatively high, and the confluency was almost 100 %. hCMEC/D3 and hiPSCs-derived BMECs reached their maximum values at different times (respectively 48 H and 72 H after seeding onto pre-coated 24-well transwells). At 72 H, hiPSCs-derived BMECs were pure. Moreover, this thesis's maximum TEER times were the starting times of ICC, flow cytometry, and permeability studies.

The TEER value of hiPSCs-derived BMECs was nearly 11 Ω x cm^2. There was no accurate TEER value for BBBs, leading to a variety of TEER values of BMECs in the literature. The varieties in TEER may be due to the position and angle of electrodes while measuring the TEER and the variables described in the results section, on which TEER values are dependent. Additionally, hiPSCs used in the thesis were not obtained commercially as a cell line, such as IMR90-4. They were transduced from human blood. Therefore, it reveals the originality of this thesis study compared to other studies in the literature.

hiPSC-derived BMECs were frozen on day 8 if not used immediately. Levels of gene expressions might be affected by the freezing process of non-purified BMEC-like cells as well as the changes in differentiation protocol, such as cell seeding density, which could further change the differences in brain ECs-related gene expression profiles between BMECs, hCMEC/D3, and hiPSCs (Delsing et al., 2018).

According to the RT-qPCR profiling of this thesis study, SLC2A1, TFRC, OCLN, and ZO-1 genes' expressions were higher in hiPSCs-derived BMECs during the differentiation process than in the hCMEC/D3 cell line (section 4.4). In hiPSCs-derived BMECs subcultured on transwells pre-coated with CoL I + FN, several genes specific to brain ECs, which are SLC2A1, OCLN, KDR, CDH5, and ABCB1 were prominently

expressed more than hCMEC/D3 (Figure 4.12B). Therefore, with the help of stem cell technology, better brain ECs could be created from hiPSCs, and the human in vitro BBB model by using hiPSCs-derived BMECs could resemble the in vivo BBB more than the BBB model with hCMEC/D3 monolayers.

hiPSCs transduced via SeV vectors from PBMCs exhibited pluripotency genes expressions such as endogenous OCT4, SOX2, and NANOG (Appendix 8) (Fusaki, Ban, Nishiyama, Saeki, & Hasegawa, 2009; Ye & Wang, 2018).

The numbers in gene expressions differed at the steps of the differentiation process of hiPSCs to BMECs, including induction, expansion, and purification by subculture. Here, RA was an essential factor for inducing expressions of brain ECs-specific genes and inhibiting hiPSCs-specific genes (Hanley, Rastegarlari, & Nathwani, 2010; J. Zhang et al., 2015). For example, the thesis study found that the expressions of pluripotency transcription factor genes in hiPSCs-derived BMECs were almost nonexistent when they expanded in the EC medium with RA and bFGF. Also, the expression of SLC2A1 was significantly affected by RA and bFGF treatment. Even though non-purified BMEC-like cells expressed this gene on day 10, withdrawing RA from the EC culture media on the same day decreased its expression (T. Qian et al., 2017). Furthermore, its expression profile by hiPSCs was almost the same as that of hCMEC/D3, which could be possible according to a study by Al-Ahmad et al. It may be because cells isolated from PBMCs possess glucose transporters (Al-Ahmad, 2017; Neal et al., 2019).

Out of the investigated brain ECs-specific genes in this thesis study, TFRC is an essential gene for RMT, enabling the transport of antibodies of anti-TfR across the BBB and having the potential for improving drug delivery to the brain by acting as drug transporters (Di Marco et al., 2020; Goldeman et al., 2021). In the thesis study, hiPSCs-derived BMECs expressed this gene, and that expression increased when the cells were purified by subculturing.

TJs encode the OCLN gene. hiPSCs-derived BMECs expressed the OCLN gene at high levels. Its expression increased during induction and was protected during expansion,

although the RA lowered its level. At day 11, its expression by purified BMECs was almost 5 times higher than the expression of this gene in hCMEC/D3, which was consistent with the ICC where TJs formed better in hiPSCs-derived BMECs than hCMEC/D3. Also, ZO-1 expression increased day-by-day, and EC medium plus RA significantly increased levels of ZO-1 expression, reaching the highest level on day 10, similarly in the literature (T. Qian et al., 2017).

KDR was highly expressed by hiPSCs-derived BMEC during their purification process due to the growth of ECs, and this expression was much higher than that of hCMEC/D3.

hiPSCs-derived BMECs expressed CDH5 expression profile after treatment with RA-included EC culture media, as in literature (T. Qian et al., 2017). Although there was no or little detection of CDH5 expression in the induction process with UM on days 0 and 6, non-purified BMEC-like cells cultured in EC media starting at day 8 suddenly expressed this gene and acquired it during purification by subculture on pre-coated transwells showing the maturation of brain ECs. However, it was lower on days 11 and 12 compared to the second day of purification, day 10 (Lippmann et al., 2012). Therefore, an ECM mixture with collagens and fibronectin as coating material and EC media could be another crucial factor affecting brain EC-specific gene expression.

Permeability assays informed whether the fluorescent molecules crossed the BBBs and BBTBs before reaching the healthy brain or brain side with tumors. As mentioned in section 4.5, brain ECs in pre-coated transwells decreased the spontaneous crossing of FD4 molecules in both BBB models (monolayers of hCMEC/D3 or hiPSCs-derived BMECs). This finding demonstrated the development of the BBBs as a protective membrane. In BBB and BBTB models, the transport of FD4 molecules was carried by the paracellular diffusion pathway and directly related to the number of TJs presenting on brain ECs. Based on this information, the passage of FD4 in the BBB model with hiPSCs-derived BMECs was more straightforward than in models with hCMEC/D3 thanks to better TJs' expression, and adding tumor cells to both models decreased the spontaneous passage of these molecules. Similarly, hCMEC/D3 monolayers lowered the passage of MQDs, and the presence of U87 decreased this passage even more, which might be due

to proteins presenting on brain ECs for inhibiting MQDs to cross the BBB or the presence of impaired pathway specific for MQDs passage. However, BBTB with hiPSCs-derived BMECs and U87 led to leaks on brain ECs, improving the passage of MQDs to the brain side. The reason behind the differences in findings of permeability studies with FD4 and MQDs in different groups of the models may be molecules' passage or NMs through BBB is related to properties of those molecules or NMs and the transporters or inhibitors expressed in the BBBs or BBTBs (Fong, 2015). Also, the adhesion of brain ECs on semipermeable membranes may follow an unpredictable pattern and result in unreliable permeability measurements (Gomes et al., 2016; Naik & Cucullo, 2012).

In both BBTB models, $Ti_3C_2T_x$ MQDs, shown to possess autofluorescence properties, were tracked by flow cytometry after crossing brain ECs. They were given to the brain ECs from the upper side of the transwells, crossed the barriers, and entered the tumor cell. However, these uptakes were different numerically. This difference may be since ABCB1 encoding the transporters of efflux mechanism like P-gp was expressed more in hiPSCs-derived BMECs than hCMEC/D3 (Delsing et al., 2018). From this result, the penetration of some molecules, like MQDs as NMs in this thesis, can be inhibited; they can easily pumped out before reaching brain tumors, and therefore, limited effectiveness can occur in BBB models with hiPSCs-derived BMECs (Figure 4.18) (Löscher & Potschka, 2005; Mahringer & Fricker, 2016; Praça et al., 2019).

6. CONCLUSION

BBB models in vitro have been utilized for several decades and have significantly contributed to studying cellular and molecular mechanisms involved in BBB formation and development. BBTB models in vitro have been beneficial for understanding the environment of neurological diseases and, thus, better treating them.

BBB integrity can be assessed in vitro by measuring TEER and evaluating cell monolayer permeability with molecules.

Researchers have used primary brain ECs and brain EC lines in the beginning for modeling human BBBs; however, they cannot create the exact phenotypes and properties of the BBB. For this reason, improvements in the use of iPSCs to develop iPSCs-derived BBB models provide information about several CNS transportation and signaling mechanisms for GBM therapy with nanosystems.

Human cells are essential when investigating human-specific transporters, receptors, or immunological concerns. Thus, applying highly purified BMECs derived from hiPSCs of human PBMCs could represent a significant advancement in BBB research, such as drug permeability studies, neurological disease modelings, and finding novel systems for disease therapy. Besides, treating BMECs with RA-included EC media during their differentiation and purifying them on ECMs are crucial to creating a well-developed characterization of brain ECs.

Nanotechnology and the use of NMs, even with their various combinations, in tumor therapy have become popular among researchers owing to the excellent physiochemical properties of NMs to fight against growing multiple tumor cell types, especially GBM. In this context, pre-clinical and clinical studies with novel NMs are increasing in a way researchers cannot ignore. MQDs were comparatively new in CNS-related research and nanomedicine areas against brain tumors.

The hiPSCs-derived BBB model developed in the thesis study exhibits promising barrier properties. It may serve as a personalized and pivotal BBB model in vitro for pharmaceutics and nanotechnology in exploring BBB permeability to prospective therapeutic agents.

In the realm of BBB-related studies, MQDs stand out as a preferred choice for researchers. Their ease of trackability, wettability, immunomodulation effects, surface chemistry rich in functional groups, and electrical conductivity provide a robust foundation for confident research decisions.

For future experiments, the BBTB model could be developed by isolating brain tumors from a patient with GBM and primarily culturing them. Other cells, like glial cells, astrocytes, and pericytes derived from hiPSCs, might be cultured together in 2D or a microfluid chip in 3D to fully develop the human BBB model. Also, hiPSCs can be transduced from the blood of other humans, and differences in BBB anatomy and physiology between humans could be investigated to enhance the research for patient-specific modeling in GBM therapy.

Additionally, BBB studies using humanized rodents might be conducted to trace the molecules better and more accurately analyze the desired therapeutic effect of NMs. As for NMs, different analyses to understand their use and impact in the BBB, such as confocal microscopy to image the spatial distribution of NMs as well as their uptake by the U87 cells, Raman spectroscopy to identify the chemical changes in GBM with and w/o NM, and permeability with inhibitors of transport mechanisms to investigate which way the NMs use for crossing BBB might be conducted.

REFERENCES

Abbott, N. J. (2013). Blood–brain barrier structure and function and the challenges for CNS drug delivery. *Journal of inherited metabolic disease, 36*(3), 437-449.

Abbott, N. J., Dolman, D. E., Drndarski, S., & Fredriksson, S. M. (2012). An improved in vitro blood–brain barrier model: rat brain endothelial cells co-cultured with astrocytes. *Astrocytes: Methods and Protocols*, 415-430.

Abbott, N. J., Patabendige, A. A., Dolman, D. E., Yusof, S. R., & Begley, D. J. (2010). Structure and function of the blood–brain barrier. *Neurobiology of disease, 37*(1), 13-25.

Abbott, N. J., Rönnbäck, L., & Hansson, E. (2006). Astrocyte–endothelial interactions at the blood–brain barrier. *Nature reviews neuroscience, 7*(1), 41-53.

Al-Ahmad, A. J. (2017). Comparative study of expression and activity of glucose transporters between stem cell-derived brain microvascular endothelial cells and hCMEC/D3 cells. *American Journal of Physiology-Cell Physiology, 313*(4), C421-C429.

Alahmari, A. (2021). Blood-brain barrier overview: structural and functional correlation. *Neural Plasticity, 2021*.

Alimonti, J. B., Ribecco-Lutkiewicz, M., Sodja, C., Jezierski, A., Stanimirovic, D. B., Liu, Q., . . . Bani-Yaghoub, M. (2018). Zika virus crosses an in vitro human blood brain barrier model. *Fluids and Barriers of the CNS, 15*, 1-9.

Argaw, A. T., Gurfein, B. T., Zhang, Y., Zameer, A., & John, G. R. (2009). VEGF-mediated disruption of endothelial CLN-5 promotes blood-brain barrier breakdown. *Proceedings of the National Academy of Sciences, 106*(6), 1977-1982.

Arvanitis, C. D., Ferraro, G. B., & Jain, R. K. (2020). The blood–brain barrier and blood–tumour barrier in brain tumours and metastases. *Nature Reviews Cancer, 20*(1), 26-41.

Azad, T. D., Pan, J., Connolly, I. D., Remington, A., Wilson, C. M., & Grant, G. A. (2015). Therapeutic strategies to improve drug delivery across the blood-brain barrier. *Neurosurgical focus, 38*(3), E9.

Bagchi, S., Chhibber, T., Lahooti, B., Verma, A., Borse, V., & Jayant, R. D. (2019). In-vitro blood-brain barrier models for drug screening and permeation studies: an overview. *Drug Design, Development and Therapy, 13*, 3591.

Bamji-Mirza, M., Callaghan, D., Najem, D., Shen, S., Hasim, M. S., Yang, Z., & Zhang, W. (2014). Stimulation of insulin signaling and inhibition of JNK-AP1 activation protect cells from amyloid-β-induced signaling dysregulation and inflammatory response. *Journal of Alzheimer's Disease, 40*(1), 105-122.

Benson, K., Cramer, S., & Galla, H.-J. (2013). Impedance-based cell monitoring: barrier properties and beyond. *Fluids and Barriers of the CNS, 10*(1), 1-11.

Blanchard, J. W., Bula, M., Davila-Velderrain, J., Akay, L. A., Zhu, L., Frank, A., . . . Lin, Y.-T. (2020). Reconstruction of the human blood–brain barrier in vitro reveals a pathogenic mechanism of APOE4 in pericytes. *Nature medicine, 26*(6), 952-963.

Boltman, T., Meyer, M., & Ekpo, O. (2023). Diagnostic and Therapeutic Approaches for Glioblastoma and Neuroblastoma Cancers Using Chlorotoxin Nanoparticles. *Cancers, 15*(13), 3388.

Booth, R., & Kim, H. (2012). Characterization of a microfluidic in vitro model of the blood-brain barrier (μBBB). *Lab on a Chip, 12*(10), 1784-1792.

Bowman, P. D., Betz, A. L., Ar, D., Wolinsky, J. S., Penney, J. B., Shivers, R. R., & Goldstein, G. W. (1981). Primary culture of capillary endothelium from rat brain. *In vitro, 17*, 353-362.

Bowman, P. D., Ennis, S. R., Rarey, K. E., Lorris Betz, A., & Goldstein, G. W. (1983). Brain microvessel endothelial cells in tissue culture: A model for study of blood-brain barrier permeability. *Annals of Neurology: Official Journal of the American Neurological Association and the Child Neurology Society, 14*(4), 396-402.

Brooks, D. (2009). The endosomal network. *International journal of clinical pharmacology and therapeutics, 47*, S9-17.

Burek, M., Salvador, E., & Förster, C. Y. (2012). Generation of an immortalized murine brain microvascular endothelial cell line as an in vitro blood brain barrier model. *JoVE (Journal of Visualized Experiments)*(66), e4022.

Cafiso, D. S. (2017). Influence of charges and dipoles on macromolecular adsorption and permeability. In *Permeability and stability of lipid bilayers* (pp. 179-195): CRC Press.

Calabrese, G., De Luca, G., Nocito, G., Rizzo, M. G., Lombardo, S. P., Chisari, G., . . . Conoci, S. (2021). Carbon dots: an innovative tool for drug delivery in brain tumors. *International journal of molecular sciences, 22*(21), 11783.

Canfield, S. G., Stebbins, M. J., Morales, B. S., Asai, S. W., Vatine, G. D., Svendsen, C. N., . . . Shusta, E. V. (2017). An isogenic blood–brain barrier model comprising brain endothelial cells, astrocytes, and neurons derived from human induced pluripotent stem cells. *Journal of neurochemistry, 140*(6), 874-888.

Cardoso, F. L., Brites, D., & Brito, M. A. (2010). Looking at the blood–brain barrier: molecular anatomy and possible investigation approaches. *Brain research reviews, 64*(2), 328-363.

Cecchelli, R., Aday, S., Sevin, E., Almeida, C., Culot, M., Dehouck, L., . . . Ferreira, L. (2014). A stable and reproducible human blood-brain barrier model derived from hematopoietic stem cells. *PloS one, 9*(6), e99733.

Ceylan, A., Uyar, R., Çelik, D., Rafieerad, A., Çinar, O. O., Summak, G. Y., . . . Turktas, M. (2024). Spatial transcriptomics reveals the interplay between cancer and immune cells directed by MXene quantum dots. *Nano today, 56*, 102285.

Chakraborty, P., Das, S. S., Dey, A., Chakraborty, A., Bhattacharyya, C., Kandimalla, R., . . . Kant, S. (2022). Quantum dots: The cutting-edge nanotheranostics in brain cancer management. *Journal of controlled release, 350*, 698-715.

Chang, C.-Y., Ting, H.-C., Liu, C.-A., Su, H.-L., Chiou, T.-W., Lin, S.-Z., . . . Ho, T.-J. (2020). Induced pluripotent stem cell (iPSC)-based neurodegenerative disease models for phenotype recapitulation and drug screening. *Molecules, 25*(8), 2000.

Cilingir, E. K., Hettiarachchi, S. D., Zhou, Y., Ferreira, B. C., Vanni, S., Leblanc, R. M., & Graham, R. M. (2022). Cell-nucleus Targeted Peptide Tethered Quadruple Carbon Dots for Treatment of High-grade Gliomas.

Coisne, C., Dehouck, L., Faveeuw, C., Delplace, Y., Miller, F., Landry, C., . . . Tremblay, P. (2005). Mouse syngenic in vitro blood–brain barrier model: a new tool to examine inflammatory events in cerebral endothelium. *Laboratory investigation, 85*(6), 734-746.

Cucullo, L., Couraud, P.-O., Weksler, B., Romero, I.-A., Hossain, M., Rapp, E., & Janigro, D. (2008). Immortalized human brain endothelial cells and flow-based vascular modeling: a marriage of convenience for rational neurovascular studies. *Journal of Cerebral Blood Flow & Metabolism, 28*(2), 312-328.

Czupalla, C. J., Liebner, S., & Devraj, K. (2014). In vitro models of the blood–brain barrier. *Cerebral Angiogenesis: Methods and Protocols*, 415-437.

Daneman, R. (2012). The blood–brain barrier in health and disease. *Annals of neurology, 72*(5), 648-672.

Daneman, R., & Prat, A. (2015). The blood–brain barrier. *Cold Spring Harbor perspectives in biology, 7*(1), a020412.

Daneman, R., Zhou, L., Agalliu, D., Cahoy, J. D., Kaushal, A., & Barres, B. A. (2010). The mouse blood-brain barrier transcriptome: a new resource for understanding the development and function of brain endothelial cells. *PloS one, 5*(10), e13741.

de Rus Jacquet, A., Denis, H. L., Cicchetti, F., & Alpaugh, M. (2021). Current and future applications of induced pluripotent stem cell-based models to study pathological proteins in neurodegenerative disorders. *Molecular Psychiatry, 26*(7), 2685-2706.

Dehouck, M. P., Méresse, S., Delorme, P., Fruchart, J. C., & Cecchelli, R. (1990). An easier, reproducible, and mass-production method to study the blood–brain barrier in vitro. *Journal of neurochemistry, 54*(5), 1798-1801.

Deligne, C., Hachani, J., Duban-Deweer, S., Meignan, S., Leblond, P., Carcaboso, A. M., . . . Gosselet, F. (2020). Development of a human in vitro blood–brain tumor barrier model of diffuse intrinsic pontine glioma to better understand the chemoresistance. *Fluids and Barriers of the CNS, 17*, 1-15.

Delsing, L., Dönnes, P., Sánchez, J., Clausen, M., Voulgaris, D., Falk, A., . . . Hicks, R. (2018). Barrier properties and transcriptome expression in human iPSC-derived models of the blood–brain barrier. *Stem cells, 36*(12), 1816-1827.

Delsing, L., Herland, A., Falk, A., Hicks, R., Synnergren, J., & Zetterberg, H. (2020). Models of the blood-brain barrier using iPSC-derived cells. *Molecular and Cellular Neuroscience, 107*, 103533.

Deng, K., Zhang, L., Gao, W., Lin, X., Long, X., Wang, Y., & Wu, M. (2023). A functional carbon dots induce ferroptosis by suppressing PLPP4 activity to inhibit glioblastoma growth. *Chemical Engineering Journal, 475*, 146473.

Di Marco, A., Vignone, D., Gonzalez Paz, O., Fini, I., Battista, M. R., Cellucci, A., . . . Khetarpal, V. (2020). Establishment of an in vitro human blood-brain barrier model derived from induced pluripotent stem cells and comparison to a porcine cell-based system. *Cells, 9*(4), 994.

Dube, T., Kumar, N., Bishnoi, M., & Panda, J. J. (2021). Dual blood–brain barrier–glioma targeting peptide–poly (levodopamine) hybrid nanoplatforms as potential near infrared phototheranostic agents in glioblastoma. *Bioconjugate chemistry, 32*(9), 2014-2031.

Eberli, D., & Atala, A. (2006). Tissue engineering using adult stem cells. *Methods in enzymology, 420*, 287-302.

Ebrahimi Shahmabadi, H., Movahedi, F., Koohi Moftakhari Esfahani, M., Alavi, S. E., Eslamifar, A., Mohammadi Anaraki, G., & Akbarzadeh, A. (2014). Efficacy of Cisplatin-loaded polybutyl cyanoacrylate nanoparticles on the glioblastoma. *Tumor Biology, 35*, 4799-4806.

Eigenmann, D. E., Xue, G., Kim, K. S., Moses, A. V., Hamburger, M., & Oufir, M. (2013). Comparative study of four immortalized human brain capillary endothelial cell lines, hCMEC/D3, hBMEC, TY10, and BB19, and optimization of culture conditions, for an in vitro blood–brain barrier model for drug permeability studies. *Fluids and Barriers of the CNS, 10*(1), 1-17.

Fan, X., Liu, L., Jin, X., Wang, W., Zhang, S., & Tang, B. (2019). MXene Ti 3 C 2 T x for phase change composite with superior photothermal storage capability. *Journal of Materials Chemistry A, 7*(23), 14319-14327.

Fang, J. H., Lai, Y. H., Chiu, T. L., Chen, Y. Y., Hu, S. H., & Chen, S. Y. (2014). Magnetic Core–Shell Nanocapsules with Dual-Targeting Capabilities and Co-Delivery of Multiple Drugs to Treat Brain Gliomas. *Advanced Healthcare Materials, 3*(8), 1250-1260.

Fong, C. W. (2015). Permeability of the blood–brain barrier: molecular mechanism of transport of drugs and physiologically important compounds. *The Journal of membrane biology, 248*(4), 651-669.

Förster, C., Burek, M., Romero, I. A., Weksler, B., Couraud, P. O., & Drenckhahn, D. (2008). Differential effects of hydrocortisone and TNFα on tight junction proteins in an in vitro model of the human blood–brain barrier. *The Journal of physiology, 586*(7), 1937-1949.

Furuse, M., Hata, M., Furuse, K., Yoshida, Y., Haratake, A., Sugitani, Y., . . . Tsukita, S. (2002). Claudin-based tight junctions are crucial for the mammalian epidermal barrier: a lesson from claudin-1–deficient mice. *The Journal of cell biology, 156*(6), 1099-1111.

Furuse, M., Sasaki, H., & Tsukita, S. (1999). Manner of interaction of heterogeneous claudin species within and between tight junction strands. *The Journal of cell biology, 147*(4), 891-903.

Fusaki, N., Ban, H., Nishiyama, A., Saeki, K., & Hasegawa, M. (2009). Efficient induction of transgene-free human pluripotent stem cells using a vector based on

Sendai virus, an RNA virus that does not integrate into the host genome. *Proceedings of the Japan Academy, Series B, 85*(8), 348-362.

Gaillard, P. J., & de Boer, A. G. (2000). Relationship between permeability status of the blood–brain barrier and in vitro permeability coefficient of a drug. *European journal of pharmaceutical sciences, 12*(2), 95-102.

Gaillard, P. J., Voorwinden, L. H., Nielsen, J. L., Ivanov, A., Atsumi, R., Engman, H., . . . Breimer, D. D. (2001). Establishment and functional characterization of an in vitro model of the blood–brain barrier, comprising a co-culture of brain capillary endothelial cells and astrocytes. *European journal of pharmaceutical sciences, 12*(3), 215-222.

Gao, S., Li, J., Jiang, C., Hong, B., & Hao, B. (2015). Plasmid pORF-hTRAIL targeting to glioma using transferrin-modified polyamidoamine dendrimer. *Drug Design, Development and Therapy*, 1-11.

Goldeman, C., Andersen, M., Al-Robai, A., Buchholtz, T., Svane, N., Ozgür, B., . . . Saaby, L. (2021). Human induced pluripotent stem cells (BIONi010-C) generate tight cell monolayers with blood-brain barrier traits and functional expression of large neutral amino acid transporter 1 (SLC7A5). *European journal of pharmaceutical sciences, 156*, 105577.

Gomes, M. J., Mendes, B., Martins, S., & Sarmento, B. (2016). Cell-based in vitro models for studying blood–brain barrier (BBB) permeability. In *Concepts and models for drug permeability studies* (pp. 169-188): Elsevier.

Griep, L. M., Wolbers, F., de Wagenaar, B., ter Braak, P. M., Weksler, B. B., Romero, I. A., . . . van den Berg, A. (2013). BBB on chip: microfluidic platform to mechanically and biochemically modulate blood-brain barrier function. *Biomedical microdevices, 15*, 145-150.

Griffith, J. I., Rathi, S., Zhang, W., Zhang, W., Drewes, L. R., Sarkaria, J. N., & Elmquist, W. F. (2020). Addressing BBB heterogeneity: a new paradigm for drug delivery to brain tumors. *Pharmaceutics, 12*(12), 1205.

Hakkarainen, J. J., Rilla, K., Suhonen, M., Ruponen, M., & Forsberg, M. M. (2014). Re-evaluation of the role of P-glycoprotein in in vitro drug permeability studies with the bovine brain microvessel endothelial cells. *Xenobiotica, 44*(3), 283-294.

Han, S., Zheng, H., Lu, Y., Sun, Y., Huang, A., Fei, W., . . . Li, F. (2018). A novel synergetic targeting strategy for glioma therapy employing borneol combination with angiopep-2-modified, DOX-loaded PAMAM dendrimer. *Journal of drug targeting, 26*(1), 86-94.

Hanley, J., Rastegarlari, G., & Nathwani, A. C. (2010). An introduction to induced pluripotent stem cells. *British journal of haematology, 151*(1), 16-24.

Hatherell, K., Couraud, P.-O., Romero, I. A., Weksler, B., & Pilkington, G. J. (2011). Development of a three-dimensional, all-human in vitro model of the blood–brain barrier using mono-, co-, and tri-cultivation Transwell models. *Journal of neuroscience methods, 199*(2), 223-229.

Hayashi, K., Nakao, S., Nakaoke, R., Nakagawa, S., Kitagawa, N., & Niwa, M. (2004). Effects of hypoxia on endothelial/pericytic co-culture model of the blood–brain barrier. *Regulatory peptides, 123*(1-3), 77-83.

He, Y., Yao, Y., Tsirka, S. E., & Cao, Y. (2014). Cell-culture models of the blood–brain barrier. *Stroke, 45*(8), 2514-2526.

Helms, H. C., Abbott, N. J., Burek, M., Cecchelli, R., Couraud, P.-O., Deli, M. A., . . . Shusta, E. V. (2016). In vitro models of the blood–brain barrier: an overview of commonly used brain endothelial cell culture models and guidelines for their use. *Journal of Cerebral Blood Flow & Metabolism, 36*(5), 862-890.

Helms, H. C., Hersom, M., Kuhlmann, L. B., Badolo, L., Nielsen, C. U., & Brodin, B. (2014). An electrically tight in vitro blood–brain barrier model displays net brain-to-blood efflux of substrates for the ABC transporters, P-gp, Bcrp and Mrp-1. *The AAPS journal, 16*, 1046-1055.

Helms, J., Kremer, S., Merdji, H., Clere-Jehl, R., Schenck, M., Kummerlen, C., . . . Ohana, M. (2020). Neurologic features in severe SARS-CoV-2 infection. *New England Journal of Medicine, 382*(23), 2268-2270.

Henrich-Noack, P., Nikitovic, D., Neagu, M., Docea, A. O., Engin, A. B., Gelperina, S., . . . Gozes, I. (2019). The blood–brain barrier and beyond: Nano-based neuropharmacology and the role of extracellular matrix. *Nanomedicine: Nanotechnology, Biology and Medicine, 17*, 359-379.

Hoheisel, D., Nitz, T., Franke, H., Wegener, J., Hakvoort, A., Tilling, T., & Galla, H.-J. (1998). Hydrocortisone reinforces the blood–brain barrier properties in a serum free cell culture system. *Biochemical and biophysical research communications, 244*(1), 312-316.

Hollmann, E. K., Bailey, A. K., Potharazu, A. V., Neely, M. D., Bowman, A. B., & Lippmann, E. S. (2017). Accelerated differentiation of human induced pluripotent stem cells to blood–brain barrier endothelial cells. *Fluids and Barriers of the CNS, 14*(1), 1-13.

Jamieson, J. J., Linville, R. M., Ding, Y. Y., Gerecht, S., & Searson, P. C. (2019). Role of iPSC-derived pericytes on barrier function of iPSC-derived brain microvascular endothelial cells in 2D and 3D. *Fluids and Barriers of the CNS, 16*, 1-16.

Jensen, S. A., Day, E. S., Ko, C. H., Hurley, L. A., Luciano, J. P., Kouri, F. M., . . . Cutler, J. I. (2013). Spherical nucleic acid nanoparticle conjugates as an RNAi-based therapy for glioblastoma. *Science translational medicine, 5*(209), 209ra152-209ra152.

Jeong, Y.-I., Jin, S.-G., Kim, I.-Y., Pei, J., Wen, M., Jung, T.-Y., . . . Jung, S. (2010). Doxorubicin-incorporated nanoparticles composed of poly (ethylene glycol)-grafted carboxymethyl chitosan and antitumor activity against glioma cells in vitro. *Colloids and Surfaces B: Biointerfaces, 79*(1), 149-155.

Joo, F. (1973). A procedure for the isolation of capillaries from rat brain. *Cytobios, 8*, 41-48.

Jung, Y.-S., & Park, J.-I. (2020). Wnt signaling in cancer: therapeutic targeting of Wnt signaling beyond β-catenin and the destruction complex. *Experimental & Molecular Medicine, 52*(2), 183-191.

Kalra, K., & Tomar, P. C. (2014). Stem cell: basics, classification and applications. *American Journal of Phytomedicine and Clinical Therapeutics, 2*(7), 919-930.

Katt, M. E., Linville, R. M., Mayo, L. N., Xu, Z. S., & Searson, P. C. (2018). Functional brain-specific microvessels from iPSC-derived human brain microvascular endothelial cells: the role of matrix composition on monolayer formation. *Fluids and Barriers of the CNS, 15*, 1-12.

Katt, M. E., Mayo, L. N., Ellis, S. E., Mahairaki, V., Rothstein, J. D., Cheng, L., & Searson, P. C. (2019). The role of mutations associated with familial neurodegenerative disorders on blood–brain barrier function in an iPSC model. *Fluids and Barriers of the CNS, 16*(1), 1-13.

Kim, B. J., Bee, O. B., McDonagh, M. A., Stebbins, M. J., Palecek, S. P., Doran, K. S., & Shusta, E. V. (2017). Modeling group B Streptococcus and blood-brain barrier interaction by using induced pluripotent stem cell-derived brain endothelial cells. *Msphere, 2*(6), 10.1128/msphere. 00398-00317.

Kim, Y. H., Kim, K.-J., D'Argenio, D. Z., & Crandall, E. D. (2021). Characteristics of passive solute transport across primary rat alveolar epithelial cell monolayers. *Membranes, 11*(5), 331.

Kubotera, H., Ikeshima-Kataoka, H., Hatashita, Y., Allegra Mascaro, A. L., Pavone, F. S., & Inoue, T. (2019). Astrocytic endfeet re-cover blood vessels after removal by laser ablation. *Scientific reports, 9*(1), 1263.

Lalatsa, A., & Butt, A. M. (2018). Physiology of the blood–brain barrier and mechanisms of transport across the BBB. In *Nanotechnology-Based Targeted Drug Delivery Systems for Brain Tumors* (pp. 49-74): Elsevier.

Lalatsa, A., Schätchlein, A., & Uchegbu, I. F. (2012). *Nanostructures Overcoming the Blood-Brain Barrier: Physiological Considerations and Mechanistic Issues*: Royal Society of Chemistry, London, UK.

Lam, M. S., Aw, J. J., Tan, D., Vijayakumar, R., Lim, H. Y. G., Yada, S., . . . Ang, B. T. (2023). Unveiling the influence of tumor microenvironment and spatial heterogeneity on temozolomide resistance in glioblastoma using an advanced human in vitro model of the blood-brain barrier and glioblastoma. *Small, 19*(52), 2302280.

Lee, S. W. L., Campisi, M., Osaki, T., Possenti, L., Mattu, C., Adriani, G., . . . Chiono, V. (2020). Modeling nanocarrier transport across a 3D in vitro human blood-brain–barrier microvasculature. *Advanced Healthcare Materials, 9*(7), 1901486.

Li, J., Kong, J., Ma, S., Li, J., Mao, M., Chen, K., . . . Yuan, H. (2021). Exosome-coated 10b carbon dots for precise boron neutron capture therapy in a mouse model of glioma in situ. *Advanced Functional Materials, 31*(24), 2100969.

Li, S., Amat, D., Peng, Z., Vanni, S., Raskin, S., De Angulo, G., . . . Leblanc, R. M. (2016). Transferrin conjugated nontoxic carbon dots for doxorubicin delivery to target pediatric brain tumor cells. *Nanoscale, 8*(37), 16662-16669.

Li, Y., He, H., Jia, X., Lu, W.-L., Lou, J., & Wei, Y. (2012). A dual-targeting nanocarrier based on poly (amidoamine) dendrimers conjugated with transferrin and tamoxifen for treating brain gliomas. *Biomaterials, 33*(15), 3899-3908.

Lim, R. G., Quan, C., Reyes-Ortiz, A. M., Lutz, S. E., Kedaigle, A. J., Gipson, T. A., . . . Casale, M. S. (2017). Huntington's disease iPSC-derived brain microvascular endothelial cells reveal WNT-mediated angiogenic and blood-brain barrier deficits. *Cell reports, 19*(7), 1365-1377.

Lin, E.-Y., Chen, Y.-S., Li, Y.-S., Chen, S.-R., Lee, C.-H., Huang, M.-H., . . . Lin, S.-Z. (2020). Liposome consolidated with cyclodextrin provides prolonged drug retention resulting in increased drug bioavailability in brain. *International journal of molecular sciences, 21*(12), 4408.

Lippmann, E. S., Al-Ahmad, A., Azarin, S. M., Palecek, S. P., & Shusta, E. V. (2014). A retinoic acid-enhanced, multicellular human blood-brain barrier model derived from stem cell sources. *Scientific reports, 4*(1), 1-10.

Lippmann, E. S., Azarin, S. M., Kay, J. E., Nessler, R. A., Wilson, H. K., Al-Ahmad, A., . . . Shusta, E. V. (2012). Derivation of blood-brain barrier endothelial cells from human pluripotent stem cells. *Nature biotechnology, 30*(8), 783-791.

Liu, S., Zhong, Z., Zhang, C., Zhou, Y., Fu, C., & Xu, X. (2022). Targeted therapy for the treatment of gliomas with multifunctional orange emissive carbon dots. *Nanoscale Advances, 4*(3), 894-903.

Liu, Z., Ji, X., He, D., Zhang, R., Liu, Q., & Xin, T. (2022). Nanoscale Drug Delivery Systems in Glioblastoma. *Nanoscale Research Letters, 17*(1), 1-25.

Liyanage, P. Y., Zhou, Y., Al-Youbi, A. O., Bashammakh, A. S., El-Shahawi, M. S., Vanni, S., . . . Leblanc, R. M. (2020). Pediatric glioblastoma target-specific efficient delivery of gemcitabine across the blood–brain barrier via carbon nitride dots. *Nanoscale, 12*(14), 7927-7938.

Locatelli, E., Bost, W., Fournelle, M., Llop, J., Gil, L., Arena, F., . . . Comes Franchini, M. (2014). Targeted polymeric nanoparticles containing gold nanorods: a therapeutic approach against glioblastoma. *Journal of nanoparticle research, 16*, 1-9.

Lopez-Ramirez, M. A., Fischer, R., Torres-Badillo, C. C., Davies, H. A., Logan, K., Pfizenmaier, K., . . . Romero, I. A. (2012). Role of caspases in cytokine-induced barrier breakdown in human brain endothelial cells. *The Journal of Immunology, 189*(6), 3130-3139.

Löscher, W., & Potschka, H. (2005). Role of drug efflux transporters in the brain for drug disposition and treatment of brain diseases. *Progress in neurobiology, 76*(1), 22-76.

Lu, T. M., Barcia Duran, J. G., Houghton, S., Rafii, S., Redmond, D., & Lis, R. (2021). Human induced pluripotent stem cell-derived brain endothelial cells: Current controversies. *Frontiers in Physiology, 12*, 642812.

Lu, W. (2012). Adsorptive-mediated brain delivery systems. *Current pharmaceutical biotechnology, 13*(12), 2340-2348.

Lu, Y., Han, S., Zheng, H., Ma, R., Ping, Y., Zou, J., . . . Li, F. (2018). A novel RGDyC/PEG co-modified PAMAM dendrimer-loaded arsenic trioxide of glioma targeting delivery system. *International journal of nanomedicine*, 5937-5952.

Macdonald, J. A., Murugesan, N., & Pachter, J. S. (2010). Endothelial cell heterogeneity of blood-brain barrier gene expression along the cerebral microvasculature. *Journal of neuroscience research, 88*(7), 1457-1474.

Madane, R. G., & Mahajan, H. S. (2016). Curcumin-loaded nanostructured lipid carriers (NLCs) for nasal administration: design, characterization, and in vivo study. *Drug delivery, 23*(4), 1326-1334.

Madani, F., Morovvati, H., Webster, T. J., Asaadi, S. N., Rezayat, S. M., Hadjighassem, M., . . . Adabi, M. (2024). Combinatorial chemotherapy via poloxamer 188 surface-modified PLGA nanoparticles that traverse the blood-brain-barrier in a glioblastoma model.

Mahringer, A., & Fricker, G. (2016). ABC transporters at the blood–brain barrier. *Expert opinion on drug metabolism & toxicology, 12*(5), 499-508.

Mansur, A. A., Paiva, M. R., Cotta, O. A., Silva, L. M., Carvalho, I. C., Capanema, N. S., . . . Ecco, R. (2022). Carboxymethylcellulose biofunctionalized ternary quantum dots for subcellular-targeted brain cancer nanotheranostics. *International journal of biological macromolecules, 210*, 530-544.

Mayor, S., & Pagano, R. E. (2007). Pathways of clathrin-independent endocytosis. *Nature reviews Molecular cell biology, 8*(8), 603-612.

Mc Carthy, D. J., Malhotra, M., O'Mahony, A. M., Cryan, J. F., & O'Driscoll, C. M. (2015). Nanoparticles and the blood-brain barrier: advancing from in-vitro models towards therapeutic significance. *Pharmaceutical research, 32*(4), 1161-1185.

Mendes, B., Marques, C., Carvalho, I., Costa, P., Martins, S., Ferreira, D., & Sarmento, B. (2015). Influence of glioma cells on a new co-culture in vitro blood–brain barrier model for characterization and validation of permeability. *International journal of pharmaceutics, 490*(1-2), 94-101.

Mischeck, U., Meyer, J., & Galla, H.-J. (1989). Characterization of γ-glutamyl transpeptidase activity of cultured endothelial cells from porcine brain capillaries. *Cell and tissue research, 256*, 221-226.

Miura, Y., Takenaka, T., Toh, K., Wu, S., Nishihara, H., Kano, M. R., . . . Koyama, H. (2013). Cyclic RGD-linked polymeric micelles for targeted delivery of platinum anticancer drugs to glioblastoma through the blood–brain tumor barrier. *ACS nano, 7*(10), 8583-8592.

Mo, F., Pellerino, A., Soffietti, R., & Rudà, R. (2021). Blood–brain barrier in brain tumors: biology and clinical relevance. *International journal of molecular sciences, 22*(23), 12654.

Morita, K., Sasaki, H., Furuse, M., & Tsukita, S. (1999). Endothelial claudin: claudin-5/TMVCF constitutes tight junction strands in endothelial cells. *The Journal of cell biology, 147*(1), 185-194.

Naik, P., & Cucullo, L. (2012). In vitro blood–brain barrier models: current and perspective technologies. *Journal of pharmaceutical sciences, 101*(4), 1337-1354.

Nakagawa, S., Deli, M. A., Kawaguchi, H., Shimizudani, T., Shimono, T., Kittel, A., . . . Niwa, M. (2009). A new blood–brain barrier model using primary rat brain endothelial cells, pericytes and astrocytes. *Neurochemistry international, 54*(3-4), 253-263.

Nakagawa, S., Deli, M. A., Nakao, S., Honda, M., Hayashi, K., Nakaoke, R., . . . Niwa, M. (2007). Pericytes from brain microvessels strengthen the barrier integrity in primary cultures of rat brain endothelial cells. *Cellular and molecular neurobiology, 27*, 687-694.

Nance, E., Pun, S. H., Saigal, R., & Sellers, D. L. (2021). Drug delivery to the central nervous system. *Nature Reviews Materials*, 1-18.

Natarajan, R., Northrop, N., & Yamamoto, B. (2017). Fluorescein Isothiocyanate (FITC)-Dextran Extravasation as a Measure of Blood-Brain Barrier Permeability. *Current protocols in neuroscience, 79*(1), 9.58. 51-59.58. 15.

Neal, E. H., Marinelli, N. A., Shi, Y., McClatchey, P. M., Balotin, K. M., Gullett, D. R., . . . Wikswo, J. P. (2019). A simplified, fully defined differentiation scheme for producing blood-brain barrier endothelial cells from human iPSCs. *Stem cell reports, 12*(6), 1380-1388.

Neuhaus, W., Lauer, R., Oelzant, S., Fringeli, U. P., Ecker, G. F., & Noe, C. R. (2006). A novel flow based hollow-fiber blood–brain barrier in vitro model with immortalised cell line PBMEC/C1–2. *Journal of biotechnology, 125*(1), 127-141.

Neuwelt, E., Abbott, N. J., Abrey, L., Banks, W. A., Blakley, B., Davis, T., . . . Nutt, J. (2008). Strategies to advance translational research into brain barriers. *The Lancet Neurology, 7*(1), 84-96.

Nitta, T., Hata, M., Gotoh, S., Seo, Y., Sasaki, H., Hashimoto, N., . . . Tsukita, S. (2003). Size-selective loosening of the blood-brain barrier in claudin-5–deficient mice. *The Journal of cell biology, 161*(3), 653-660.

Obermeier, B., Daneman, R., & Ransohoff, R. M. (2013). Development, maintenance and disruption of the blood-brain barrier. *Nature medicine, 19*(12), 1584-1596.

Ohtsuki, S., Ikeda, C., Uchida, Y., Sakamoto, Y., Miller, F., Glacial, F., . . . Kubo, Y. (2013). Quantitative targeted absolute proteomic analysis of transporters, receptors and junction proteins for validation of human cerebral microvascular endothelial cell line hCMEC/D3 as a human blood–brain barrier model. *Molecular pharmaceutics, 10*(1), 289-296.

Oikari, L. E., Pandit, R., Stewart, R., Cuní-López, C., Quek, H., Sutharsan, R., . . . de Boer, C. M. (2020). Altered brain endothelial cell phenotype from a familial Alzheimer mutation and its potential implications for amyloid clearance and drug delivery. *Stem cell reports, 14*(5), 924-939.

Papadopoulos, M., Saadoun, S., Binder, D., Manley, G., Krishna, S., & Verkman, A. (2004). Molecular mechanisms of brain tumor edema. *Neuroscience, 129*(4), 1009-1018.

Pardridge, W. M. (2005). The blood-brain barrier: bottleneck in brain drug development. *NeuroRx, 2*, 3-14.

Pardridge, W. M., Eisenberg, J., & Cefalu, W. T. (1985). Absence of albumin receptor on brain capillaries in vivo or in vitro. *American Journal of Physiology-Endocrinology And Metabolism, 249*(3), E264-E267.

Park, T.-E., Mustafaoglu, N., Herland, A., Hasselkus, R., Mannix, R., FitzGerald, E. A., . . . Benz, M. (2019). Hypoxia-enhanced Blood-Brain Barrier Chip recapitulates human barrier function and shuttling of drugs and antibodies. *Nature communications, 10*(1), 1-12.

Pasteuning-Vuhman, S., de Jongh, R., Timmers, A., & Pasterkamp, R. J. (2021). Towards advanced iPSC-based drug development for neurodegenerative disease. *Trends in molecular medicine, 27*(3), 263-279.

Patabendige, A., & Abbott, N. J. (2014). Primary porcine brain microvessel endothelial cell isolation and culture. *Current protocols in neuroscience, 69*(1), 3.27. 21-23.27. 17.

Patabendige, A., Skinner, R. A., & Abbott, N. J. (2013). Establishment of a simplified in vitro porcine blood–brain barrier model with high transendothelial electrical resistance. *Brain research, 1521*, 1-15.

Patabendige, A., Skinner, R. A., Morgan, L., & Abbott, N. J. (2013). A detailed method for preparation of a functional and flexible blood–brain barrier model using porcine brain endothelial cells. *Brain research, 1521*, 16-30.

Patel, V., & Shah, J. (2023). Anti-cancer and neuroprotective effects of conjugated graphene quantum dot in brain tumor-bearing rat model. *Nano Express, 4*(4), 045010.

Perini, G., Palmieri, V., Ciasca, G., D'Ascenzo, M., Primiano, A., Gervasoni, J., . . . Papi, M. (2020). Enhanced chemotherapy for glioblastoma multiforme mediated by functionalized graphene quantum dots. *Materials, 13*(18), 4139.

Perriere, N., Demeuse, P., Garcia, E., Regina, A., Debray, M., Andreux, J. P., . . . Couraud, P. O. (2005). Puromycin-based purification of rat brain capillary endothelial cell cultures. Effect on the expression of blood–brain barrier-specific properties. *Journal of neurochemistry, 93*(2), 279-289.

Perrin, S. (2014). Preclinical research: Make mouse studies work. *Nature, 507*(7493), 423-425.

Phoenix, T. N., Patmore, D. M., Boop, S., Boulos, N., Jacus, M. O., Patel, Y. T., . . . Perreault, S. (2016). Medulloblastoma genotype dictates blood brain barrier phenotype. *Cancer cell, 29*(4), 508-522.

Poller, B., Gutmann, H., Krähenbühl, S., Weksler, B., Romero, I., Couraud, P. O., . . . Huwyler, J. (2008). The human brain endothelial cell line hCMEC/D3 as a human blood-brain barrier model for drug transport studies. *Journal of neurochemistry, 107*(5), 1358-1368.

Pong, S., Lizano, P., & Karmacharya, R. (2020). Derivation, expansion, cryopreservation and characterization of brain microvascular endothelial cells from human induced pluripotent stem cells. *JoVE (Journal of Visualized Experiments)*(165), e61629.

Ponio, J. B.-D., El-Ayoubi, F., Glacial, F., Ganeshamoorthy, K., Driancourt, C., Godet, M., . . . Uzan, G. (2014). Instruction of circulating endothelial progenitors in vitro

towards specialized blood-brain barrier and arterial phenotypes. *PloS one, 9*(1), e84179.

Prabhakarpandian, B., Shen, M.-C., Nichols, J. B., Mills, I. R., Sidoryk-Wegrzynowicz, M., Aschner, M., & Pant, K. (2013). SyM-BBB: a microfluidic blood brain barrier model. *Lab on a Chip, 13*(6), 1093-1101.

Praça, C., Rosa, S. C., Sevin, E., Cecchelli, R., Dehouck, M.-P., & Ferreira, L. S. (2019). Derivation of brain capillary-like endothelial cells from human pluripotent stem cell-derived endothelial progenitor cells. *Stem cell reports, 13*(4), 599-611.

Prashanth, A., Donaghy, H., Stoner, S. P., Hudson, A. L., Wheeler, H. R., Diakos, C. I., . . . McKelvey, K. J. (2021). Are in vitro human blood–brain–tumor-barriers suitable replacements for in vivo models of brain permeability for novel therapeutics? *Cancers, 13*(5), 955.

Pulgar, V. M. (2019). Transcytosis to cross the blood brain barrier, new advancements and challenges. *Frontiers in neuroscience, 12*, 1019.

Pun, P. B., Lu, J., & Moochhala, S. (2009). Involvement of ROS in BBB dysfunction. *Free radical research, 43*(4), 348-364.

Qian, M., Du, Y., Wang, S., Li, C., Jiang, H., Shi, W., . . . Huang, R. (2018). Highly crystalline multicolor carbon nanodots for dual-modal imaging-guided photothermal therapy of glioma. *ACS applied materials & interfaces, 10*(4), 4031-4040.

Qian, T., Maguire, S. E., Canfield, S. G., Bao, X., Olson, W. R., Shusta, E. V., & Palecek, S. P. (2017). Directed differentiation of human pluripotent stem cells to blood-brain barrier endothelial cells. *Science advances, 3*(11), e1701679.

Qiao, L., Sun, T., Zheng, X., Zheng, M., & Xie, Z. (2018). Exploring the optimal ratio of d-glucose/l-aspartic acid for targeting carbon dots toward brain tumor cells. *Materials Science and Engineering: C, 85*, 1-6.

Qiao, R., Jia, Q., Huwel, S., Xia, R., Liu, T., Gao, F., . . . Gao, M. (2012). Receptor-mediated delivery of magnetic nanoparticles across the blood–brain barrier. *ACS nano, 6*(4), 3304-3310.

Rafieerad, A., Yan, W., Amiri, A., & Dhingra, S. (2020). Bioactive and trackable MXene quantum dots for subcellular nanomedicine applications. *Materials & Design, 196*, 109091.

Rafieerad, A., Yan, W., Sequiera, G. L., Sareen, N., Abu-El-Rub, E., Moudgil, M., & Dhingra, S. (2019). Application of Ti3C2 MXene quantum dots for immunomodulation and regenerative medicine. *Advanced Healthcare Materials, 8*(16), 1900569.

Ragnaill, M. N., Brown, M., Ye, D., Bramini, M., Callanan, S., Lynch, I., & Dawson, K. A. (2011). Internal benchmarking of a human blood–brain barrier cell model for screening of nanoparticle uptake and transcytosis. *European journal of pharmaceutics and biopharmaceutics, 77*(3), 360-367.

Rahman, N. A., & Meyding-Lamadé, U. (2016). Immortalized endothelial cell lines for in vitro blood-brain barrier models.

Raleigh, D. R., Boe, D. M., Yu, D., Weber, C. R., Marchiando, A. M., Bradford, E. M., . . . Shen, L. (2011). Occludin S408 phosphorylation regulates tight junction protein interactions and barrier function. *Journal of Cell Biology, 193*(3), 565-582.

Rascher, G., Fischmann, A., Kröger, S., Duffner, F., Grote, E.-H., & Wolburg, H. (2002). Extracellular matrix and the blood-brain barrier in glioblastoma multiforme: spatial segregation of tenascin and agrin. *Acta neuropathologica, 104*, 85-91.

Raut, S., Patel, R., & Al-Ahmad, A. (2020). Induced pluripotent stem cells derived brain endothelial cells from patients suffering from familial form of Alzheimer's disease display impaired barrier function and cell metabolism.

Reddy, S., Tatiparti, K., Sau, S., & Iyer, A. K. (2021). Recent advances in nano delivery systems for blood-brain barrier (BBB) penetration and targeting of brain tumors. *Drug Discovery Today, 26*(8), 1944-1952.

Reuter, B., Rodemer, C., Grudzenski, S., Meairs, S., Bugert, P., Hennerici, M. G., & Fatar, M. (2015). Effect of simvastatin on MMPs and TIMPs in human brain endothelial cells and experimental stroke. *Translational Stroke Research, 6*, 156-159.

Ribecco-Lutkiewicz, M., Sodja, C., Haukenfrers, J., Haqqani, A. S., Ly, D., Zachar, P., . . . Rukhlova, M. (2018). A novel human induced pluripotent stem cell blood-brain barrier model: Applicability to study antibody-triggered receptor-mediated transcytosis. *Scientific reports, 8*(1), 1873.

Rieker, C., Migliavacca, E., Vaucher, A., Mayer, F. C., Baud, G., Marquis, J., . . . McLachlan, M. (2019). Apolipoprotein E4 expression causes gain of toxic function in isogenic human induced pluripotent stem cell-derived endothelial cells. *Arteriosclerosis, thrombosis, and vascular biology, 39*(9), e195-e207.

Roux, G. L., Jarray, R., Guyot, A.-C., Pavoni, S., Costa, N., Théodoro, F., . . . Kiyan, Y. (2019). Proof-of-concept study of drug brain permeability between in vivo human brain and an in vitro iPSCs-human blood-brain barrier model. *Scientific reports, 9*(1), 16310.

Rubin, L., Hall, D., Porter, S., Barbu, K., Cannon, C., Horner, H., . . . Morales, J. (1991). A cell culture model of the blood-brain barrier. *The Journal of cell biology, 115*(6), 1725-1735.

Sallem, F., Haji, R., Vervandier-Fasseur, D., Nury, T., Maurizi, L., Boudon, J., . . . Millot, N. (2019). Elaboration of trans-resveratrol derivative-loaded superparamagnetic iron oxide nanoparticles for glioma treatment. *Nanomaterials, 9*(2), 287.

Santaguida, S., Janigro, D., Hossain, M., Oby, E., Rapp, E., & Cucullo, L. (2006). Side by side comparison between dynamic versus static models of blood–brain barrier in vitro: a permeability study. *Brain research, 1109*(1), 1-13.

Seo, S., Nah, S. Y., Lee, K., Choi, N., & Kim, H. N. (2022). Triculture model of in vitro BBB and its application to study BBB-associated chemosensitivity and drug delivery in glioblastoma. *Advanced Functional Materials, 32*(10), 2106860.

Shi, H., Sun, S., Xu, H., Zhao, Z., Han, Z., Jia, J., . . . Yu, R. (2020). Combined delivery of temozolomide and siPLK1 using targeted nanoparticles to enhance temozolomide sensitivity in glioma. *International journal of nanomedicine*, 3347-3362.

Shimizu, F., Sano, Y., Tominaga, O., Maeda, T., Abe, M.-a., & Kanda, T. (2013). Advanced glycation end-products disrupt the blood–brain barrier by stimulating the release of transforming growth factor–β by pericytes and vascular endothelial growth factor and matrix metalloproteinase–2 by endothelial cells in vitro. *Neurobiology of aging, 34*(7), 1902-1912.

Siddharthan, V., Kim, Y. V., Liu, S., & Kim, K. S. (2007). Human astrocytes/astrocyte-conditioned medium and shear stress enhance the barrier properties of human brain microvascular endothelial cells. *Brain research, 1147*, 39-50.

Stamatovic, S. M., Keep, R. F., & Andjelkovic, A. V. (2008). Brain endothelial cell-cell junctions: how to "open" the blood brain barrier. *Current neuropharmacology, 6*(3), 179-192.

Stebbins, M. J., Wilson, H. K., Canfield, S. G., Qian, T., Palecek, S. P., & Shusta, E. V. (2016). Differentiation and characterization of human pluripotent stem cell-derived brain microvascular endothelial cells. *Methods, 101*, 93-102.

Stowasser, C. (2008). The Dipole Potential of Lipid Membranes-An Overview.

Su, J. J., Osoegawa, M., Matsuoka, T., Minohara, M., Tanaka, M., Ishizu, T., . . . Kira, J.-i. (2006). Upregulation of vascular growth factors in multiple sclerosis: correlation with MRI findings. *Journal of the neurological sciences, 243*(1-2), 21-30.

Su, Z., Xing, L., Chen, Y., Xu, Y., Yang, F., Zhang, C., . . . Xiao, Y. (2014). Lactoferrin-modified poly (ethylene glycol)-grafted BSA nanoparticles as a dual-targeting carrier for treating brain gliomas. *Molecular pharmaceutics, 11*(6), 1823-1834.

Sun, J., Ou, W., Han, D., Paganini-Hill, A., Fisher, M. J., & Sumbria, R. K. (2022). Comparative studies between the murine immortalized brain endothelial cell line (bEnd. 3) and induced pluripotent stem cell-derived human brain endothelial cells for paracellular transport. *PloS one, 17*(5), e0268860.

Sweeney, M. D., Sagare, A. P., & Zlokovic, B. V. (2018). Blood–brain barrier breakdown in Alzheimer disease and other neurodegenerative disorders. *Nature Reviews Neurology, 14*(3), 133-150.

Syvänen, S., Lindhe, Ö., Palner, M., Kornum, B. R., Rahman, O., Långström, B., . . . Hammarlund-Udenaes, M. (2009). Species differences in blood-brain barrier transport of three positron emission tomography radioligands with emphasis on P-glycoprotein transport. *Drug metabolism and disposition, 37*(3), 635-643.

Tai, L. M., Loughlin, A. J., Male, D. K., & Romero, I. A. (2009). P-glycoprotein and breast cancer resistance protein restrict apical-to-basolateral permeability of human brain endothelium to amyloid-β. *Journal of Cerebral Blood Flow & Metabolism, 29*(6), 1079-1083.

Takahashi, K., Tanabe, K., Ohnuki, M., Narita, M., Ichisaka, T., Tomoda, K., & Yamanaka, S. (2007). Induction of pluripotent stem cells from adult human fibroblasts by defined factors. *cell, 131*(5), 861-872.

Tarbell, J. M. (2010). Shear stress and the endothelial transport barrier. *Cardiovascular research, 87*(2), 320-330.

Theumer, A., Gräfe, C., Bähring, F., Bergemann, C., Hochhaus, A., & Clement, J. H. (2015). Superparamagnetic iron oxide nanoparticles exert different cytotoxic effects on cells grown in monolayer cell culture versus as multicellular spheroids. *Journal of Magnetism and Magnetic Materials, 380*, 27-33.

Urich, E., Lazic, S. E., Molnos, J., Wells, I., & Freskgård, P.-O. (2012). Transcriptional profiling of human brain endothelial cells reveals key properties crucial for predictive in vitro blood-brain barrier models. *PloS one, 7*(5), e38149.

Van Tellingen, O., Yetkin-Arik, B., De Gooijer, M., Wesseling, P., Wurdinger, T., & De Vries, H. (2015). Overcoming the blood–brain tumor barrier for effective glioblastoma treatment. *Drug Resistance Updates, 19*, 1-12.

Veiseh, O., Sun, C., Fang, C., Bhattarai, N., Gunn, J., Kievit, F., . . . Ellenbogen, R. G. (2009). Specific targeting of brain tumors with an optical/magnetic resonance imaging nanoprobe across the blood-brain barrier. *Cancer research, 69*(15), 6200-6207.

Vignone, D., Gonzalez Paz, O., Fini, I., Cellucci, A., Auciello, G., Battista, M. R., . . . Khetarpal, V. (2022). Modelling the Human Blood–Brain Barrier in Huntington Disease. *International journal of molecular sciences, 23*(14), 7813.

Wagner, E. F., & Risau, W. (1994). *Oncogenes in the study of endothelial cell growth and differentiation.* Paper presented at the Seminars in cancer biology.

Wang, J., Liu, Y., Morsch, M., Lu, Y., Shangguan, P., Han, L., . . . Liu, S. (2022). Brain-Targeted Aggregation-Induced-Emission Nanoparticles with Near-Infrared Imaging at 1550 nm Boosts Orthotopic Glioblastoma Theranostics. *Advanced Materials, 34*(5), 2106082.

Wang, X., Meng, N., Wang, S., Zhang, Y., Lu, L., Wang, R., . . . Ran, D. (2019). Non-immunogenic, low-toxicity and effective glioma targeting MTI-31 liposomes. *Journal of controlled release, 316*, 381-392.

Wang, Y., Huo, T., Jiang, H., Xie, Y., Zhang, X., Nie, H., . . . Hao, T. (2021). Sugar-originated carbon nanodots selectively damage the tumor and enhance the sensitivity of chemotherapy. *Nano today, 38*, 101200.

Weksler, B., Romero, I. A., & Couraud, P.-O. (2013). The hCMEC/D3 cell line as a model of the human blood brain barrier. *Fluids and Barriers of the CNS, 10*(1), 1-10.

Weksler, B., Subileau, E., Perriere, N., Charneau, P., Holloway, K., Leveque, M., . . . Turowski, P. (2005). Blood-brain barrier-specific properties of a human adult brain endothelial cell line. *The FASEB journal, 19*(13), 1872-1874.

Wilson, H. K., Canfield, S. G., Hjortness, M. K., Palecek, S. P., & Shusta, E. V. (2015). Exploring the effects of cell seeding density on the differentiation of human pluripotent stem cells to brain microvascular endothelial cells. *Fluids and Barriers of the CNS, 12*(1), 1-12.

Wilson, H. K., Faubion, M. G., Hjortness, M. K., Palecek, S. P., & Shusta, E. V. (2016). Cryopreservation of brain endothelial cells derived from human induced pluripotent stem cells is enhanced by rho-associated coiled coil-containing kinase inhibition. *Tissue Engineering Part C: Methods, 22*(12), 1085-1094.

Wolburg, H., Wolburg-Buchholz, K., Liebner, S., & Engelhardt, B. (2001). Claudin-1, claudin-2 and claudin-11 are present in tight junctions of choroid plexus epithelium of the mouse. *Neuroscience letters, 307*(2), 77-80.

Workman, M. J., & Svendsen, C. N. (2020). Recent advances in human iPSC-derived models of the blood–brain barrier. *Fluids and Barriers of the CNS, 17*(1), 1-10.

Wu, Y.-C., Sonninen, T.-M., Peltonen, S., Koistinaho, J., & Lehtonen, Š. (2021). Blood–brain barrier and neurodegenerative diseases—modeling with iPSC-derived brain cells. *International journal of molecular sciences, 22*(14), 7710.

Xiang, Y., Liang, L., Wang, X., Wang, J., Zhang, X., & Zhang, Q. (2011). Chloride channel-mediated brain glioma targeting of chlorotoxin-modified doxorubicine-loaded liposomes. *Journal of controlled release, 152*(3), 402-410.

Yan, W., Rafieerad, A., Alagarsamy, K. N., Saleth, L. R., Arora, R. C., & Dhingra, S. (2023). Immunoengineered MXene nanosystem for mitigation of alloantigen presentation and prevention of transplant vasculopathy. *Nano today, 48*, 101706.

Ye, H., & Wang, Q. (2018). Efficient generation of non-integration and feeder-free induced pluripotent stem cells from human peripheral blood cells by Sendai virus. *Cellular Physiology and Biochemistry, 50*(4), 1318-1331.

Yeon, J. H., Na, D., Choi, K., Ryu, S.-W., Choi, C., & Park, J.-K. (2012). Reliable permeability assay system in a microfluidic device mimicking cerebral vasculatures. *Biomedical microdevices, 14*, 1141-1148.

Yilmazer, A., Alagarsamy, K. N., Gokce, C., Summak, G. Y., Rafieerad, A., Bayrakdar, F., . . . Unal, M. A. (2023). Low Dose of Ti3C2 MXene Quantum Dots Mitigate SARS-CoV-2 Infection. *Small Methods, 7*(8), 2300044.

Zhang, J., Gao, Y., Yu, M., Wu, H., Ai, Z., Wu, Y., . . . Zhang, Y. (2015). Retinoic acid induces embryonic stem cell differentiation by altering both encoding RNA and microRNA expression. *PloS one, 10*(7), e0132566.

Zhang, Y., Fu, X., Jia, J., Wikerholmen, T., Xi, K., Kong, Y., . . . Li, Z. (2020). Glioblastoma therapy using codelivery of cisplatin and glutathione peroxidase targeting siRNA from iron oxide nanoparticles. *ACS applied materials & interfaces, 12*(39), 43408-43421.

Zhang, Y., Li, C. S., Ye, Y., Johnson, K., Poe, J., Johnson, S., . . . Madhu, C. (2006). Porcine brain microvessel endothelial cells as an in vitro model to predict in vivo blood-brain barrier permeability. *Drug metabolism and disposition, 34*(11), 1935-1943.

Zhang, Y., Zhang, L., Hu, Y., Jiang, K., Li, Z., Lin, Y.-Z., . . . Lu, W. (2018). Cell-permeable NF-κB inhibitor-conjugated liposomes for treatment of glioma. *Journal of controlled release, 289*, 102-113.

Zhao, J., Li, D., Ma, J., Yang, H., Chen, W., Cao, Y., & Liu, P. (2021). Increasing the accumulation of aptamer AS1411 and verapamil conjugated silver nanoparticles in tumor cells to enhance the radiosensitivity of glioma. *Nanotechnology, 32*(14), 145102.

Zhou, Y., Liyanage, P. Y., Devadoss, D., Guevara, L. R. R., Cheng, L., Graham, R. M., . . . El-Shahawi, M. S. (2019). Nontoxic amphiphilic carbon dots as promising drug nanocarriers across the blood–brain barrier and inhibitors of β-amyloid. *Nanoscale, 11*(46), 22387-22397.

Zhu, Y., Liang, J., Gao, C., Wang, A., Xia, J., Hong, C., . . . Ren, H. (2021). Multifunctional ginsenoside Rg3-based liposomes for glioma targeting therapy. *Journal of controlled release, 330*, 641-657.

APPENDICES

APPENDIX 1 Primary & secondary antibodies of bbb used for immunocytochemistry

Primary Antibodies				
Name	**Species & Class**	**Vendor & Lot Number**	**Fixative & Blocking Solution**	**Dilution**
PECAM1 (CD31) (1 mg/mL)	Mouse Monoclonal	Abcam, ab9498	Cold MeOH, 1% BSA + 0.1% TritonX_100 in DPBS (1X)	1:1000
Occludin (OCLN) (1 mg/mL)	Mouse Monoclonal	Abcam, ab242202		1:100
Secondary Antibodies				
Species Reactivity	**Host**	**Vendor & Lot Number**	**Conjugate**	**Dilution**
Mouse	Donkey	Abcam, ab150113	Alexa Fluor 488 (AF488)	1:500

APPENDIX 2 Primers of BBB & hiPSCs for RT-qPCR

Gene Name	Forward Sequence (5' to 3') & Melting Temperature	Reverse Sequence (3' to 5') & Melting Temperature	Length (between 80-150 bp)
GAPDH	AGCCACATCGCTCAGACA 59.0 ºC	GCCCAATACGACCAAATC 57.0 ºC	66
SLC2A1	AACTCTTCAGCCAGGGTCCAC 62.9 ºC	CACAGTGAAGATGATGAAGAC 53.0 ºC	140
CDH5	GGCCAGGTATGAGATCGTGG 62.8 ºC	TCTTGCAGAGTGACCAGCAC 60.2 ºC	90
ABCB1	GCCTGGCAGCTGGAAGACAAATAC 64.4 ºC	ATGGCCAAAATCACAAGGGTTAGC 61.0 ºC	-
OCLN	GACTTCAGGCAGCCTCGTTAC 61.3 ºC	GCCAGTTGTGTAGTCTGTCTCA 58.0 ºC	132
ZO-1	ACCAGTAAGTCGTCCTGATCC 58.1 ºC	TCGGCCAAATCTTCTCACTCC 63.8 ºC	128
CD31	GAGTATTACTGCACAGCCTTCA 57.2 ºC	AACCACTGCAATAAGTCCTTTC 57.4 ºC	117
TFRC	GCACAGCTCTCCTATTGAAAC 56.7 ºC	GGTATCCCTCTAGCCATTCAG 57.8 ºC	147
KDR	GTACATAGTTGTCGTTGTAGG 49.9 ºC	TCAATCCCCACATTTAGTTC 55.0 ºC	132
PAX2	TCAAGTCGAGTCTATCTGCATCC 60.8 ºC	CATGTCACGACCAGTCACAAC 60.1 ºC	92
SOX2	ACAGCAAATGACAGCTGC 57.0 ºC	TCGGCATCGCGGTTTTT- 52.0 ºC	68
OCT4	AGCAAAACCCGGAGGAGT 56.0 ºC	CCACATCGGCCTGTGTAT 61.0 ºC	114
NANOG	ATGCCTCACACGGAGACT 60.0 ºC	AGGGCTGTCCTGAATAAG 58.0 ºC	66

APPENDIX 3 Mycoplasma detection of hCMEC/D3

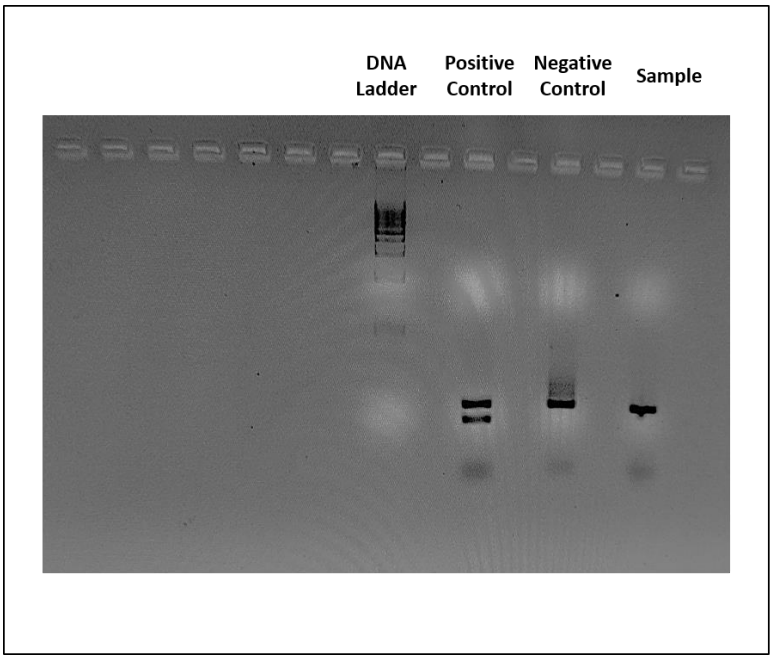

APPENDIX 4 L-lactate dehydrogenase (LDH) analysis

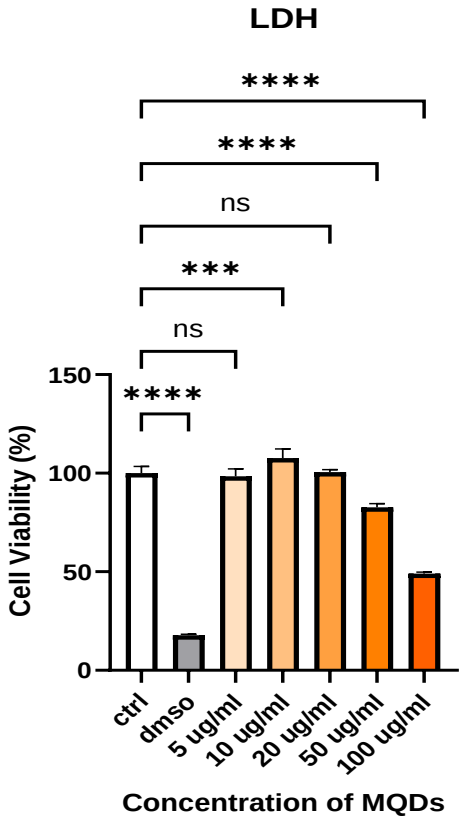

Cytotoxicity of MQDs on hCMEC/D3 after 24 H by LDH Assay (ns: non significant, *p < 0.05 with standard errors)

APPENDIX 5 Gene Expression Profiles of hCMEC/D3 by RT-qPCR

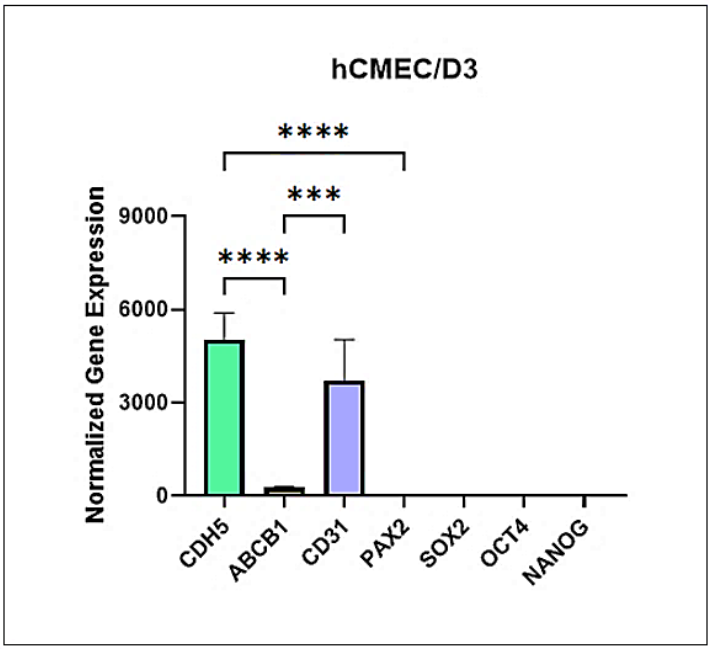

Normalized Gene Expressions of hCMEC/D3 on CoL1-coated flasks at passage +4 according to hiPSCs at passage 25, *p < 0.05 with standard errors

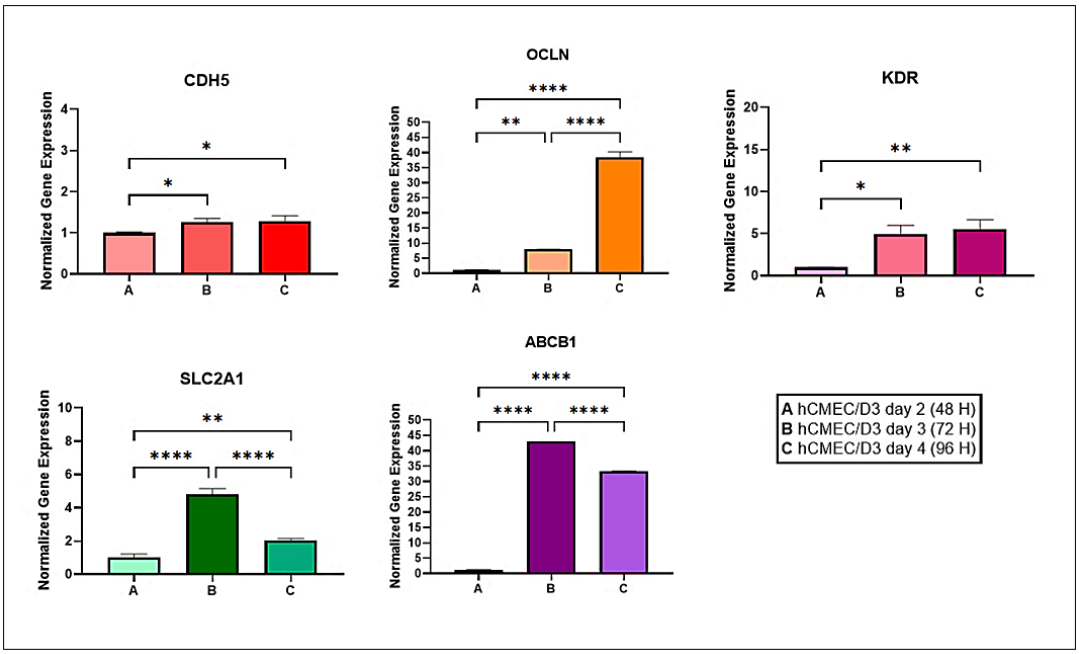

Normalized Gene Expressions of hCMEC/D3 at different times immediately after seeding on 24 transwells pre-coated with CoL1 according to sample A (the sample which maximum TEER was observed), *p < 0.05 with standard errors

APPENDIX 6 RT-qPCR analysis of hiPSCs-derived BMECs, hiPSCs and hCMEC/D3 showing %GAPDH

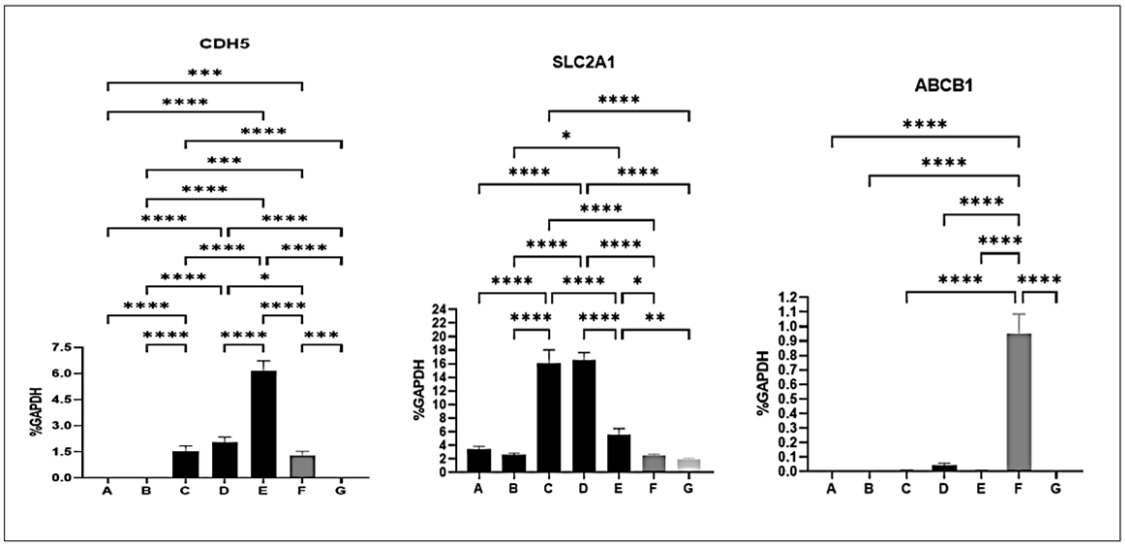

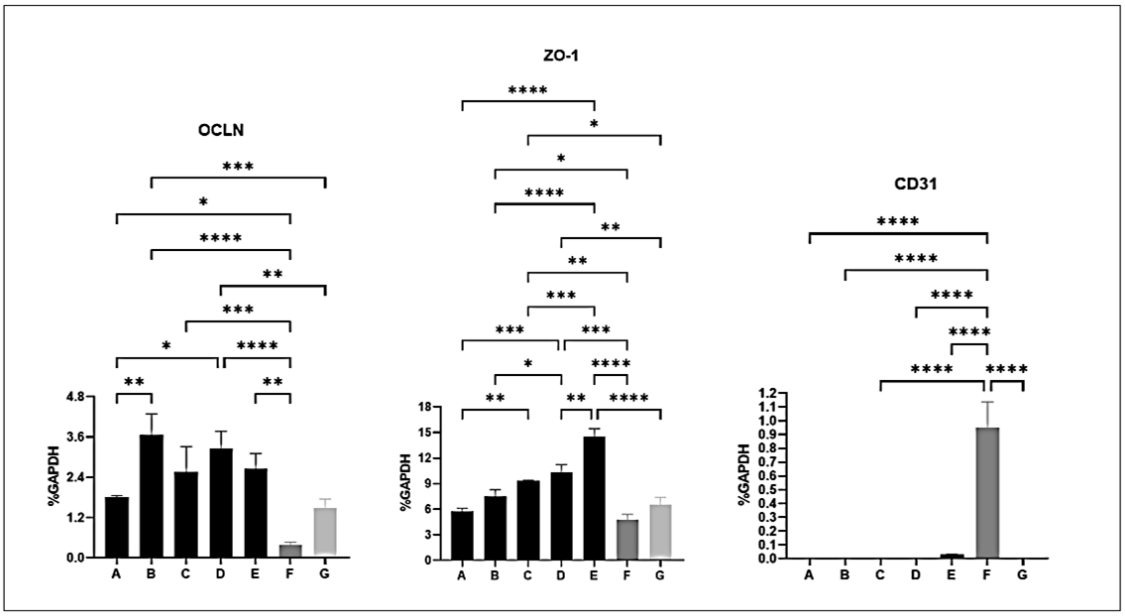

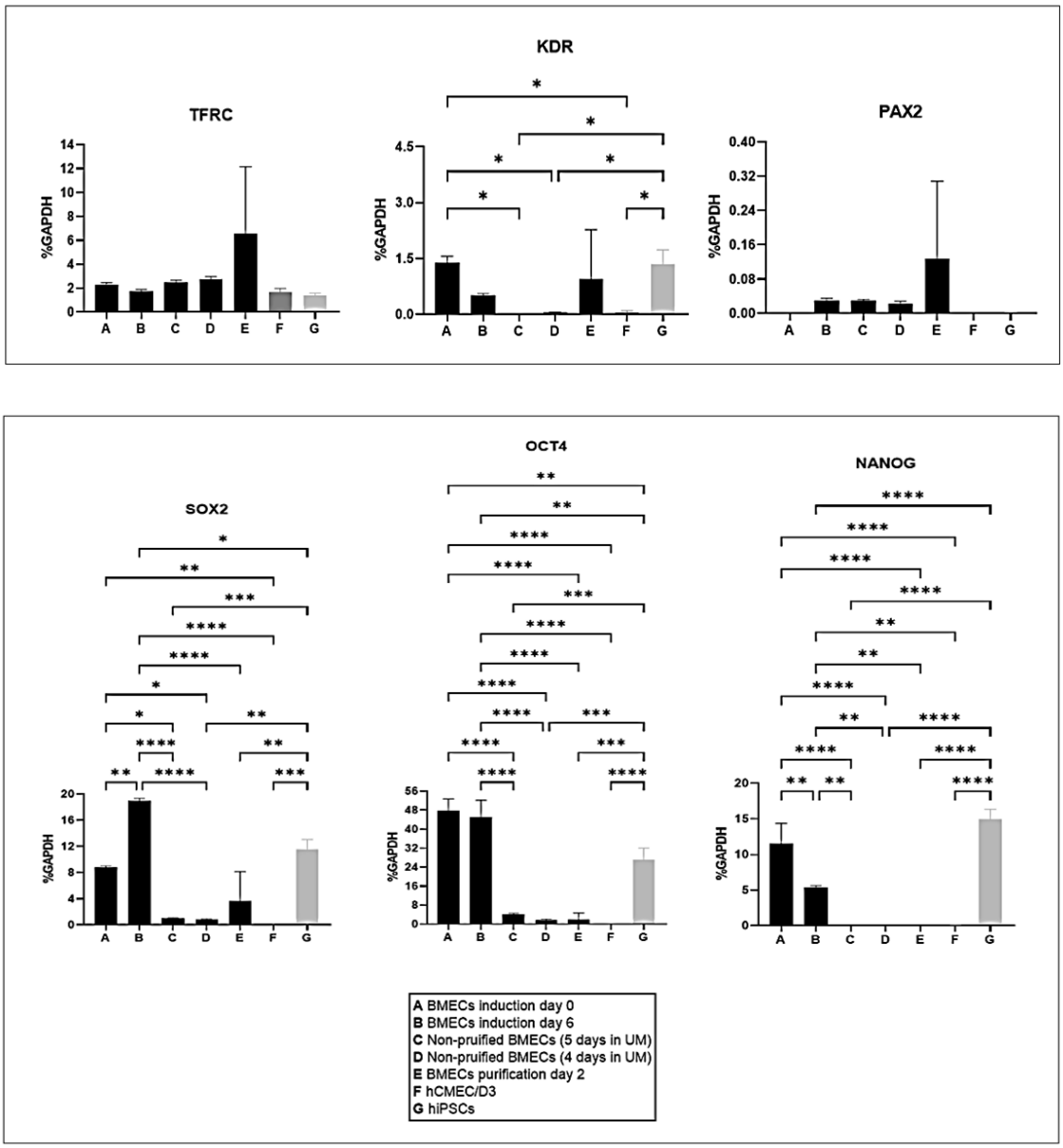

Gene Expressions of hiPSCs-derived BMECs throughout the differentiation, hiPSCs at passage 25, and hCMEC/D3 at passage +4, with GAPDH as the loading control, *p < 0.05 with standard errors

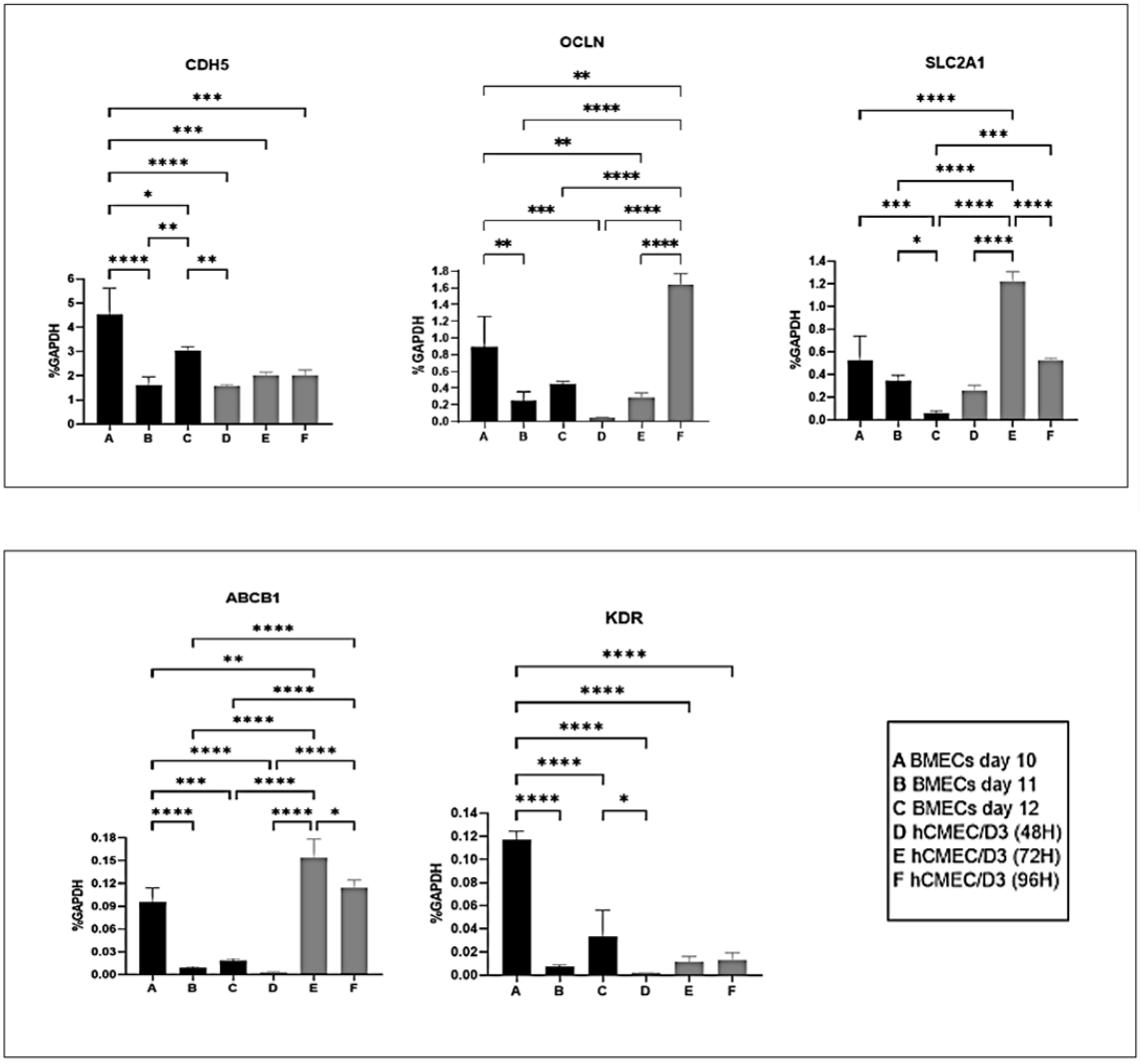

Gene Expressions of hiPSCs-derived BMECs on CoL1 + FN coated-transwells during subculture and hCMEC/D3 on CoL1-coated transwells at different times, with GAPDH as the loading control, *p < 0.05 with standard errors

APPENDIX 7 Ethics committee approval for the isolation of iPSCs from human blood cells, PBMCs

İNSAN ARAŞTIRMALARI ETİK KURULU KARAR FORMU

ETİK KURULUN ADI	ANKARA ÜNİVERSİTESİ TIP FAKÜLTESİ İNSAN ARAŞTIRMALARI ETİK KURULU
AÇIK ADRES	Ankara Üniversitesi Tıp Fakültesi Morfoloji Binası 06100 Sıhhıye/ANKARA
TELEFON	0312 595 82 27
E-POSTA	tipinsanetik@ankara.edu.tr

BAŞVURU BİLGİLERİ	ARAŞTIRMANIN AÇIK ADI	Başvuru No: 2024000362-1(2024/362) uPK Hücrelerinden Elde Edilen Kan-Beyin Bariyer Modelinde Nanomalzeme Geçişinin in Vitro Modellenmesi	
	KOORDİNATÖR/SORUMLU ARAŞTIRMACI ÜNVANI/ADI/SOYADI	Doç. Dr. Açelya YILMAZER AKTUNA	
	PROJE YÜRÜTÜCÜSÜ UNVANI/ADI/SOYADI (TÜBİTAK vb. gibi kaynaklardan destek alanlar için)		
	KOORDİNATÖR/SORUMLU ARAŞTIRMACININ UZMANLIK ALANI	Tıbbi Biyoloji ve Genetik	
	KOORDİNATÖR/SORUMLU ARAŞTIRMACININ BULUNDUĞU MERKEZ	Ankara Üniversitesi Biyomedikal Mühendisliği	
	ARAŞTIRMAYA KATILAN MERKEZLER	TEK MERKEZ ☒	ÇOK MERKEZLİ ☐

KARAR BİLGİLERİ	Karar No:106-416-24	Tarih: 13 Haziran 2024
	Yukarıda bilgileri verilen başvuru dosyası ile ilgili belgeler araştırmanın/çalışmanın gerekçe, amaç, yaklaşım ve yöntemleri dikkate alınarak incelenmiş ve uygun bulunmuş olup araştırmanın/çalışmanın başvuru dosyasında belirtilen merkezde gerçekleştirilmesinde etik ve bilimsel sakınca bulunmadığına toplantıya katılan etik kurul üye tam sayısının salt çoğunluğu ile karar verilmiştir.	

İNSAN ARAŞTIRMALARI ETİK KURULU	
ÇALIŞMA ESASI	İyi Klinik Uygulamaları Kılavuzu
BAŞKANIN UNVANI / ADI / SOYADI:	Prof.Dr.Hakan ERGÜN

Unvanı/Adı/Soyadı	Uzmanlık Alanı	Kurumu	Araştırma ile ilişki		İmza
Prof.Dr.Hakan ERGÜN	Tıbbi Farmakoloji	A.Ü. Tıp Fakültesi	E ☐	H ☒	
Prof.Dr.Berna ARDA	Tıp Tarihi ve Etik	A.Ü Tıp Fakültesi	E ☐	H ☒	
Prof.Dr.Hatice İLGIN RUHİ	Tıbbi Genetik	A.Ü Tıp Fakültesi	E ☐	H ☒	
Prof.Dr Sevim AYDIN	Histoloji ve Embriyoloji	A.Ü Tıp Fakültesi	E ☐	H ☒	
Prof.Dr.Berna SAVAŞ	Tıbbi Patoloji	A.Ü Tıp Fakültesi	E ☐	H ☒	
Prof.Dr Yüksel ÜRÜN	Tıbbi Onkoloji	A.Ü.Tıp Fakültesi	E ☐	H ☒	
Prof.Dr Başak Ceyda MEÇO	Anestezyoloji ve Reanimasyon	A.Ü Tıp Fakültesi	E ☐	H ☒	
Doç.Dr Emel OKULU	Çocuk Sağlığı ve Hastalıkları	A.Ü Tıp Fakültesi	E ☐	H ☒	
Doç.Dr.Zahide Çiler BÜYÜKATALAY YALDIZ	Kulak, Burun ve Boğaz Hastalıkları	A.Ü Tıp Fakültesi	E ☐	H ☒	
Doç.Dr Rezzak YILMAZ	Nöroloji	A.Ü Tıp Fakültesi	E ☐	H ☒	
Doç.Dr Serkan AKBULUT	Cerrahi Onkoloji	A.Ü Tıp Fakültesi	E ☐	H ☒	
Doç.Dr Miraç YILDIRIM	Çocuk Sağlığı ve Hastalıkları	A.Ü, Tıp Fakültesi	E ☐	H ☒	
Dr Öğr Üyesi Can Yahya BOZTUĞ	Genel Cerrahi	A.Ü Tıp Fakültesi	E ☐	H ☒	
Dr.İrem KAR	Biyoistatistik	A.Ü Tıp Fakültesi	E ☐	H ☒	

APPENDIX 8 Characterization of hiPSCs (Colony 4)

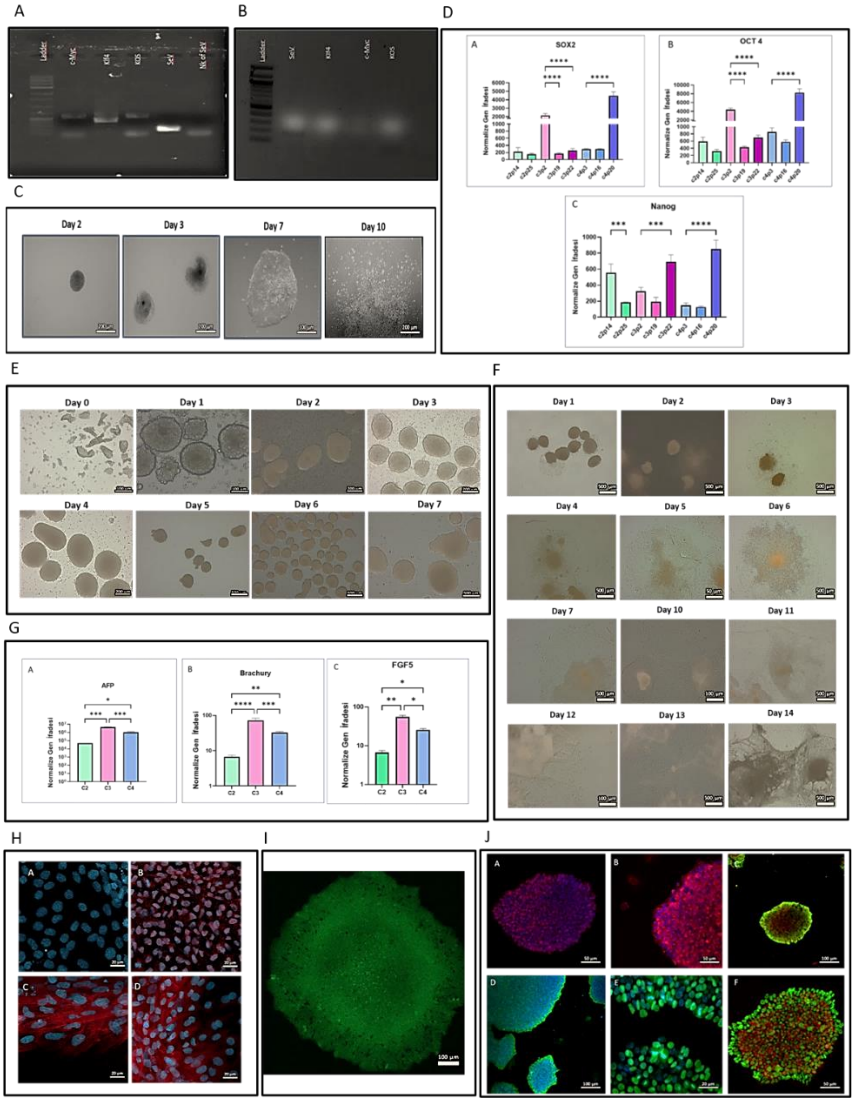

A. SeV PCR Gel Image for the Proof of Viral Transduction, B. SeV PCR Gel Image for the Prove of Viral Vectors Deletion After Passage, C. Growth of Colony 4, D. Measurement of Gene Expressions in the Following Passages by RT-qPCR (A. SOX2 Expression, B. Oct4 Expression and C. Nanog Expression), E. Embryoid Body (EB) Formation, F. EB Spontaneous Differentiation, G. RT-qPCR Results of EB Formation (A. AFP Expression, B. Brachyury Expression and C. FGF5 Expression), H. IF Staining Images of Spontaneous Differentiation (A. DAPI, B. DAPI +AFP, C. DAPI +FGF5, D. DAPI + Brachury), I. Alkaline Phosphatase Live Staining of Colony 4, J. Colony 4 Stained with PSC 4-Marker ICC Kit (A. Blue DAPI, Red Oct4 B. Blue DAPI, Red TRA-1-60, C. Red Oct4, Green SSEA4, D. Blue DAPI, Green SSEA4 E. Blue DAPI, Green Sox2 F. Red TRA-1-60, Green SOX2)